Combined Analysis of Electricity and Heat Networks

Xuezhi Liu

Institute of Energy

Cardiff University

A thesis submitted for the degree of

Doctor of Philosophy

September, 2013

Acknowledgment

This presented PhD thesis would not have been possible without the numerous, continuous guidance and help from Prof. Nick Jenkins. I appreciate his honesty and patience. His strong insights and professional writing style illuminated me in many ways, which significantly improved the thesis.

I would like to thank Dr. Jianzhong Wu for bringing me to this promising ripe research area. I thank him for his enormous helpful guidance and support in many ways.

I would like to thank Dr. Audrius Bagdanavicius for the numerous, important, constructive and fruitful discussions in technical details throughout my entire PhD journey.

I would like to thank Dr. Janaka Ekanayake for his kind support and suggestions.

I would like to thank Marc Rees for constant discussions in how to present the work clearly.

I would like to thank people in our group: Lee Thomas for helping to design the electrical network of the case study, Daniel Oluwole Adeuyi for improving the writing of some sentences, Bieshoy Awad for introducing district heating networks, and Brian Drysdale for reading Chapter 1. I also would like to thank Meysam Qadrdan and Modassar Chaudry for the discussions in the Energy Infrastructure group weekly meeting and the many friends made within the Institute of Energy.

I would like to thank Xi Hu at Oxford for improving the writing of Chapter 1, Xiaobo Hu, at China Electric Power Research Institute who visited Cardiff, for discussing the model of combined analysis, Chao Long at Glasgow for discussing electrical power flow calculation of the case study, and Brian Boyle at Cardiff for discussing the writing of Chapter 2.

I would like to acknowledge the EPSRC for their financial support through the HiDEF project and organising training and meetings. I also would like to thank the support received from Cardiff University, especially the Research Students' Skills Development Programme (RSSDP) provided by the University Graduate College; and the IT office and the research office in School of Engineering.

Finally, I would like to express my deepest appreciation to my parents and sister for their unconditional love and continuous support.

Declaration

This work has not previously been accepted in substance for any degree and is not concurrently submitted in candidature for any degree.

Signed ……..(candidate) Date …….

This thesis is being submitted in partial fulfilment of the requirements for the degree of PhD.

Signed ……..(candidate) Date …….

This thesis is the result of my own independent work/investigation, except where otherwise stated. Other sources are acknowledged by explicit references.

Signed ……..(candidate) Date …….

I hereby give consent for my thesis, if accepted, to be available for photocopying and for inter-library loan, and for the title and summary to be made available to outside organisations.

Signed …….. (candidate) Date …….

Abstract

The use of Combined Heat and Power (CHP) units, heat pumps and electric boilers increases the linkages between electricity and heat networks. In this thesis, a combined analysis was developed to investigate the performance of electricity and heat networks as an integrated whole. This was based on a model of electrical power flow and hydraulic and thermal circuits together with their coupling components (CHP units, heat pumps, electric boilers and circulation pumps). The flows of energy between the electricity and heat networks through the coupling components were taken into account.

In the combined analysis, two calculation techniques were developed. These were the decomposed and integrated electrical-hydraulic-thermal calculation techniques in the forms of the power flow and simple optimal dispatch. Using the combined analysis, the variables of the electrical and heat networks were calculated. The results of the decomposed and integrated calculations were very close. The comparison showed that the integrated calculation requires fewer iterations than the decomposed calculation.

A case study of Barry Island electricity and district heating networks was conducted. The case study examined how both electrical and heat demands in a self-sufficient system (no interconnection with external systems) were met using CHP units. A solution was demonstrated to deliver the electrical and heat energy from the CHP units to the consumers through electrical and heat networks.

The combined analysis can be used for the design and operation of integrated heat and electricity systems for energy supply to buildings. This will increase the flexibility of the electricity and heat supply systems for facilitating the integration of intermittent renewable energy.

Contents

List of Figures

List of Tables

Nomenclature

Variables

V	Voltage (V)
θ	Voltage angle (rad)
P	Electrical real power (MW_e)
Q	Electrical reactive power (MVar)
S	Electrical complex power (MVA)
Φ	Heat power (MW_{th})
$\dot{m}$	Mass flow rate within each pipe (kg/s)
$\dot{m}_q$	Injected mass flow rate at each node (kg/s)
T_s	Supply temperature at a node in the supply network (°C)
T_o	Return temperature at the outlet of a node before mixing in the return network (°C)
T_r	Return temperature at a node after mixing in the return network (°C)
T_a	Ambient temperature (°C)
T'_s	Difference between T_s and T_a
T'_r	Difference between T_r and T_a
T_{start}	Temperature at the start node of a pipe (°C)
T_{end}	Temperature at the end node of a pipe (°C)
h_f	Head loss (m) within a pipe
H	Head level (m)
H_c	Minimum allowable head differential (m)
H_p	Pump head (m)
$\boldsymbol{A}$	Network incidence matrix
$\boldsymbol{B}$	Loop incidence matrix
C_p	Specific heat of water (J/(kg·K))
λ	Overall heat transfer coefficient per unit length (W/(m·K))
c_m	Heat to power ratio
c'_m	Equivalent heat-to-power ratio of a composite CHP and heat pump system

Z	Z ratio that describes the trade-off between heat supplied to site and electrical power
K	Resistance coefficient of each pipe
L	Pipe length (m)
D	Pipe diameter (m)
ρ	Water density (kg/m^3)
g	Gravitational acceleration (kg·m/s^2).
f	Friction factor
Re	Reynolds number
ε	Roughness of a pipe (m)
v	Flow velocity (m/s)
μ	Kinematic viscosity of water (m^2/s).
$\boldsymbol{J}$	Jacobian matrix
$\Delta\boldsymbol{F}$	Vector of mismatches
$\boldsymbol{x}$	Vector of unknown state variables
$\mathbf{C}$	Matrix of coefficients
$\boldsymbol{b}$	Column vector of solutions
P_{CHP}	Electrical power output of a CHP unit (MW_e)
Φ_{CHP}	Useful heat output of a CHP unit (MW_{th})
P_{hp}	Electrical power consumed from a heat pump (MW_e)
Φ_{hp}	Heat power supplied from a heat pump (MW_{th})
P_{con}	Electrical power generation of an extraction steam turbine CHP unit in full condensing mode (MW_e)
α	Percentage of a fraction of electrical power from the CHP unit modulated to drive the heat pump
η_e	Electrical efficiency of an extraction steam turbine CHP unit in full condensing mode
F_{in}	Fuel input rate (MW)
η_b	Efficiency of an electric boiler
COP	Coefficient of performance
η_p	Efficiency of a circulation pump
P_p	Electrical power consumed (MW_e) by a circulation pump
$\dot{m}_p$	Mass flow rate (kg/s) through a criculation pump

P_p	Consumed electrical power (MW_e) by a circulation pump
ℓ	A set which includes all the pipes in the critical route with the largest pressure drop in a heat network
Y	Admittance matrix
Real	Real part of a complex expression
Imag	Imaginary part of a complex expression
$f_{i,source}$	Fuel cost of Source *i* (£/*h*)
λ	Incremental fuel cost (£/MWh)
n_{node}	Number of nodes in heat networks
n_{load}	Number of loads in heat networks
n_{loop}	Number of loops in heat networks
n_{pipe}	Number of pipes in heat networks
N	Number of busbars in electricity networks

Subscripts and Superscripts

p	pump
hp	heat pump
b	boiler
e	electrical network
h	heat network
sp	specified

Chapter 1 - Introduction

1.1 Background

It is known that the largest contribution to greenhouse gas emissions arises from the energy supply sector – the burning of coal, natural gas, and oil for the generation of electricity and heat. In the UK, this contributed 34.5% to the total emissions in 2011 as shown in Figure 1.1 [1]. The UK has set an ambitious target for cutting the greenhouse gas emissions by 80% by 2050 compared to 1990 levels [2], and a target of 15% of energy supply from renewable sources by 2020 [3]. To achieve these targets, the contribution from renewable energy has to be increased significantly.

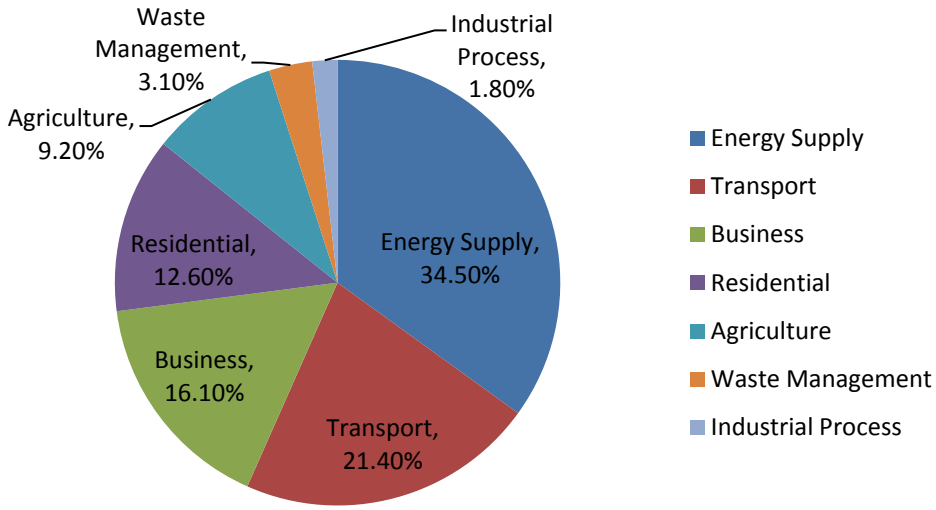

Figure 1.1: 2011 UK Greenhouse gas emissions by source sector [1]

The large-scale integration of renewable power into the electricity supply is necessary for future renewable energy systems [4]. Balancing electricity demand and supply in such systems will be challenging. This

is because the output of renewables such as wind is intermittent and it is not easy to modulate the output of renewables to follow a particular load profile. Thus, the flexibility of energy supply system that can accommodate intermittent renewables will become important.

The energy supply system is usually considered as individual sub-systems with separate energy vectors (e.g. electricity, heat, gas and hydrogen). In addition to electricity, heat is a major contributor to greenhouse gas emissions. Almost half (44%) of the final energy consumed in the UK is used to provide heat [5]. The Renewable Heat Incentive (RHI) is a policy promoting renewable heat technologies, which aims to encourage the uptake of renewable sources such as biomass boilers, heat pumps and solar thermal systems [6].

In the present Smart Grid vision, the role of electricity is most prominent with limited consideration of other energy networks. However, there is much benefit to be gained by considering the energy system as an integrated whole. Energy flows can be controlled, loads supplied from alternative sources and so security of energy supply increased. The most energy efficient operating regime can be determined and energy losses, costs or gaseous emissions minimised. Independent planning and operation of energy networks is unlikely to yield an overall optimum, since synergies between the different energy vectors cannot be exploited. Thus, an integration of energy systems is highly desirable [7].

One possibility to integrate electricity and heat networks is to use district heating systems. Combined Heat and Power (CHP) units and boilers connected to district heating systems and heat pumps act as linkages between electricity and heat networks. These allow a coupling of the electricity and heat networks, and make use of synergies of the two networks for energy storage and the utilisation of distributed renewable energy. The coupling components (CHP units, heat pumps, electric boilers and circulation pumps) increase flexibility for equalising the fluctuations from the renewable energy. Flexibility is achieved through the optimisation of electric power consumption in heat pumps and supply in CHP units. As the penetration of the coupling components increases,

the interaction of electricity and heat networks becomes tighter and modelling electricity and heat networks as a whole becomes increasingly important.

1.2 Electricity and District Heating Networks

1.2.1 Electricity Networks

Transmission networks refer to the bulk transfer of power by high-voltage links between central generation and load centres. Distribution networks, on the other hand, describe the distribution of this power to consumers by means of lower voltage networks (see Figure 1.2) [8]. Generators usually produce voltages in the range 11-25kV, which is increased by transformers to the main transmission voltage. At substations the connections between the various components of the system, such as lines and transformers, are made and the switching of these components is carried out [8].

Distribution networks differ from transmission networks in several ways, apart from their voltage levels. The number of branches -is much higher in distribution networks and the general structure or topology is different. A typical system consists of a step-down (e.g.33/11kV) on-load tap-changing transformer at a bulk supply point feeding a number of circuits which can vary in length from a few hundred metres to several kilometres. A series of step-down three-phase transformers (e.g.11kV/433V) are spaced along the route and from these are supplied the consumer three-phase, four-wire networks which give 240V single-phase supplies to houses and similar loads [8].

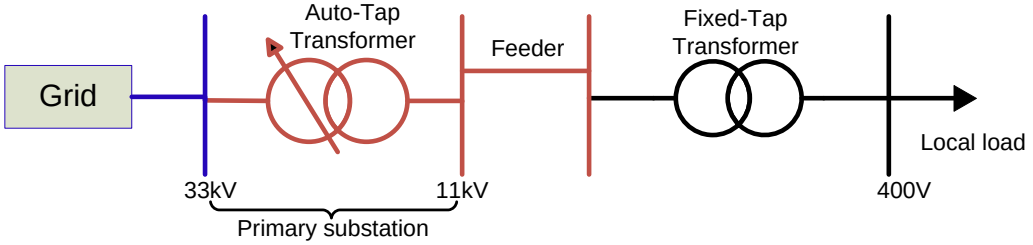

Figure 1.2: Electrical distribution network [9]

1.2.2 District Heating Networks

District Heating Networks usually consist of supply and return pipes that deliver heat, in the form of hot water or steam, from the point of generation of the heat to the consumers [10, 11] (see Figure 1.3). The supply line carries the flow water at temperatures of 70°C to 120°C and the return line carries the return water after the heat has been extracted at temperatures of 30°C to 70°C. The heat is transferred to conventional heating systems within the building either directly or indirectly through a heat exchanger which provides a separation of the two water based systems [12, 13]. A circulation pump powered by electricity is located at the heat plant and substation to create and maintain pressure difference between the supply and return pipelines [14].

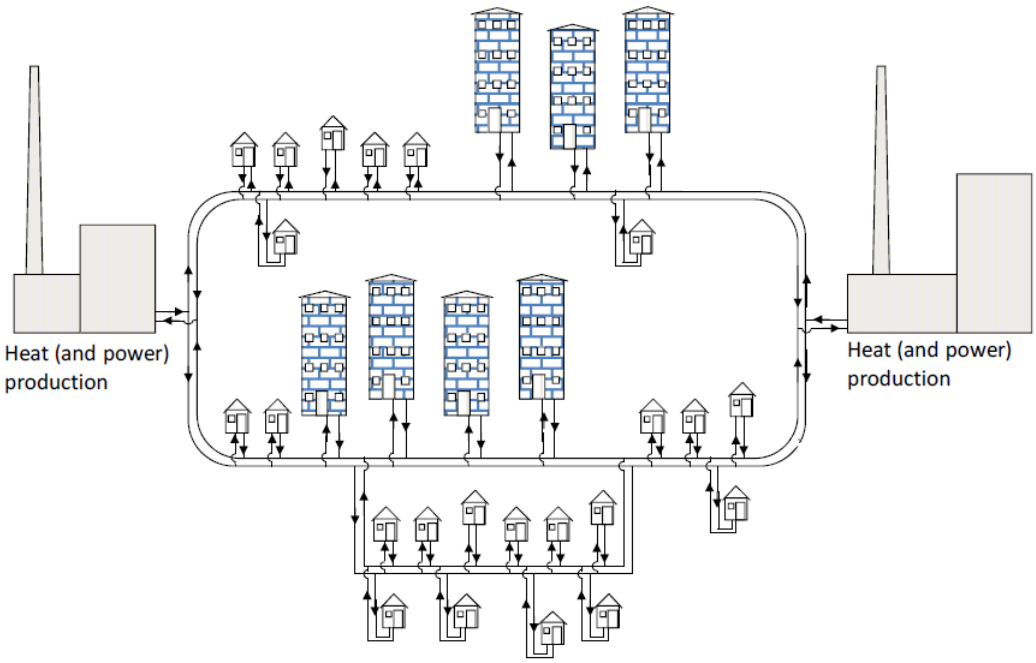

Figure 1.3: A simplified district heating network with two heat production units [15]

District heating systems, which are well-developed in a number of Northern European countries such as Denmark and Sweden, are very promising for energy saving and carbon emission reduction [12, 16, 17]. Energy systems using CHP and district heating are common in many countries and are reviewed in the literature [10]. District heating networks have a very low penetration in the UK. Although the UK has an extensive gas network that provides gas supplies to households, unlike a number of European countries, it does not have a very widely distributed heat

networks [18]. Nevertheless, some of the UK's largest towns and cities either already have district heating or are in the process of establishing such schemes, examples include the city-wide heat networks in Sheffield and Nottingham [10, 19].

Heat networks require significant deployment of new infrastructure and therefore face a number of barriers to wide deployment. The low penetration of district heating to date in the UK is partly due to the relatively high cost of providing heat through district heating in comparison with conventional gas or electric-based heating systems, notably the cost of installing the pipes [12, 20-24]. A commercially viable heat network requires a constant, large and consistent heat load, limiting its suitability to specific locations [20, 21]. Besides, district heating networks are complex projects, which have long lead-in times and are coupled with lengthy payback periods [21]. Furthermore, there is currently no separately regulated market for heat in the UK, unlike electricity or gas [20].

Although district heating networks face challenges, it offers many benefits: increased energy efficiency; reduced fossil fuel consumption and the ability to use local renewable energy resources [17, 25]. The local heat sources are: low-grade heat generated from thermal power stations, heat pumps, biomass CHP or boilers, solar thermal, industrial waste heat and geothermal [5, 12, 22, 26-28]. District Heating can also offer significant electricity demand-side management in relation to intermittent wind output [29]. A number of Government White Papers have cited district heating networks as an important enabler for the more efficient utilisation of gas and the diffusion of renewable heating technologies [30, 31].

1.3 Interdependencies between Electricity and Heat Networks

CHP units, heat pumps, electric boilers and circulation pumps are the coupling components between electricity and heat networks. These coupling components allow flows of energy between electricity and heat

networks. The CHP units generate electricity and heat simultaneously. Heat pumps use a small quantity of electricity to leverage heat from the surroundings to higher temperatures, using a compressor similar to a refrigerator [22, 32]. Electric boilers convert electricity to heat directly. Circulation pumps consume electricity to circulate water in the district heating network.

Heat pumps and CHP/district heating are core heating technologies, which could play a key role in meeting the UK and global heat demand in an emissions constrained future [5, 28, 33, 34]. CHP can deliver energy and carbon savings of up to 30% by reducing energy lost as waste heat compared to separate electrical and heat power generation from the same fuel [35]. The global deployment of heat pumps, solar thermal and CHP in the IEA scenario to 2050 is shown in Figure 1.4 [36]. This data indicates that the link between electricity and heat networks is increasing. The larger the penetration of CHP/district heating and heat pumps, the stronger the links between electricity and heat networks.

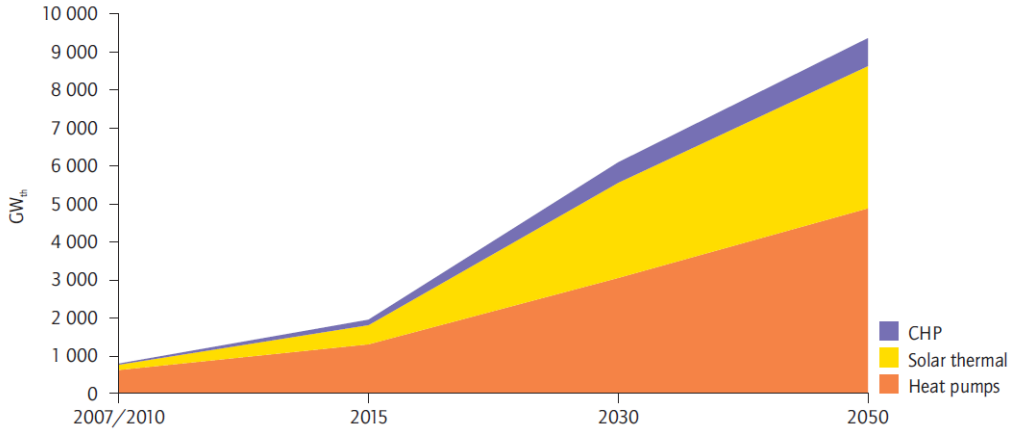

Figure 1.4: Global deployment of heating technologies in the IEA scenario, 2007/2010 to 2050 (GW_{th})

In an energy system with increased CHP/district heating and heat pumps, the conversion to heat facilitates system operation and the use of storages. For example, excess electricity can be converted to heat, stored as heat in a tank or in the system when there is a surplus of electricity from intermittent renewables [5, 26]. Using CHP with heat accumulation to integrate intermittent renewable electricity supplies such

as wind power into electricity systems has been demonstrated in various countries [37]. In Germany, the demonstration project used biogas CHP and hydropower to balance fluctuations in wind and solar power [38]. Pilot projects such as: feeding heat or hydrogen from weather-dependent renewables into district heating or gas networks were launched [39, 40].

Thus, it becomes increasingly important to consider electricity and heating systems as a whole to consider the synergy effects.

1.4 Modelling Review

Several conceptual approaches for modelling the integration of energy systems have been published. Examples include energy hubs [7, 41], multi-energy systems and distributed multi-generation [42-45], community energy [43], smart energy systems [4, 46], and integrated energy systems [10].

A generic framework for steady-state and optimisation of energy systems is investigated by Geidl & Andersson [41]. The coupling between multiple energy carriers are modelled by the use of energy hubs [47]. In the modelling of energy hubs [41], electricity, natural gas, and district heat input powers are converted to electricity and heat output powers through an efficiency coupling matrix. Smart multi-energy systems were described by Mancarella et al [42, 48, 49]. In multi-energy systems, coupling of electricity, heat/cooling and gas networks through distribution infrastructure takes place through various distributed technologies such as CHP, micro-CHP, heat pump, solar thermal, photovoltaic, storage and heat networks. In a community energy scheme [47], a transformer substation in the electrical power system links the gas network and a local heat network on the community scale, with sources installed at this substation. Low temperature heat networks compatible with waste heat from CHP, electric or engine driven heat pumps, or solar thermal was used. Integrated energy systems focusing on the role of CHP and district heating were described by the CHPA [10].

Methods have been developed to investigate combined electricity and natural gas networks [7, 50-54], in which gas turbine generators provide

the linkage between gas and electricity networks. A general approach was described to execute a single gas and power flow analysis in a unified framework based on the Newton-Raphson formulation [53]. There have been a few studies that have investigated combined electricity and heat networks, e.g. the energy hub model [7], the energy interconnector model [55] and an integrated optimal power flow for electricity and heat networks [56]. The simultaneous transmission of heat, electricity, and chemical energy in one single device was modelled [55]. The integration of technical design, green house gas emissions analysis and financial analysis models for integrated community energy systems was modelled by Rees [57, 58]. In these models the electrical, thermal and gas power flows were calculated independently and linked through generating units.

The role of the coupling components (CHP units, heat pumps and electric boilers) was investigated, i.e., a strategy [59], the economic value [60], a technical approach [61, 62], and the impact of future heat demand [63]. It is concluded that the increased diversity of heat delivery – with gas, heat networks and electric heating all playing major roles, may facilitate the difficult move towards a decarbonised future [64-66].

For individual heat network calculation, PSS SINCAL Heating [67] is a commercial software for planning large networks. Using the Hardy-Cross method, the simulation program can determine the operating points in any number of meshed networks.

The Hardy-Cross method dealt with one loop at a time. The Newton-Raphson method considered all loops simultaneously [11]. The Newton-Raphson method was used to solve the electrical power flow. For the sake of combining with the thermal model and further combining with the electrical power flow, the Newton-Raphson method was used to solve the hydraulic equations. Consistently, the Newton-Raphson method was chosen to solve a unified formulation of the hydraulic-thermal equations and the electrical power flow equations in this thesis.

1.5 Research Objective

The penetration of CHP units, heat pumps and electric boilers increases the linkages between electricity and heat networks. The objective of this thesis is to develop a combined analysis to investigate the performance of electricity and heat networks as an integrated whole and maximise synergy effects. The combined analysis can be used for the design and operation of integrated heat and electricity systems for energy supply to buildings. This will increase the flexibility of the electricity and heat supply systems for facilitating the integration of intermittent renewable energy. The combined analysis has taken into account the flows of energy between the electricity and heat networks through the coupling components (CHP units, heat pumps, electric boilers and circulation pumps).

The research framework is shown in Figure 1.5.

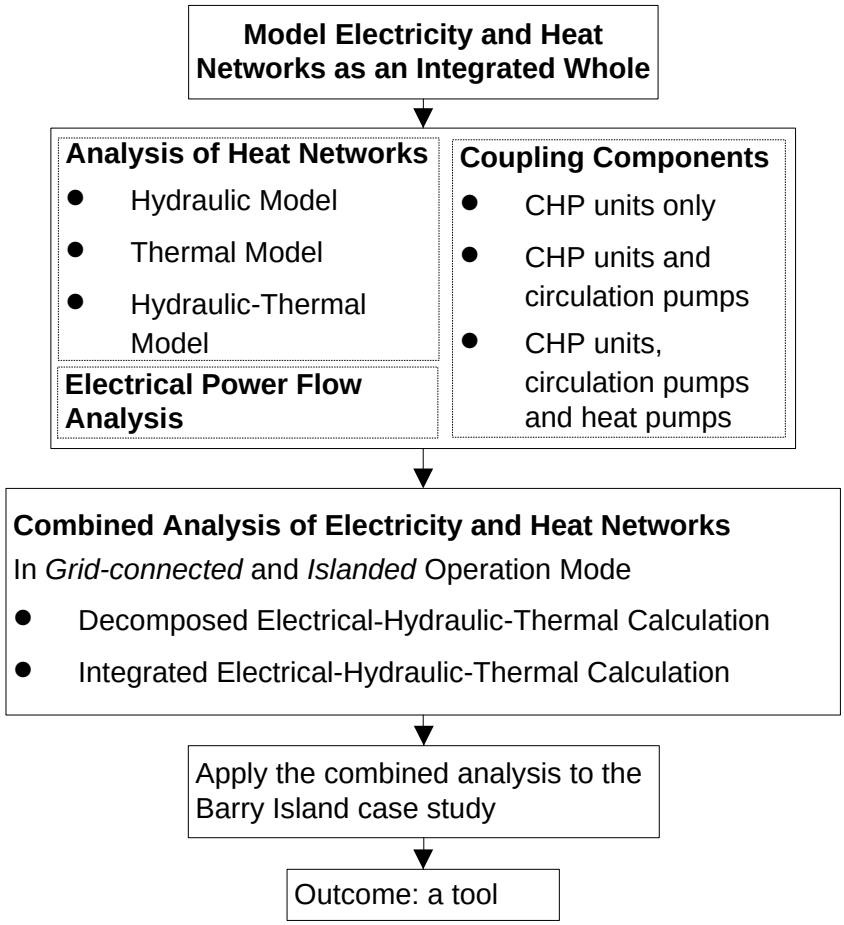

Figure 1.5: Research Framework

1.6 Thesis Structure

The description of each chapter is as follows:

Chapter 1 presents the introduction.

Chapter 2 describes an analysis of district heating networks. A hydraulic-thermal model (decomposed and integrated calculations) was developed to investigate the performance of a district heating network.

Chapter 3 describes a combined analysis of electricity and heat networks. Two calculation techniques (decomposed and integrated electrical-hydraulic-thermal calculations) were developed. This is based on a model of electrical power flow and hydraulic and thermal circuits together with their coupling components.

In Chapter 4, a case study of Barry Island examined how both electrical and heat demands in a self-sufficient system (no interconnection with external systems) were met using CHP units.

Chapter 5 presents the conclusions drawn, the main findings and recommendations for future work.

Chapter 2 - Analysis of District Heating Networks

District Heating Networks usually consist of supply and return pipes that deliver heat, in the form of hot water or steam, from the point of generation of the heat to the end consumers [10, 11]. In a simulation of a district heating network, the variables are: pressure and mass flow rates in the hydraulic model; supply and return temperatures and heat power in the thermal model. Hydraulic and thermal analysis is carried out to determine the mass flow rates within each pipe and the supply and return temperatures at each node. Usually, hydraulic analysis is carried out before the thermal analysis [11, 67-69]. It is common to perform hydraulic calculations using the Hardy-Cross or Newton-Raphson method [11, 67-70]. The Hardy-Cross method considers each loop independently and the Newton-Raphson method considers all loops simultaneously [11]. The decomposed hydraulic and thermal analysis of a pipe network using the Newton-Raphson method is described in the literature [68].

According to the literature [11, 67, 71, 72], the source supply temperatures and the load return temperatures are specified; the injected mass flow rates or the heat power supplied or consumed at all the nodes except one are specified. Based on these assumptions, an integrated hydraulic-thermal model of district heating networks, the so-called thermal power flow by the Newton-Raphson method was presented in

this Chapter. In the hydraulic model, the network description is based on a graph-theoretical method. In the thermal model, a matrix approach was used.

2.1 Hydraulic Model

The modelling of a district heating network is similar to that of an electrical network. For electrical network and district heating network, the analogy of three basic rules is shown in Table 2.1. The first two laws describe the linear algebraic constraints on branch current and voltage (or flow and pipe pressure drop in a district heating network), that are independent of the branch characteristics [11]. The description of the first two laws based on the graph theoretical method is described in the literature [73, 74].

Table 2.1: Analogy of rules in electrical network and district heating network

Electrical network	Kirchhoff's current law	Kirchhoff's voltage law	Ohm's law
District heating network	Continuity of flow	Loop pressure equation	Head loss equation

For illustration purpose, a simplified district heating network with a loop is shown in Figure 2.1. Since supply and return networks are identical, the supply network is only considered in the hydraulic model.

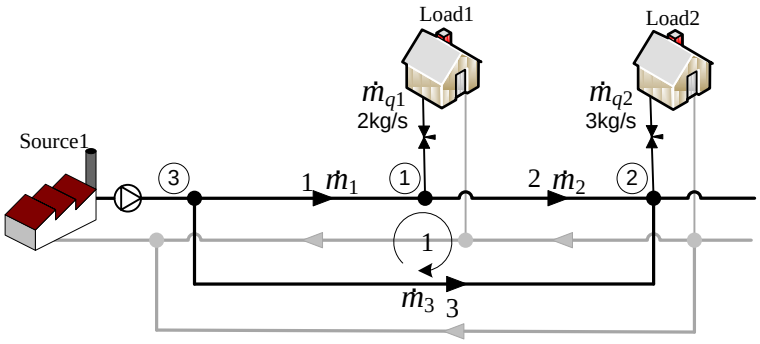

Figure 2.1: A district heating network with a loop

2.1.1 Continuity of Flow

The continuity of flow is expressed as: the mass flow that enters into a node is equal to the mass flow that leaves the node plus the flow consumption at the node, i.e.

$$\left(\sum \dot{m}\right)_{in} - \left(\sum \dot{m}\right)_{out} = \dot{m}_q \qquad (2.1)$$

where $\dot{m}$ is the mass flow (kg/s) within each pipe; $\dot{m}_q$ is the mass flow (kg/s) through each node injected from a source or discharged to a load.

To describe the continuity of flow in a matrix form, the network incidence matrix ***A*** with n_{node} = 3 rows and n_{pipe} = 3 columns is defined, where n_{node} is the number of nodes and n_{pipe} is the number of pipes. Each element of the matrix *A* describes [74]

+1, if the flow in a pipe comes into a node;

-1, if the flow in a pipe leaves a node;

0, if no connection from a pipe to a node.

$\boldsymbol{\dot{m}_q}$ is the vector of the mass flow (kg/s) through each node injected from a source or discharged to a load. The element is positive if the flow leaves the node and negative if it comes into the node.

For the network as shown in Figure 2.1, the network incidence matrix and the nodal mass flow rates are

$$\boldsymbol{A} = \begin{array}{c} \\ \text{Node No.} \end{array} \begin{array}{c} \begin{array}{ccc} \text{Pipe No.} & & \\ 1 & 2 & 3 \end{array} \\ \begin{array}{c} 1 \\ 2 \\ 3 \end{array} \begin{bmatrix} 1 & -1 & 0 \\ 0 & 1 & 1 \\ -1 & 0 & -1 \end{bmatrix} \end{array} \qquad \boldsymbol{\dot{m}_q} = \begin{bmatrix} 2 \\ 3 \\ -5 \end{bmatrix} \qquad (2.2)$$

For node 1, the continuity of flow is expressed as

$$\dot{m}_1 - \dot{m}_2 = 2 \text{ or}$$
$$A(1,1) \cdot \dot{m}_1 + A(1,2) \cdot \dot{m}_2 + A(1,3) \cdot \dot{m}_3 = \dot{m}_q(1) \qquad (2.3)$$

Thus for the entire hydraulic network, the continuity of flow is expressed as

$$\boldsymbol{A}\,\dot{\boldsymbol{m}} = \dot{\boldsymbol{m}}_{\boldsymbol{q}} \tag{2.4}$$

The continuity of flow is applied at all nodes in a network, but one is redundant because of it being linearly dependent on others and is chosen arbitrarily for exclusion. Thus, in the following context, the incidence matrix $\boldsymbol{A}$ of the network in Figure 2.1 is also written as $\boldsymbol{A} = \begin{bmatrix} 1 & -1 & 0 \\ 0 & 1 & 1 \end{bmatrix}$.

2.1.2 Loop Pressure Equation

Head loss is the pressure change in meters due to the pipe friction. The loop pressure equation states that the sum of head losses around a closed loop must equal to zero.

$$\sum h_f = 0 \tag{2.5}$$

where h_f is the head losses within a pipe, which is the difference of the pressure head H at the start and end nodes within a pipe.

The loop incidence matrix $\boldsymbol{B}$ with n_{loop} = 1 rows and n_{pipe} = 3 columns is defined, where n_{loop} is the number of loops and n_{pipe} is the number of pipes. Each element of the matrix B describes [74]

+1, if the flow in a pipe is the same direction as the definition;

-1, if the flow in a pipe is the opposite direction as the definition;

0, if a pipe is not part of the loop.

For the network as shown in Figure 2.1, the loop incidence matrix is

$$\boldsymbol{B} = \begin{array}{c} \\ \text{Loop No.} \\ 1 \end{array} \begin{array}{c} \text{Pipe No.} \\ \begin{array}{ccc} 1 & 2 & 3 \end{array} \\ \begin{bmatrix} 1 & 1 & -1 \end{bmatrix} \end{array} \tag{2.6}$$

For loop 1, the equation (2.5) is expressed as

$$h_{f1} + h_{f2} - h_{f3} = 0 \text{ or}$$
$$B(1,1) \cdot h_{f1} + B(1,2) \cdot h_{f2} + B(1,3) \cdot h_{f3} = 0 \quad (2.7)$$

Thus correspondingly for the entire hydraulic network

$$\boldsymbol{B}\, \boldsymbol{h}_f = 0 \quad (2.8)$$

where $\boldsymbol{B}$ is the loop incidence matrix that relates the loops to the pipes; and $\boldsymbol{h}_f$ is the vector of the head losses (m).

2.1.3 Head Loss Equation

The relation between the flow and the head losses along each pipe is

$$\boldsymbol{h}_f = \boldsymbol{K}\, \dot{\boldsymbol{m}}|\dot{\boldsymbol{m}}| \quad (2.9)$$

where $\boldsymbol{K}$ is the vector of the resistance coefficients of each pipe calculated using equation (2.11). *K* generally depends largely on the diameter of a pipe.

Hence, equation (2.8) is expressed as

$$\boldsymbol{B}\, \boldsymbol{K}\, \dot{\boldsymbol{m}}|\dot{\boldsymbol{m}}| = \sum_{j=1}^{n_{pipe}} B_{ij} K_j \dot{m}_j \left|\dot{m}_j\right| = 0 \quad (2.10)$$

where n_{pipe} is the number of pipes; *i* is the index of loops and *j* is the index of pipes.

The resistance coefficient *K* of a pipe is calculated from the friction factor f

$$K = \frac{8Lf}{D^5 \rho^2 \pi^2 g} \quad (2.11)$$

where *L* is the pipe length (m); *D* is the pipe diameter (m); ρ is water density (kg/m^3); and *g* is gravitational acceleration (kg·m/s^2).

The friction factor f generally depends on Reynolds number Re.

For laminar flow (Re<2320)

$$f = \frac{64}{Re} \tag{2.12}$$

For the more frequent turbulent flow (Re>4000), the friction factor *f* is calculated by

$$\frac{1}{\sqrt{f}} = -2log_{10}\left(\frac{\epsilon/D}{3.7} + \frac{2.51}{Re\sqrt{f}}\right) \tag{2.13}$$

where ε is the roughness of a pipe (m). The implicit equation (2.13) is solved by the method adopted in the reference [75].

For 2300 < Re < 4000, linear interpolation is used.

Reynolds number Re is calculated from the flow velocity

$$Re = \frac{\nu D}{\mu} \tag{2.14}$$

where *v* is the flow velocity (m/s); μ is kinematic viscosity of water (m^2/s).

The flow velocity is calculated from the mass flow rate

$$\nu = \frac{\dot{m}}{\rho\pi D^2/4} \tag{2.15}$$

2.2 Solution of the Hydraulic Model

2.2.1 Newton-Raphson Method

The Newton-Raphson method [76, 77] is based on Taylor Series expansion of *f*(*x*) about an operating point x_0

$$f(x) = f(x_0) + \left.\frac{\partial f}{\partial x}\right|_{x=x_0}(x - x_0) + \left.\frac{\partial^2 f}{\partial x^2}\right|_{x=x_0}(x - x_0)^2 + \cdots \tag{2.16}$$

Neglecting the higher order terms in equation (2.16) since the value of $(x - x_0)$ is small enough and solving the linear approximation of $f(x) = 0$ for x gives

$$x = x_0 - \left[\left.\frac{\partial f}{\partial x}\right|_{x=x_0}\right]^{-1} f(x_0) \tag{2.17}$$

The Newton-Raphson method replaces the old value $x^{(i)}$ by the new value $x^{(i+1)}$ for the iterative solution as shown below

$$x^{(i+1)} = x^{(i)} - J^{-1} f\left(x^{(i)}\right) \tag{2.18}$$

where *i* is the iteration time; and $\boldsymbol{J}$ is Jacobian matrix

$$J = \left.\frac{\partial f}{\partial x}\right|_{x=x^{(i)}} \tag{2.19}$$

Equation (2.18) is repeated until the mismatch $f\left(x^{(i)}\right)$ is less than a specified tolerance, or the algorithm diverges.

For a set of nonlinear equations (2.20)

$$\boldsymbol{F}(\boldsymbol{x}) = \begin{cases} \boldsymbol{F}_1(\boldsymbol{x}_1, \boldsymbol{x}_2, \cdots, \boldsymbol{x}_n) = 0 \\ \boldsymbol{F}_2(\boldsymbol{x}_1, \boldsymbol{x}_2, \cdots, \boldsymbol{x}_n) = 0 \\ \vdots \\ \boldsymbol{F}_n(\boldsymbol{x}_1, \boldsymbol{x}_2, \cdots, \boldsymbol{x}_n) = 0 \end{cases} \tag{2.20}$$

where *n* is the number of equations.

The Newton-Raphson method is generalised to multiple dimensions, and the iterative form is

$$\begin{bmatrix} \boldsymbol{x}_1^{(i+1)} \\ \boldsymbol{x}_2^{(i+1)} \\ \vdots \\ \boldsymbol{x}_n^{(i+1)} \end{bmatrix} = \begin{bmatrix} \boldsymbol{x}_1^{(i)} \\ \boldsymbol{x}_2^{(i)} \\ \vdots \\ \boldsymbol{x}_n^{(i)} \end{bmatrix} - \left[\boldsymbol{J}^{(i)}\right]^{-1} \begin{bmatrix} \boldsymbol{F}_1\left(\boldsymbol{x}^{(i)}\right) \\ \boldsymbol{F}_2\left(\boldsymbol{x}^{(i)}\right) \\ \vdots \\ \boldsymbol{F}_n\left(\boldsymbol{x}^{(i)}\right) \end{bmatrix} \tag{2.21}$$

Hence, the Jacobian matrix $\boldsymbol{J}$ is given by

$$\boldsymbol{J} = \begin{bmatrix} \frac{\partial \boldsymbol{F}_1}{\partial \boldsymbol{x}_1} & \frac{\partial \boldsymbol{F}_1}{\partial \boldsymbol{x}_2} & \cdots & \frac{\partial \boldsymbol{F}_1}{\partial \boldsymbol{x}_n} \\ \frac{\partial \boldsymbol{F}_2}{\partial \boldsymbol{x}_1} & \frac{\partial \boldsymbol{F}_2}{\partial \boldsymbol{x}_2} & \cdots & \frac{\partial \boldsymbol{F}_2}{\partial \boldsymbol{x}_n} \\ \vdots & \vdots & \ddots & \vdots \\ \frac{\partial \boldsymbol{F}_n}{\partial \boldsymbol{x}_1} & \frac{\partial \boldsymbol{F}_n}{\partial \boldsymbol{x}_2} & \cdots & \frac{\partial \boldsymbol{F}_n}{\partial \boldsymbol{x}_n} \end{bmatrix} \tag{2.22}$$

2.2.2 Radial District Heating Network

For a radial network as shown in Figure 2.2, given the nodal flows $\dot{\boldsymbol{m}}_q$, a set of linear continuity equations (2.4) for the hydraulic model is solved to calculate the pipe mass flow rates $\dot{\boldsymbol{m}}$. The continuity of flow is applied to all nodes, but one is redundant because of it being linearly dependent on others and is chosen arbitrarily for exclusion. The number of the independent flow continuity equations is exactly the same as the number of unknown pipe flows, and the flows are computed without considering the pressure at all. Thus, applying equation (2.4) to node 1 and node 2 in Figure 2.2 to obtain

$$\begin{aligned} \dot{m}_1 - \dot{m}_2 &= 2 \\ \dot{m}_2 &= 3 \end{aligned} \tag{2.23}$$

The linear continuity equations (2.23) for a radial network can be easily solved using the command '/','\', or 'linsolve' in MATLAB. After $\dot{\boldsymbol{m}}$ is obtained, the head loss along each pipe is calculated using equation (2.9) and then the head at each node is calculated accordingly.

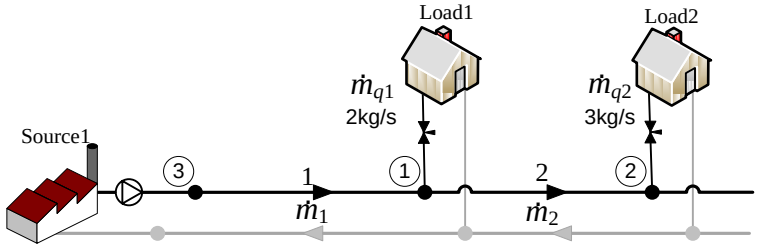

Figure 2.2: A radial district heating network

2.2.3 Meshed District Heating Network

For a meshed network as shown in Figure 2.1, the number of unknown pipe flows is larger than the number of the independent flow continuity equations. Therefore, in addition to the linear continuity equation (2.4), the nonlinear loop pressure equation (2.10) for each loop is considered.

Given the nodal flows $\dot{\boldsymbol{m}}_q$, the combined equations (2.4) and (2.10) can be written in the forms of unknown pipe mass flow rates $\dot{m}$, unknown pressure head h, or unknown corrective mass flow rates $\Delta\dot{m}$. The three systems of equations for the solution of the hydraulic model of meshed

district heating networks shown in Table 2.2 are discussed in the literature [11, 69].

Table 2.2: Three systems of equations in hydraulic model

Type	$\dot{m}$-equations	h-equations	$\Delta\dot{m}$-equations
Unknown variables	Mass flow rates	Pressure head levels	Corrective mass flow rates
Method	Newton-Raphson	Newton-Raphson	Newton-Raphson or Hardy-Cross

The three systems of equations solved by the Newton-Raphson or Hardy-Cross method are explained by a simple example and a more complicated example in the Appendix A. It is reported that the formulations of $\dot{m}$-equations and $\Delta\dot{m}$-equations can be effectively used to overcome at least some of the convergence problems associated with the nodal formulation of h-equations [78]. The $\dot{m}$-equations with unknown mass flow rates in each pipe solved by the Newton-Raphson method is discussed in this section. Using equation (2.21), the iterative form of the Newton-Raphson method for this hydraulic calculation is

$$\begin{bmatrix} \dot{\boldsymbol{m}}_1^{(i+1)} \\ \dot{\boldsymbol{m}}_2^{(i+1)} \\ \vdots \\ \dot{\boldsymbol{m}}_{n_{pipe}}^{(i+1)} \end{bmatrix} = \begin{bmatrix} \dot{\boldsymbol{m}}_1^{(i)} \\ \dot{\boldsymbol{m}}_2^{(i)} \\ \vdots \\ \dot{\boldsymbol{m}}_{n_{pipe}}^{(i)} \end{bmatrix} - \left[\boldsymbol{J}^{(i)}\right]^{-1} \begin{bmatrix} \Delta\boldsymbol{F}_1(\dot{\boldsymbol{m}}) \\ \Delta\boldsymbol{F}_2(\dot{\boldsymbol{m}}) \\ \vdots \\ \Delta\boldsymbol{F}_{n_{pipe}}(\dot{\boldsymbol{m}}) \end{bmatrix} \tag{2.24}$$

where $\Delta\boldsymbol{F}$ is the vector of mismatches; $\boldsymbol{J}$ is Jacobian matrix; i is the iteration time; and n_{pipe} is the number of pipes.

Following equation (2.20), the vector of mismatches $\Delta\boldsymbol{F}$ consisting of the flow continuity equation (2.4) and the loop pressure equation (2.10) is given by

$$\begin{bmatrix} \Delta\boldsymbol{F}_1(\dot{\boldsymbol{m}}) \\ \Delta\boldsymbol{F}_2(\dot{\boldsymbol{m}}) \\ \vdots \\ \Delta\boldsymbol{F}_{n_{pipe}}(\dot{\boldsymbol{m}}) \end{bmatrix} = \begin{bmatrix} \boldsymbol{A}\,\dot{\boldsymbol{m}} - \dot{\boldsymbol{m}}_q \\ \boldsymbol{B}\boldsymbol{K}\,\dot{\boldsymbol{m}}|\dot{\boldsymbol{m}}| \end{bmatrix} \tag{2.25}$$

where the upper part of $\Delta \boldsymbol{F}$ is $(n_{node} - 1) \times 1$ and the lower part of $\Delta \boldsymbol{F}$ is $n_{loop} \times 1$. n_{pipe} is the number of pipes, n_{node} is the number of nodes and n_{loop} is the number of loops.

Hence, following equation (2.22), $\boldsymbol{J}$ is given by

$$\boldsymbol{J} = \begin{bmatrix} \frac{\partial \boldsymbol{F}_1}{\partial \dot{\boldsymbol{m}}_1} & \frac{\partial \boldsymbol{F}_1}{\partial \dot{m}_2} & \cdots & \frac{\partial \boldsymbol{F}_1}{\partial \dot{\boldsymbol{m}}_{n_{pipe}}} \\ \frac{\partial \boldsymbol{F}_2}{\partial \dot{\boldsymbol{m}}_1} & \frac{\partial \boldsymbol{F}_2}{\partial \dot{\boldsymbol{m}}_2} & \cdots & \frac{\partial \boldsymbol{F}_2}{\partial \dot{\boldsymbol{m}}_{n_{pipe}}} \\ \vdots & \vdots & \ddots & \vdots \\ \frac{\partial \boldsymbol{F}_{n_{pipe}}}{\partial \dot{\boldsymbol{m}}_1} & \frac{\partial \boldsymbol{F}_{n_{pipe}}}{\partial \dot{\boldsymbol{m}}_2} & \cdots & \frac{\partial \boldsymbol{F}_{n_{pipe}}}{\partial \dot{\boldsymbol{m}}_{n_{pipe}}} \end{bmatrix} = \begin{bmatrix} \boldsymbol{A} \\ \boldsymbol{2BK}\,|\dot{\boldsymbol{m}}| \end{bmatrix} \tag{2.26}$$

where the upper part of $\boldsymbol{J}$ is $(n_{node} - 1) \times n_{pipe}$ and the lower part of $\boldsymbol{J}$ is $n_{loop} \times n_{pipe}$.

For the network shown in Figure 2.1, the parameters of each pipe are: L= 400m, D = 0.15m, $\boldsymbol{\varepsilon}$ = 1.25×10^{-3}m, μ = 0.294×10^{-6}m^2/s.

The continuity of flow at node 1 and node 2 in Figure 2.1 is expressed using equation (2.4)

$$\begin{aligned} \dot{m}_1 - \dot{m}_2 &= 2 \\ \dot{m}_2 + \dot{m}_3 &= 3 \end{aligned} \tag{2.27}$$

The sum of pressure head around the loop in Figure 2.1 is expressed using equation (2.10)

$$\begin{aligned} &\sum_{j=1}^{3} B_{1,j} K_j \dot{m}_j |\dot{m}_j| \\ &= K_1 \dot{m}_1 |\dot{m}_1| + K_2 \dot{m}_2 |\dot{m}_2| - K_3 \dot{m}_3 |\dot{m}_3| = 0 \end{aligned} \tag{2.28}$$

Equation (2.27) and (2.28) are then combined to calculate the pipe mass flow rates using the Newton-Raphson method.

According to equations (2.25)(2.26), $\Delta \boldsymbol{F}$ and $\boldsymbol{J}$ are

$$\Delta \boldsymbol{F} = \begin{bmatrix} \dot{m}_1 - \dot{m}_2 - 2 \\ \dot{m}_2 + \dot{m}_3 - 3 \\ K_1 \dot{m}_1 |\dot{m}_1| + K_2 \dot{m}_2 |\dot{m}_2| - K_3 \dot{m}_3 |\dot{m}_3| \end{bmatrix} \tag{2.29}$$

$$\therefore \boldsymbol{J} = \begin{bmatrix} 1 & -1 & 0 \\ 0 & 1 & 1 \\ 2K_1|\dot{m}_1| & 2K_2|\dot{m}_2| & -2K_3|\dot{m}_3| \end{bmatrix} \tag{2.30}$$

Assuming initial condition as, $\dot{\boldsymbol{m}}^{(0)} = \begin{bmatrix} \dot{m}_1^{(0)} \\ \dot{m}_2^{(0)} \\ \dot{m}_3^{(0)} \end{bmatrix} = \begin{bmatrix} 1 \\ 1 \\ 1 \end{bmatrix}$.

The pipe resistance coefficient *K* is updated at each iteration. For the first iteration,

$$\boldsymbol{K}^{(0)} = \begin{bmatrix} 0.0179 \\ 0.0179 \\ 0.0269 \end{bmatrix},$$

$$\Delta\boldsymbol{F}^{(0)} = \begin{bmatrix} -2 \\ -1 \\ 0.009 \end{bmatrix},$$

$$\boldsymbol{J}^{(0)} = \begin{bmatrix} 1 & -1 & 0 \\ 0 & 1 & 1 \\ 0.0358 & 0.0358 & -0.0537 \end{bmatrix}.$$

Following equation (2.24),

$$\dot{\boldsymbol{m}}^{(1)} = \dot{\boldsymbol{m}}^{(0)} - \left(\boldsymbol{J}^{(0)}\right)^{-1}\Delta\boldsymbol{F}^{(0)} = \begin{bmatrix} 2.786 \\ 0.786 \\ 2.214 \end{bmatrix}.$$

The procedure is repeated until the maximum element in $|\Delta\boldsymbol{F}|$ becomes less than the tolerance $\boldsymbol{\varepsilon}$ = 10^{-3}. After 3 iterations, the converged results are: $\dot{\boldsymbol{m}} = \begin{bmatrix} 2.712 \\ 0.712 \\ 2.289 \end{bmatrix}$.

To validate the results, the same network as Figure 2.1 was built in commercial software SINCAL [67]. The results are the same with SINCAL at 10^{-3} precision. A screenshot of the result $\dot{m}_3 = 2.289$ in SINCAL is shown in Figure 2.3.

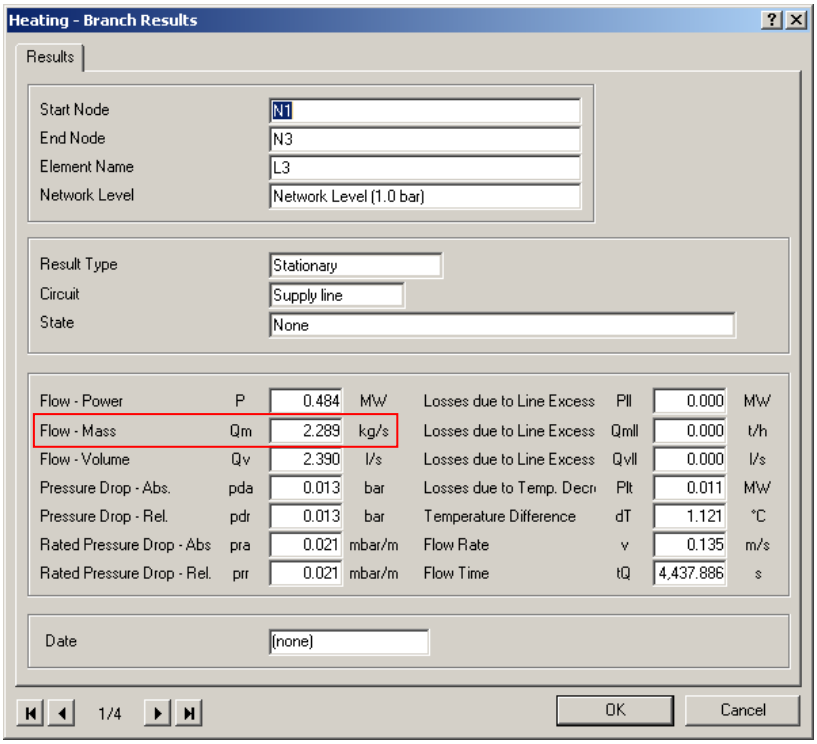

Figure 2.3: Result of the mass flow rate within pipe 3 from SINCAL

2.3 Thermal Model

The thermal model is used to determine the temperatures at each node. There are three different temperatures associated with each node (Figure 2.4): the supply temperature (T_s); the outlet temperature (T_o) and the return temperature (T_r) [79]. The outlet temperature is defined as the temperature of the flow at the outlet of each node before mixing in the return network. Usually, the supply temperatures at each source and the return temperatures at each load before mixing are specified in the thermal model [11, 67, 71, 72]. The load return temperature depends on the supply temperature, the outdoor temperature and the heat load [80-83]. For simplicity, the return temperature is assumed to be known at each load.

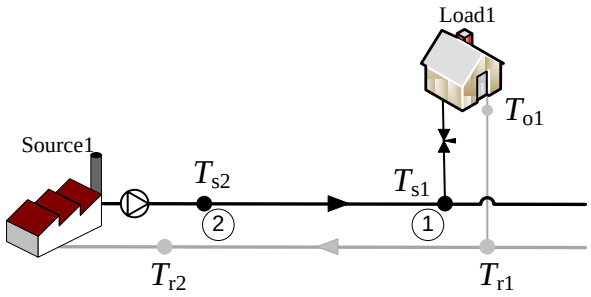

Figure 2.4: Temperatures associated with each node

The heat power is calculated using equation (2.31) [11, 83]

$$\boldsymbol{\Phi} = C_p \dot{\boldsymbol{m}}_{\boldsymbol{q}} (\boldsymbol{T}_s - \boldsymbol{T}_o) \tag{2.31}$$

where $\boldsymbol{\Phi}$ is the vector of heat power (W_{th}) consumed or supplied at each node; C_p is the specific heat of water (J/(kg·K)); and $\dot{\boldsymbol{m}}_{\boldsymbol{q}}$ is the vector of the mass flow rate (kg/s) through each node injected from a supply or discharged to a load.

The temperature at the outlet of a pipe is calculated using the temperature drop equation (2.32) and the derivation of this equation is in the Appendix B [11, 83, 84].

$$T_{end} = (T_{start} - T_a)e^{-\frac{\lambda L}{C_p \dot{m}}} + T_a \tag{2.32}$$

where T_{start} and T_{end} are the temperatures at the start node and the end node of a pipe (°C); T_a is the ambient temperature (°C); λ is the overall heat transfer coefficient of each pipe per unit length (W/(m·K)); L is the length of each pipe (m); and $\dot{m}$ is the mass flow rate (kg/s) within each pipe.

Equation (2.32) shows that if the mass flow rate within a pipe is larger, the temperature at the end node of the pipe is larger and the temperature drop along the pipe is smaller.

For brevity, denoting $T'_{start} = T_{start} - T_a$, $T'_{end} = T_{end} - T_a$, $\Psi = e^{-\frac{\lambda L}{C_p \dot{m}}}$, thus Equation (2.32) is written as

$$T'_{end} = T'_{start}\Psi \tag{2.33}$$

The temperature of water leaving a node with more than one incoming pipe is calculated as the mixture temperature of the incoming flows using (2.34). The temperature at the start of each pipe leaving the node is equal to the mixture temperature at the node [11, 73, 83].

$$\left(\sum \dot{m}_{out}\right) T_{out} = \sum (\dot{m}_{in} T_{in}) \tag{2.34}$$

where T_{out} is the mixture temperature of a node (°C); $\dot{m}_{out}$ is the mass flow rate within a pipe leaving the node (kg/s); T_{in} is the temperature of flow at the end of an incoming pipe (°C); and $\dot{m}_{in}$ is the mass flow rate within a pipe coming into the node (kg/s).

2.4 Solution of the Thermal Model

For a district heating network, the thermal model determines the supply temperatures at each load and the return temperatures at each load and source. The assumptions are specified supply temperatures at each source and return temperatures at each load before mixing and mass flow rates within each pipe [11, 67, 71, 72]. The problem becomes

complex when the thermal model equations in Section 2.3 are applied to a district heating network with arbitrary topology. Therefore, a matrix formulation of a thermal model was used and the procedures were illustrated using flowcharts. Furthermore, a general program for the thermal model in a district heating network was developed in MATLAB.

A simple meshed district heating network shown in Figure 2.5 is used to illustrate the thermal model calculation. The objective is to determine the load supply temperatures T_{s1}, T_{s2} and the source return temperature T_{r3}. The specified variables are [67]: $\dot{m}_1$ = 3kg/s, $\dot{m}_2$ = 1kg/s, $\dot{m}_3$ = 2kg/s. T_{s3} = 100°C, T_{o1} = T_{o2} = 50°C. The ambient temperature T_a = 10°C. The parameters of each pipe are [67]: L = 400m, λ = 0.2W/(m·K). C_p = 4182J/(kg·K)). Denoting $T_s' = T_s - T_a$, $T_r' = T_r - T_a$.

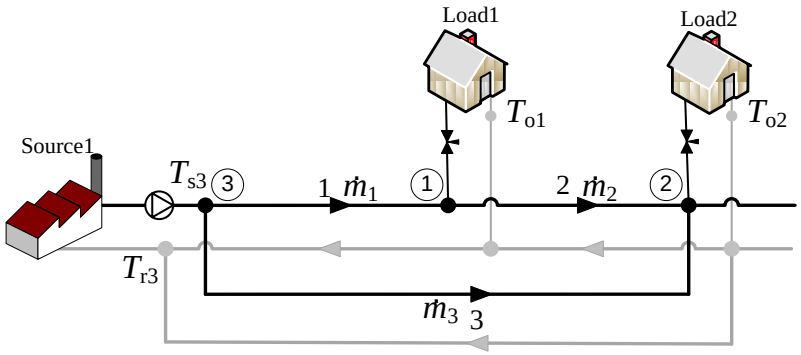

Figure 2.5: A simple district heating network with a loop

2.4.1 Supply Temperature Calculation

The objective is to determine the load supply temperatures based on the specified source supply temperatures. For the supply network shown in Figure 2.5, the incidence matrix is

$$\boldsymbol{A} = \begin{array}{c} \\ \text{Node No.} \end{array} \begin{array}{c} \begin{array}{ccc} \text{Pipe No.} & & \\ 1 & 2 & 3 \end{array} \\ \begin{bmatrix} 1 & -1 & 0 \\ 0 & 1 & 1 \\ -1 & 0 & -1 \end{bmatrix} \end{array} \begin{array}{c} \\ 1 \\ 2 \\ 3 \end{array}$$

Each element of the matrix ***A*** describes

+1, if the flow in a pipe comes into a node;

-1, if the flow in a pipe leaves a node;

0, if no connection from a pipe to a node.

The steps of the thermal calculation are performed as follows

1) Determine the mixing nodes based on the matrix ***A***. The row 2 in the matrix ***A*** has more than one element '1', which means the incoming flows mix at node 2.

2) For node 1, the supply temperature T'_{s1} is calculated using the temperature drop equation (2.33)

$$T'_{s1} = T'_{s3}\Psi_1 \tag{2.31}$$

3) For node 2, the supply temperature T'_{s2} is calculated using the temperature drop equation (2.33) and the temperature mixing equation (2.34)

$$(\dot{m}_2 + \dot{m}_3)T'_{s2} = \dot{m}_2(T'_{s1}\Psi_2) + \dot{m}_3(T'_{s3}\Psi_3) \tag{2.32}$$

4) The temperature equations (2.31) and (2.32) are combined to form a linear system of equations

$$\boldsymbol{C}_s\boldsymbol{T}'_s = \boldsymbol{b}_s \tag{2.33}$$

where $\boldsymbol{C}_s$ is the matrix of coefficients, $\boldsymbol{T}'_s$ is the column vector of variables (the load supply temperatures) and $\boldsymbol{b}_s$ is the column vector of solutions. The general procedure to form the matrix $\boldsymbol{C}_s$ and the vector $\boldsymbol{b}_s$ is illustrated using a flowchart in Figure 2.6.

$$\boldsymbol{C}_s = \begin{bmatrix} 1 & 0 \\ -\dot{m}_2\Psi_2 & \dot{m}_{q2} \end{bmatrix} \quad \boldsymbol{T}'_s = \begin{bmatrix} T'_{s1} \\ T'_{s2} \end{bmatrix} \quad \boldsymbol{b}_s = \begin{bmatrix} T'_{s3}\Psi_1 \\ \dot{m}_3 T'_{s3}\Psi_3 \end{bmatrix} \tag{2.34}$$

By substituting the specified parameters into equation (2.34)

$$\begin{bmatrix} 1 & 0 \\ -0.981 & 3 \end{bmatrix}\begin{bmatrix} T'_{s1} \\ T'_{s2} \end{bmatrix} = \begin{bmatrix} 89.428 \\ 178.287 \end{bmatrix} \tag{2.35}$$

The linear system of equations (2.35) can be solved using the command 'linsolve' in MATLAB. The results are: $T_{s1} = 99.428°\text{C}$, $T_{s2} = 98.673°\text{C}$. The supply temperature from node 1 to node 1 and then to node 2 reduces because of the heat losses.

The flowchart of supply temperature calculation is depicted in Figure 2.6, where *i*, *j* are the index of nodes, *k* is the index of pipes and water flows from node *j* to node *i* through pipe *k*.

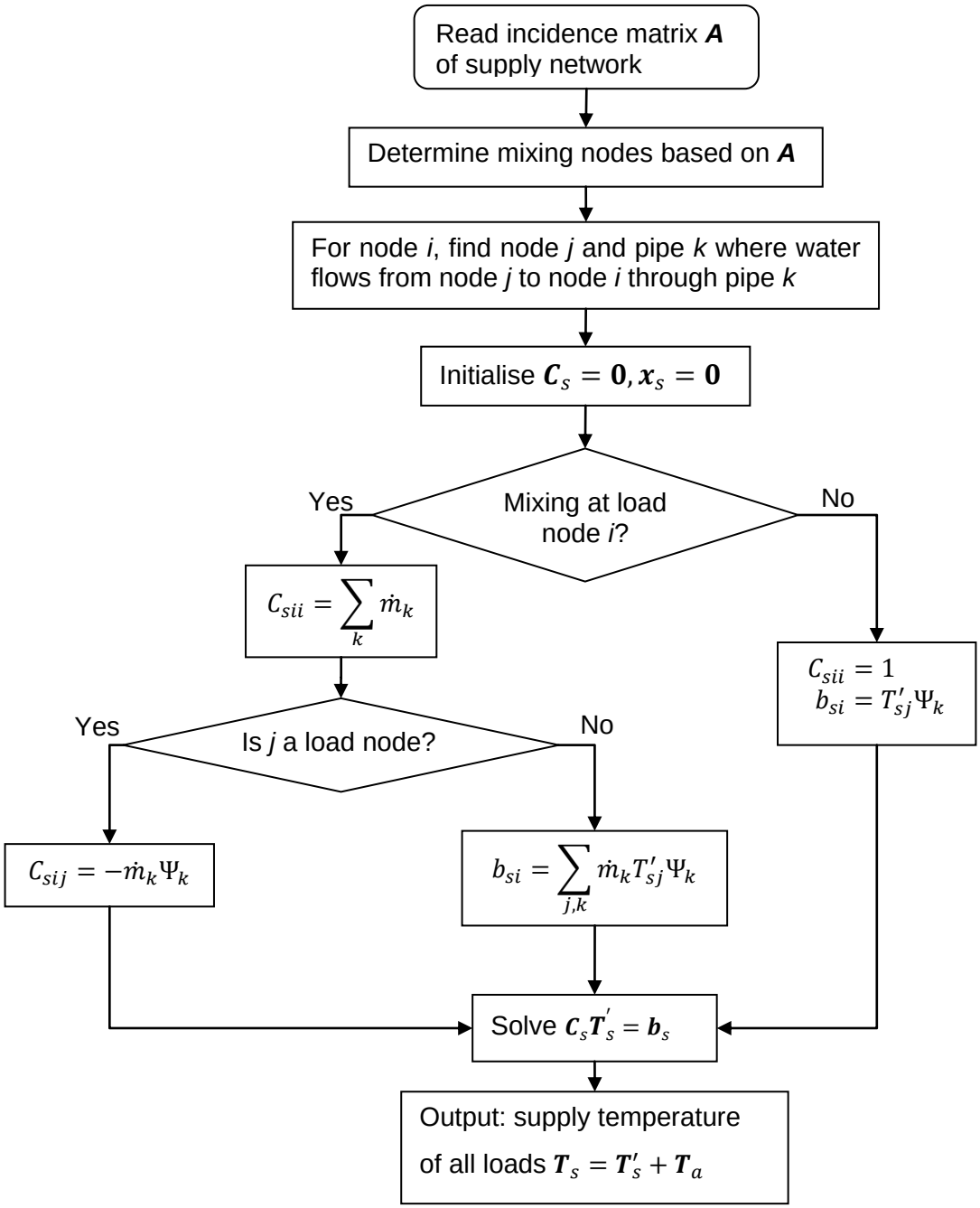

Figure 2.6: Flowchart of the supply temperature calculation

2.4.2 Return Temperature Calculation

The objective is to determine the load and source return temperatures based on the specified load outlet temperatures. For the return network shown in Figure 2.5, the incidence matrix is the inverse of the incidence matrix of the supply network.

$$(-\boldsymbol{A}) = \begin{array}{c} \\ \text{Node No.} \end{array} \begin{array}{c} \text{Pipe No.} \\ \begin{array}{ccc} 1 & 2 & 3 \end{array} \end{array} \begin{array}{c} \\ \begin{array}{c} 1 \\ 2 \\ 3 \end{array} \end{array} \begin{bmatrix} -1 & 1 & 0 \\ 0 & -1 & -1 \\ 1 & 0 & 1 \end{bmatrix}$$

The steps of the thermal calculation are similar to that of the supply network and are performed as follows

1) Determine the mixing nodes based on the matrix (-***A***). The row 1 in the matrix (-***A***) has one element ‘1’ plus one incoming flow from load 1 to the node 1 and row 3 has more than one element ‘1’, which means the incoming flows mix at the node 1 and 3.

2) For node 1, the return temperature T'_{r1} is calculated using the temperature drop equation (2.33) and the temperature mixing equation (2.34)

$$\dot{m}_1 T'_{r1} = \dot{m}_2 T'_{r2} \Psi_2 + \dot{m}_{q1} T'_{o1} \tag{2.36}$$

3) For node 2, the return temperature T'_{r2} is equal to the outlet temperature and calculated as

$$T'_{r2} = T'_{o2} \tag{2.37}$$

4) Similarly, the temperature equations (2.36) and (2.37) are combined to form a linear system of equations

$$\boldsymbol{C}_r \boldsymbol{T}'_r = \boldsymbol{b}_r \tag{2.38}$$

where $\boldsymbol{C}_r$ is the matrix of coefficients, $\boldsymbol{T}'_r$ is the column vector of variables (the load return temperatures) and $\boldsymbol{b}_r$ is the column vector of solutions. The general procedure to form matrix $\boldsymbol{C}_r$ and vector $\boldsymbol{b}_r$ is illustrated using a flowchart in Figure 2.7.

$$\boldsymbol{C}_r = \begin{bmatrix} \dot{m}_1 & -\dot{m}_2\Psi_2 \\ 0 & 1 \end{bmatrix} \quad \boldsymbol{T}'_r = \begin{bmatrix} T'_{r1} \\ T'_{r2} \end{bmatrix} \quad \boldsymbol{b}_r = \begin{bmatrix} \dot{m}_{q1}T'_{o1} \\ T'_{o2} \end{bmatrix} \tag{2.39}$$

By substituting the specified parameters into equation (2.39)

$$\begin{bmatrix} 3 & -0.981 \\ 0 & 1 \end{bmatrix} \begin{bmatrix} T'_{r1} \\ T'_{r2} \end{bmatrix} = \begin{bmatrix} 80 \\ 40 \end{bmatrix} \tag{2.40}$$

The linear system of equations (2.40) is solved using the command 'linsolve' in MATLAB. The results are: $T_{r1} = 49.747°\mathrm{C}$, $T_{r2} = 50°\mathrm{C}$

5) For source node 3, the return temperature T'_{r3} is calculated using the temperature drop equation (2.33) and the temperature mixing equation (2.34)

$$\dot{m}_{q3}T'_{r3} = \dot{m}_1(T'_{r1}\Psi_1) + \dot{m}_3(T'_{r2}\Psi_3) \tag{2.41}$$

The result is: $T_{r3} = 49.695°\mathrm{C}$.

The return temperature from node 2 to node 1 reduces because of the heat losses.

The results of the thermal model are validated together with the hydraulic model in the next section 2.5.

The flowchart of the return temperature calculation is shown in Figure 2.7.

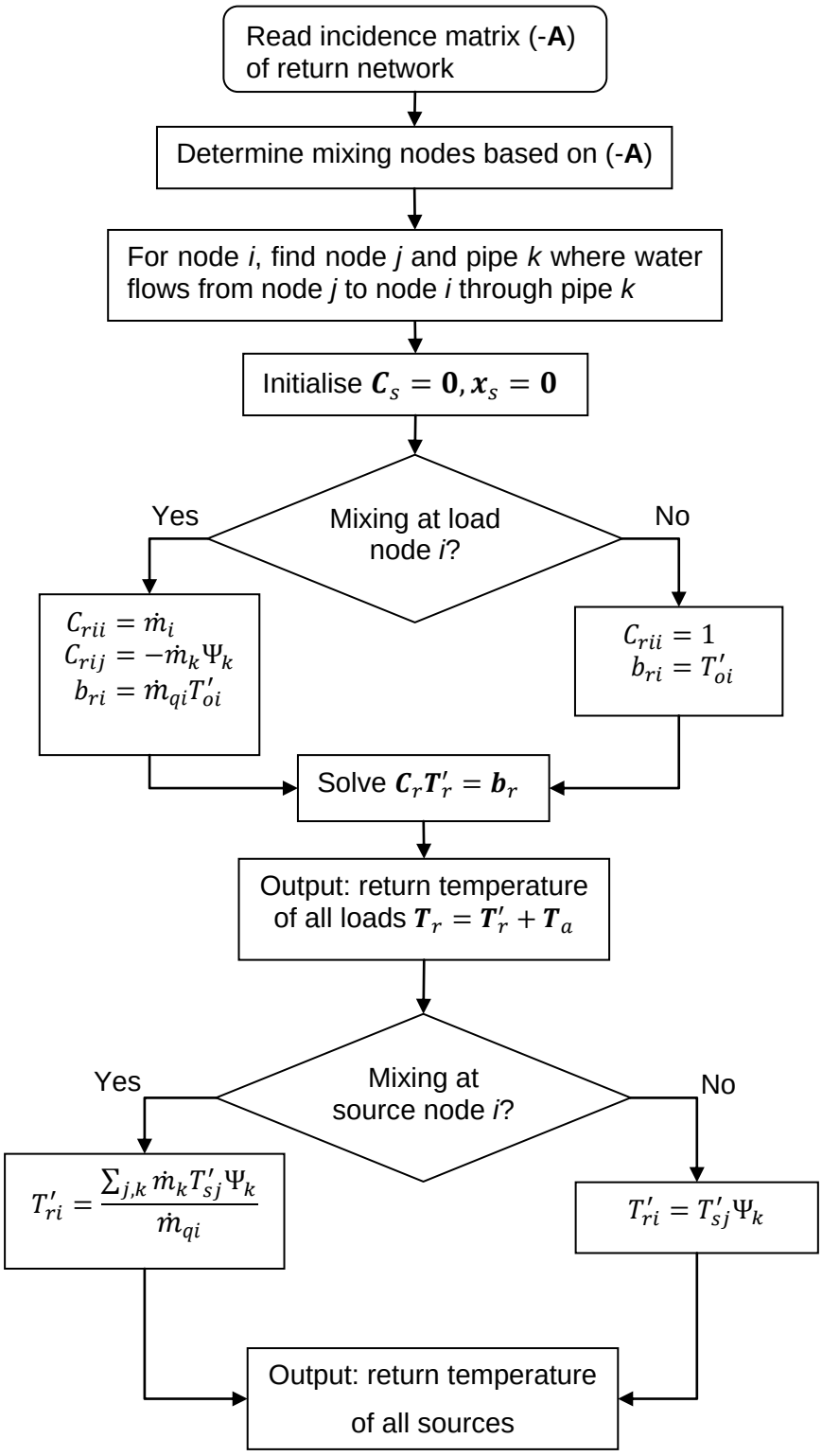

Figure 2.7: Flowchart of the return temperature calculation

2.5 Hydraulic-Thermal Model

2.5.1 Introduction

For a district heating network, the objective of the hydraulic-thermal model is to determine the mass flow rates $\dot{\boldsymbol{m}}$ within each pipe and the load supply temperatures and the source return temperatures. It is assumed that the source supply temperatures and the load return temperatures are specified; the mass flow rates $\dot{\boldsymbol{m}}_q$ or the heat power $\boldsymbol{\Phi}$ are specified at all the nodes except the slack node [11, 67, 71, 72]. The slack node is defined to be rescheduled to supply the heat power difference between the total system loads plus losses and the sum of specified heat power at the source nodes.

If the nodal injected mass flow rates $\dot{\boldsymbol{m}}_q$ is specified, the hydraulic-thermal model calculations are performed independently [68, 73]. Firstly, the pipe mass flow rates $\dot{\boldsymbol{m}}$ is calculated by the hydraulic model. Then, the results of the hydraulic model $\dot{\boldsymbol{m}}$ are substituted into the thermal model. Finally, the load supply temperatures and the source return temperatures are calculated by the thermal model.

Alternatively, if the heat power $\boldsymbol{\Phi}$ consumed or supplied at each node is specified, two methods are adopted to perform the calculation of the hydraulic-thermal model. Conventionally, the calculation is through an iterative procedure – referred to as the decomposed hydraulic-thermal calculation – between the individual hydraulic and thermal models [67]. In this thesis, an integrated hydraulic-thermal calculation was proposed, in which the hydraulic and thermal models were combined in a single system of equations.

Until now, the Newton-Raphson method has been used in the hydraulic calculation. The integrated calculation combines the individual hydraulic and thermal analyses using the Newton-Raphson approach. It takes into account the coupling between the individual hydraulic and thermal analyses. For instance, the thermal calculation cannot be performed without knowing the pipe mass flows. The hydraulic calculation cannot

be performed without knowing temperatures under the assumption that the nodal heat power are specified.

The proposed methods can handle the initial conditions with arbitrary flow directions. During each iteration of the hydraulic-thermal model, the network incidence matrix ***A*** and the loop incidence matrix ***B*** are updated according to the signs of the pipe mass flow rates. Based on matrix ***A***, the formulation of the temperature mixing equations in the thermal model is updated at each iteration.

2.5.2 Decomposed Hydraulic-Thermal Calculation

The structure of the decomposed hydraulic-thermal calculation with specified nodal heat power is shown in Figure 2.8. The iterative procedure between the individual hydraulic and thermal models is as follows

- The calculated nodal mass flow rates $\dot{\boldsymbol{m}}_{\boldsymbol{q}}$ are substituted into the hydraulic model to update the pipe mass flow rates $\dot{\boldsymbol{m}}$. For the first iteration, $\dot{\boldsymbol{m}}_{\boldsymbol{q}}$ is initialised.
- The load supply temperatures $\boldsymbol{T}_{s,load}$ and the source return temperatures $\boldsymbol{T}_{r,source}$ are updated using the thermal model.
- The calculated temperatures are fed back into the heat power equation (2.31) to update the nodal injected mass flow rates $\dot{\boldsymbol{m}}_{\boldsymbol{q}}$.

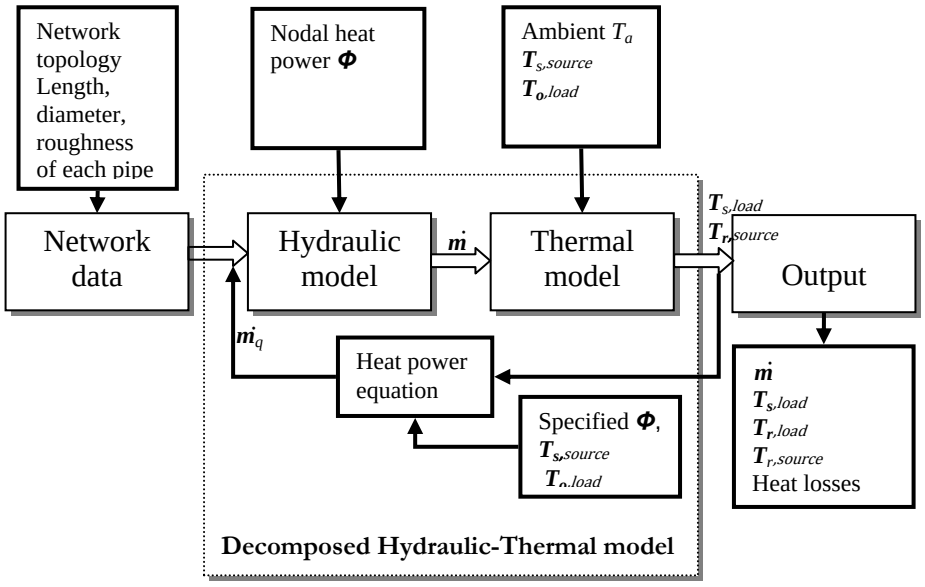

Figure 2.8: Structure of the decomposed hydraulic-thermal calculation with specified nodal heat power

The flowchart of the decomposed hydraulic-thermal calculation with specified nodal heat power is shown in Figure 2.9. Denoting $\Delta \boldsymbol{T}_{s,load} = \boldsymbol{T}_{s,load}^{(i+1)} - \boldsymbol{T}_{s,load}^{(i)}$, $\Delta \boldsymbol{T}_r = \boldsymbol{T}_r^{(i+1)} - \boldsymbol{T}_r^{(i)}$, where i is the iteration time. The initialised load supply temperatures $\boldsymbol{T}_{s,load}$ and the initialised source return temperatures $\boldsymbol{T}_{r,source}$ are substituted into the heat power equation (2.31) $\boldsymbol{\Phi} = C_p \dot{\boldsymbol{m}}_{\boldsymbol{q}} (\boldsymbol{T}_s - \boldsymbol{T}_r)$ to calculate the nodal flows $\dot{\boldsymbol{m}}_{\boldsymbol{q}}$.

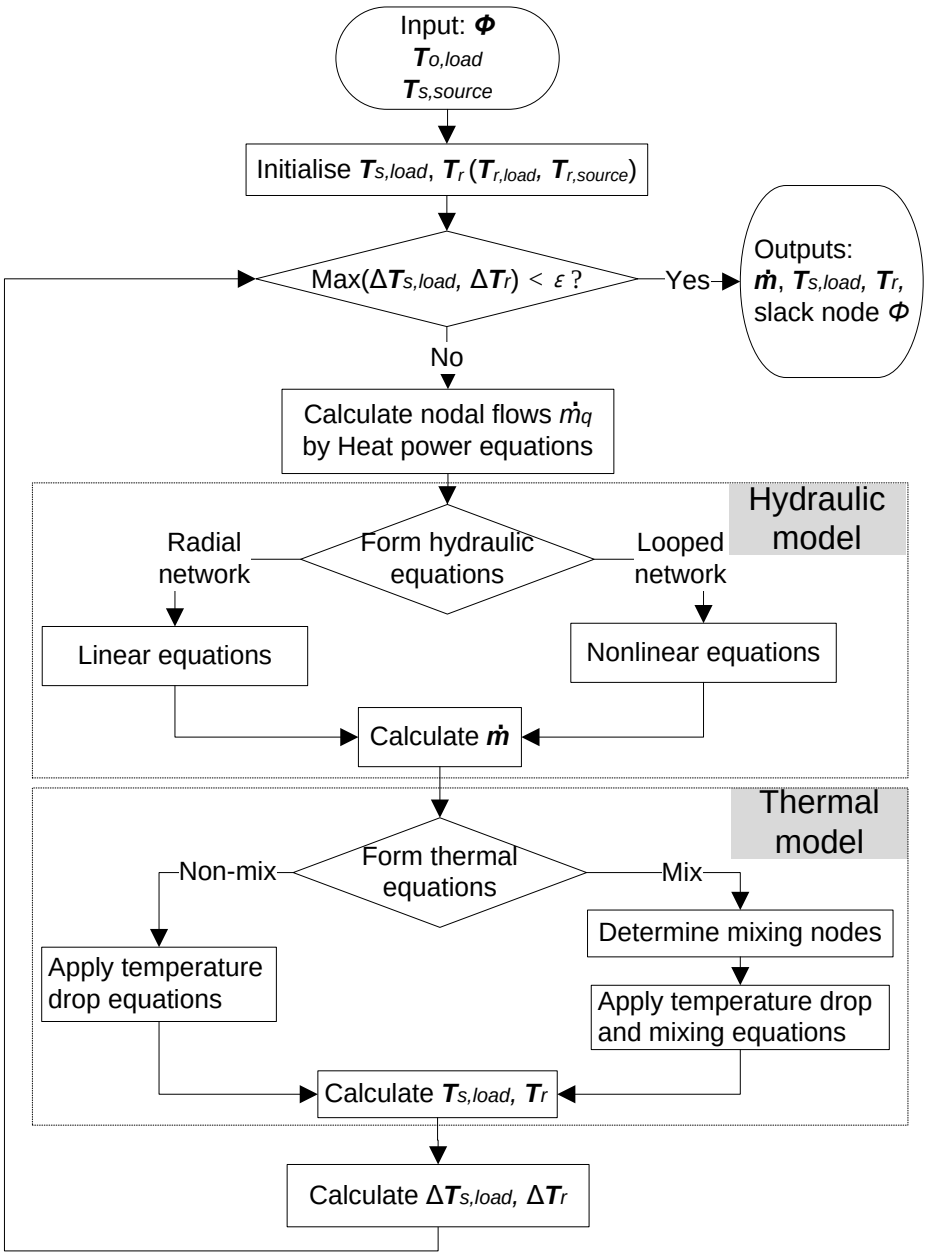

Figure 2.9: Flowchart of the decomposed hydraulic-thermal calculation with specified nodal power

A simple district heating network with a loop shown in Figure 2.10 is used to illustrate the decomposed hydraulic-thermal calculation. The objective is to determine the pipe mass flow rates $\dot{m}_1, \dot{m}_2, \dot{m}_3$ and the load supply temperatures $T_{s1,load}$, $T_{s2,load}$ and the source return temperature $T_{r1,source}$. The specified variables are [67]: $\Phi_{1,load} = \Phi_{2,load}$ = 0.3MW. $T_{s1,source}$ = 100°C, $T_{o1,load} = T_{o2,load}$ = 50°C. The ambient temperature T_a = 10°C. The parameters of each pipe are [67]: $L_1 = L_2$ = 400m, L_3 = 600m, D = 0.15m, ε = 1.25×10^{-3}m, λ = 0.2W/mK. C_p = 4182J/(kg·K)) = 4.182 × 10^{-3}MJ/(kg·K)).

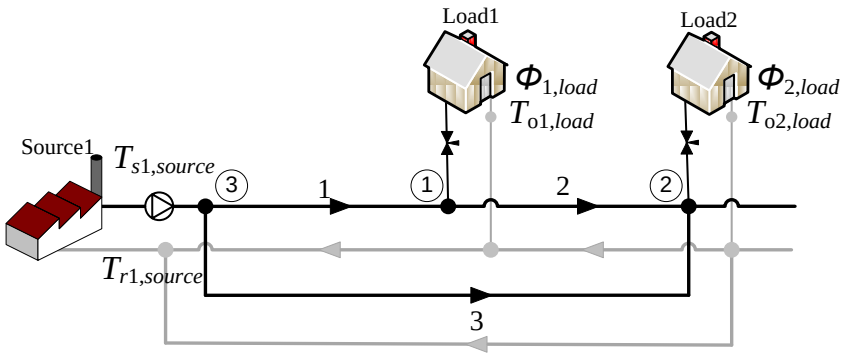

Figure 2.10: A district heating network with a loop

The continuity of flow is applied to all nodes in a network, but one is redundant because of it being linearly dependent on others and is chosen arbitrarily for exclusion. Thus, the last row of the network incidence matrix ***A*** that relates to the slack node is redundant and is chosen for exclusion.

For the supply network shown in Figure 2.10,

$$\boldsymbol{A} = \begin{array}{c} \\ \text{Node No.} \\ 1 \\ 2 \end{array} \begin{array}{c} \text{Pipe No.} \\ \begin{array}{ccc} 1 & 2 & 3 \end{array} \\ \begin{bmatrix} 1 & -1 & 0 \\ 0 & 1 & 1 \end{bmatrix} \end{array} \qquad \boldsymbol{B} = \begin{array}{c} \\ \text{Loop No.} \\ 1 \end{array} \begin{array}{c} \text{Pipe No.} \\ \begin{array}{ccc} 1 & 2 & 3 \end{array} \\ \begin{bmatrix} 1 & 1 & -1 \end{bmatrix} \end{array} \tag{2.35}$$

Each element of the matrix ***A*** describes

+1, if the flow in a pipe comes into a node;

-1, if the flow in a pipe leaves a node;

0, if no connection from a pipe to a node.

Each element of the matrix ***B*** describes

+1, if the flow in a pipe has the same direction as the definition;

-1, if the flow in a pipe has the opposite direction as the definition;

0, if pipe is not part of the loop.

Following equations (2.25) and (2.26), the vector of mismatches $\Delta \boldsymbol{F}$ and the Jacobian matrix ***J*** are

$$\Delta \boldsymbol{F} = \begin{bmatrix} \boldsymbol{A}\,\dot{\boldsymbol{m}} - \dot{\boldsymbol{m}}_{\boldsymbol{q}} \\ \boldsymbol{B}\boldsymbol{K}\dot{\boldsymbol{m}}|\dot{\boldsymbol{m}}| \end{bmatrix} = \begin{bmatrix} \dot{m}_1 - \dot{m}_2 - \dot{m}_{q1} \\ \dot{m}_2 + \dot{m}_3 - \dot{m}_{q2} \\ K_1\dot{m}_1|\dot{m}_1| + K_2\dot{m}_2|\dot{m}_2| - K_3\dot{m}_3|\dot{m}_3| \end{bmatrix} \tag{2.36}$$

$$\therefore \boldsymbol{J} = \begin{bmatrix} \boldsymbol{A} \\ \boldsymbol{2BK}\,|\dot{\boldsymbol{m}}| \end{bmatrix} = \begin{bmatrix} 1 & -1 & 0 \\ 0 & 1 & 1 \\ 2K_1|\dot{m}_1| & 2K_2|\dot{m}_2| & -2K_3|\dot{m}_3| \end{bmatrix} \tag{2.37}$$

The steps used to solve the decomposed calculation of the district heating network in Figure 2.10 are as follows

Step 1) Assume initial condition as, $T_{s1,load}^{(0)} = T_{s2,load}^{(0)} = 100°\text{C}$, $\dot{\boldsymbol{m}}^{(0)} = \begin{bmatrix} \dot{m}_1^{(0)} \\ \dot{m}_2^{(0)} \\ \dot{m}_3^{(0)} \end{bmatrix} = \begin{bmatrix} 1 \\ 1 \\ 1 \end{bmatrix}$.

Step 2) Calculate the nodal flows $\dot{\boldsymbol{m}}_{\boldsymbol{q}}$ using the heat power equation (2.31), $\dot{\boldsymbol{m}}_{\boldsymbol{q}} = \frac{\boldsymbol{\Phi}}{C_p(\boldsymbol{T}_s - \boldsymbol{T}_o)}$. For the first iteration, $\dot{m}_{q1}^{(0)} = \dot{m}_{q2}^{(0)} = 1.435$ kg/s.

Step 3) Update $\dot{\boldsymbol{m}}$ using the hydraulic model.

For the first iteration,

$$\Delta \boldsymbol{F}^{(0)} = \begin{bmatrix} -1.435 \\ 0.565 \\ 0.009 \end{bmatrix}, \quad \boldsymbol{J}^{(0)} = \begin{bmatrix} -1 & -1 & 0 \\ 0 & 1 & 1 \\ 0.0358 & 0.0358 & -0.0537 \end{bmatrix},$$

$$\Delta \dot{\boldsymbol{m}}^{(0)} = -\left(\boldsymbol{J}^{(0)}\right)^{-1} \Delta \boldsymbol{F}^{(0)} = \begin{bmatrix} 0.711 \\ -0.724 \\ 0.158 \end{bmatrix},$$

$$\dot{\boldsymbol{m}}^{(1)} = \dot{\boldsymbol{m}}^{(0)} + \Delta \dot{\boldsymbol{m}}^{(0)} = \begin{bmatrix} 1.711 \\ 0.276 \\ 1.158 \end{bmatrix}.$$

Step 4) Update $T_{s1,load}, T_{s2,load}$ using the thermal model. For the first iteration, $T_{s1,load}^{(1)} = 98.999$, $T_{s2,load}^{(1)} = 96.883$.

Step 5) This procedure is repeated from step 2) until the maximal $|\Delta \boldsymbol{T}_{s,load}|$ and $|\Delta \dot{\boldsymbol{m}}|$ become less than $\boldsymbol{\varepsilon}$.

After 4 iterations with the tolerance $\boldsymbol{\varepsilon}$ = 10^{-3}, the converged results are $\dot{m}_1 = 1.642, \dot{m}_2 = 0.177, \dot{m}_3 = 1.345$. $T_{s1,load}$ = 98.958, $T_{s2,load}$ = 97.140. $T_{r1,load}$ = 49.558, $T_{r2,load}$ = 50, $T_{r1,source}$ = 49.125.

To validate the results, the network in Figure 2.10 is analysed using commercial software SINCAL [67]. The results are the same with SINCAL at 10^{-3} precision. A screenshot of the result $T_{s1,load}$ = 98.958 in SINCAL is shown in Figure 2.11.

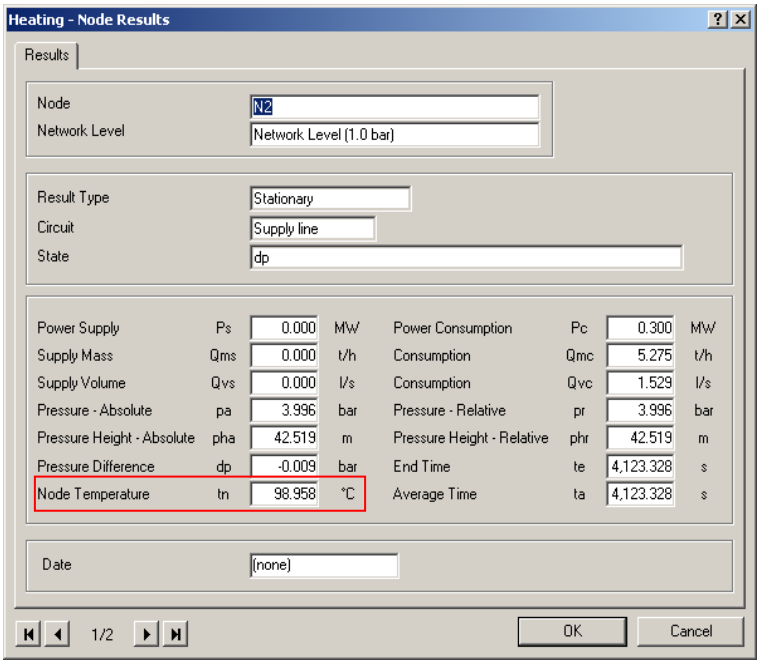

Figure 2.11: Result of the supply temperature at the load 1 from SINCAL

2.5.3 Integrated Hydraulic-Thermal Calculation

The integrated hydraulic-thermal calculation combines the individual hydraulic and thermal analyses in a single system of equations under the assumption of specified nodal heat power. The single system of equations was solved by the Newton-Raphson method with an integrated Jacobian matrix.

The system of equations for the integrated hydraulic-thermal calculation is derived from the individual hydraulic and thermal models, which is illustrated in Figure 2.12. The individual hydraulic and thermal models are linked through the pipe mass flow rates $\dot{\boldsymbol{m}}$. To form the integrated hydraulic-thermal model, a heat power equation describing the relation between the nodal heat power $\boldsymbol{\Phi}$ and the pipe mass flow rates $\dot{\boldsymbol{m}}$ is expressed as equation (2.42). It is obtained by substituting the nodal flows $\dot{\boldsymbol{m}}_{\boldsymbol{q}}$ in the continuity equation (2.4) into the heat power equation (2.31) to eliminate the intermediate variables $\dot{\boldsymbol{m}}_{\boldsymbol{q}}$.

$$\boldsymbol{\Phi} = C_p \boldsymbol{A}\, \dot{\boldsymbol{m}}(\boldsymbol{T}_s - \boldsymbol{T}_o) \tag{2.42}$$

where $\boldsymbol{\Phi}$ is the vector of heat power (MW_{th}) consumed or supplied at each node; C_p is the specific heat of water, C_p = 4.182 × 10^{-3} MJ/(kg·K)); $\boldsymbol{A}$ is the network incidence matrix, and the last row of $\boldsymbol{A}$ that relates to the slack node is redundant and is chosen for exclusion; $\dot{\boldsymbol{m}}$ is the mass flow rates (kg/s) within each pipe; $\boldsymbol{T}_s$ is the supply temperatures (°C); $\boldsymbol{T}_o$ is the outlet temperatures (°C).

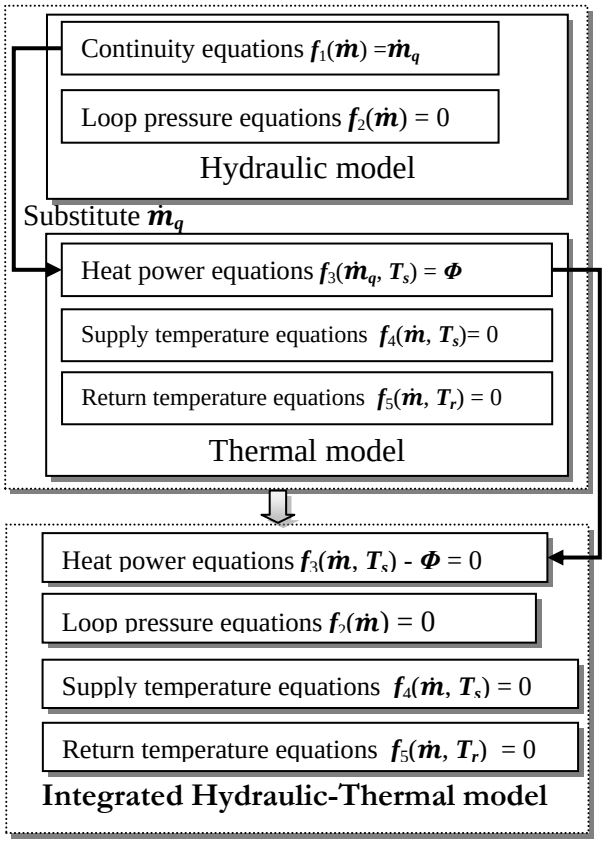

Figure 2.12: Derivation of the system of equations for the integrated hydraulic-thermal calculation

The structure for the integrated hydraulic-thermal calculation is shown in Figure 2.13.

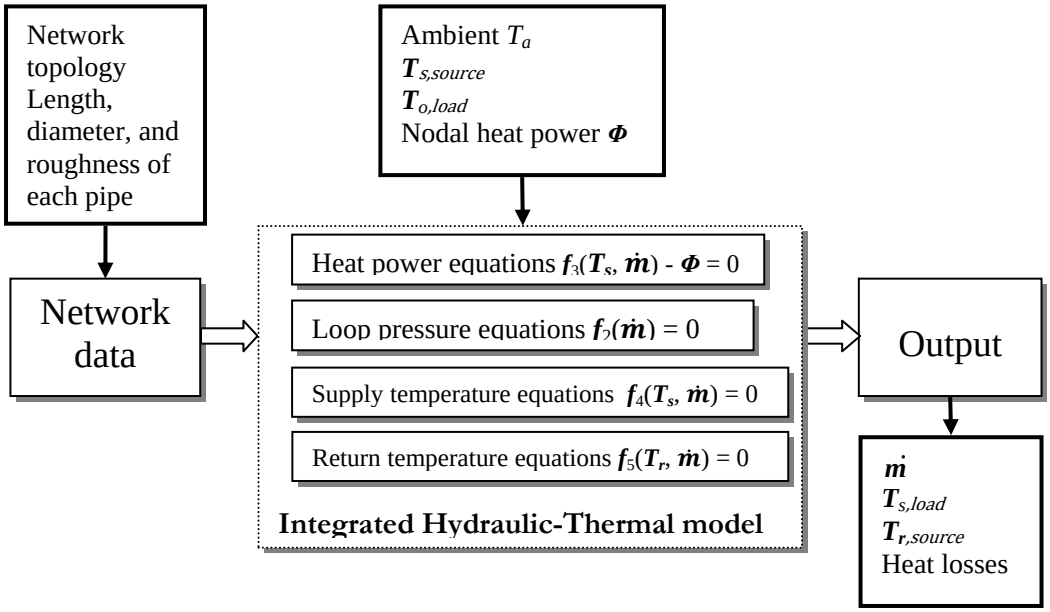

Figure 2.13: Structure of the integrated hydraulic-thermal calculation with specified nodal heat power

Following equation (2.21), the iterative form of the Newton-Raphson method for the integrated hydraulic-thermal calculation is

$$\boldsymbol{x}^{(i+1)} = \boldsymbol{x}^{(i)} - \left(\boldsymbol{J}^{(i)}\right)^{-1} \Delta \boldsymbol{F}(\boldsymbol{x}^{(i)}) \tag{2.43}$$

where i is the iteration time; $\boldsymbol{x}$ is the state variables; $\boldsymbol{J}$ is the Jacobian matrix; $\Delta\boldsymbol{F}$ is the vector of total mismatches.

$$\boldsymbol{x} = \begin{bmatrix} \dot{\boldsymbol{m}} \\ \boldsymbol{T}'_{s,load} \\ \boldsymbol{T}'_{r,load} \end{bmatrix} \tag{2.44}$$

where the three parts of $\boldsymbol{x}$ are $n_{pipe} \times 1$, $n_{load} \times 1$, $n_{load} \times 1$. n_{pipe} is the number of pipes and n_{load} is the number of loads. Denoting $T'_s = T_s - T_a$, $T'_r = T_r - T_a$.

In equation (2.43), $\Delta\boldsymbol{F}$ consists of the heat power equation (2.42), the loop pressure equation (2.10), a linear system of equations (2.33) for the supply temperatures and a linear system of equations (2.38) for the return temperatures.

$$\Delta \boldsymbol{F} =$$

$$\begin{bmatrix} \Delta \boldsymbol{\Phi} \\ \Delta \boldsymbol{p} \\ \Delta \boldsymbol{T}'_s \\ \Delta \boldsymbol{T}'_r \end{bmatrix} = \begin{bmatrix} C_p \boldsymbol{A}\, \dot{\boldsymbol{m}}(\boldsymbol{T}_s - \boldsymbol{T}_o) - \boldsymbol{\Phi}^{sp} \\ \boldsymbol{B}\, \boldsymbol{K}\, \dot{\boldsymbol{m}}|\dot{\boldsymbol{m}}| \\ \boldsymbol{A}_s \boldsymbol{T}'_{s,load} - \boldsymbol{b}_s \\ \boldsymbol{A}_r \boldsymbol{T}'_{r,load} - \boldsymbol{b}_r \end{bmatrix} \begin{matrix} \leftarrow \text{Heat power mismatches} \\ \leftarrow \text{Loop pressure mismatches} \\ \leftarrow \text{Supply temperature mismatches} \\ \leftarrow \text{Return temperature mismatches} \end{matrix} \tag{2.45}$$

where $\boldsymbol{\Phi}^{sp}$ is the specified nodal heat power. The four parts of $\Delta \boldsymbol{F}$ are $(n_{node} - 1) \times 1$, $n_{loop} \times 1$, $n_{load} \times 1$ and $n_{load} \times 1$. n_{node} is the number of nodes, and n_{load} is the number of loads, and n_{loop} is the number of loops.

Hence, following equations (2.44) and (2.45), the integrated Jacobian matrix $\boldsymbol{J}$ comprises (3 × 3 block) matrices. It is divided by the mass flow rates, the supply temperatures and the return temperatures.

$$\begin{aligned} \boldsymbol{J} &= \begin{bmatrix} J_{11} & J_{12} & J_{13} \\ J_{21} & J_{22} & J_{23} \\ J_{31} & J_{32} & J_{33} \end{bmatrix} \\ &= \begin{bmatrix} \dfrac{\partial[\Delta \boldsymbol{\Phi}; \Delta \boldsymbol{p}]}{\partial \dot{\boldsymbol{m}}} & \dfrac{\partial[\Delta \boldsymbol{\Phi}; \Delta \boldsymbol{p}]}{\partial \boldsymbol{T}'_s} & \dfrac{\partial[\Delta \boldsymbol{\Phi}; \Delta \boldsymbol{p}]}{\partial \boldsymbol{T}'_r} \\ \dfrac{\partial \Delta \boldsymbol{T}'_s}{\partial \dot{\boldsymbol{m}}} & \dfrac{\partial \Delta \boldsymbol{T}'_s}{\partial \boldsymbol{T}'_s} & \dfrac{\partial \Delta \boldsymbol{T}'_s}{\partial \boldsymbol{T}'_r} \\ \dfrac{\partial \Delta \boldsymbol{T}'_r}{\partial \dot{\boldsymbol{m}}} & \dfrac{\partial \Delta \boldsymbol{T}'_r}{\partial \boldsymbol{T}'_s} & \dfrac{\partial \Delta \boldsymbol{T}'_r}{\partial \boldsymbol{T}'_r} \end{bmatrix} \end{aligned} \tag{2.46}$$

where the block matrices in grey background are nonzero and others are zero. The nonzero elements of the off-diagonal submatrices J_{21} and J_{31} in the Jacobian matrix are the derivatives of the mixture temperatures mismatches to the mass flow rates $\dot{\boldsymbol{m}}$. Thus, they are usually very small relative to the elements of the diagonal submatrices J_{11}, J_{22} and J_{33}. This is because the small variation of mass flow rates has very small variation to the difference of the mixture temperature. For simplicity, the submatrices J_{21} and J_{31} in the Jacobian matrix are put to zero [85].

Following equations (2.45) and (2.46), $\boldsymbol{J}_{11}$ is similar to the Jacobian matrix in the hydraulic model as shown in equation (2.26).

$$\boldsymbol{J}_{11} = \begin{bmatrix} C_p \boldsymbol{A}\, (\boldsymbol{T}_s - \boldsymbol{T}_o) \\ \boldsymbol{2BK}\, |\dot{\boldsymbol{m}}| \end{bmatrix} \tag{2.47}$$

where the upper part of $\boldsymbol{J}_{11}$ is $(n_{node} - 1) \times n_{pipe}$; the lower part of $\boldsymbol{J}_{11}$ is $n_{loop} \times n_{pipe}$.

Following equations (2.45) and (2.46), $\boldsymbol{J}_{12}$ is expressed as

$$\boldsymbol{J}_{12} = Diag\left[C_p \boldsymbol{A}\, \dot{\boldsymbol{m}}\right] \tag{2.48}$$

where $\boldsymbol{J}_{12}$ is $n_{pipe} \times n_{load}$. *Diag* [*E*] represents a matrix with the elements *E* on the diagonal.

Following equations (2.45) and (2.46), $\boldsymbol{J}_{22}$ and $\boldsymbol{J}_{33}$ are equal to the coefficients matrix for supply and return networks in the thermal model.

$$\begin{aligned} \boldsymbol{J}_{22} &= \boldsymbol{A}_s \\ \boldsymbol{J}_{33} &= \boldsymbol{A}_r \end{aligned} \tag{2.49}$$

where $\boldsymbol{J}_{22}$ is $n_{load} \times n_{load}$ and $\boldsymbol{J}_{33}$ is $n_{load} \times n_{load}$.

To illustrate the integrated hydraulic-thermal calculation, the model equations are applied to the district heating network in Figure 2.10. Thus, $n_{pipe} = 3$, $n_{node} = 3$, $n_{load} = 2$ and $n_{loop} = 1$.

Following equation (2.44), the state variables $\boldsymbol{x}$ for the network shown in Figure 2.10 is given by

$$\boldsymbol{x} = \begin{bmatrix} \dot{m}_1 \\ \dot{m}_2 \\ \dot{m}_3 \\ T'_{s1} \\ T'_{s2} \\ T'_{r1} \\ T'_{r2} \end{bmatrix} \tag{2.50}$$

Following equation (2.45), the vector of total mismatches $\Delta \boldsymbol{F}$ for the network in Figure 2.10 consists of the heat power equation (2.45), the loop pressure equation (2.28), a linear system of equations for the supply temperatures (2.34) and a linear system of equations for the return temperatures (2.39). $\Delta \boldsymbol{F}$ for the network shown in Figure 2.10 is given by

$$\Delta \boldsymbol{F} = \begin{bmatrix} \begin{bmatrix} C_p \begin{bmatrix} 1 & -1 & 0 \\ 0 & 1 & 1 \end{bmatrix} \begin{bmatrix} \dot{m}_1 \\ \dot{m}_2 \\ \dot{m}_3 \end{bmatrix} \left(\begin{bmatrix} T'_{s1} \\ T'_{s2} \end{bmatrix} - \begin{bmatrix} T'_{o1} \\ T'_{o2} \end{bmatrix} \right) - \begin{bmatrix} \emptyset_1^{sp} \\ \emptyset_2^{sp} \end{bmatrix} \end{bmatrix} \\ [K_1 \dot{m}_1 |\dot{m}_1| + K_2 \dot{m}_2 |\dot{m}_2| - K_3 \dot{m}_3 |\dot{m}_3|] \\ \begin{bmatrix} 1 & 0 \\ -\dot{m}_2 \Psi_2 & \dot{m}_{q2} \end{bmatrix} \begin{bmatrix} T'_{s1} \\ T'_{s2} \end{bmatrix} - \begin{bmatrix} T'_{s3} \Psi_1 \\ \dot{m}_3 T'_{s3} \Psi_3 \end{bmatrix} \\ \begin{bmatrix} \dot{m}_1 & -\dot{m}_2 \Psi_2 \\ 0 & 1 \end{bmatrix} \begin{bmatrix} T'_{r1} \\ T'_{r2} \end{bmatrix} - \begin{bmatrix} \dot{m}_{q1} T'_{o1} \\ T'_{o2} \end{bmatrix} \end{bmatrix} \tag{2.51}$$

where the last row of $\boldsymbol{A}$ that relates to the slack node is redundant and is chosen for exclusion. $\boldsymbol{A} = \begin{bmatrix} 1 & -1 & 0 \\ 0 & 1 & 1 \end{bmatrix}$.

Hence, following equation (2.46), the Jacobian matrix is expressed as

$$\boldsymbol{J} = \begin{bmatrix} J_{11} & J_{12} & J_{13} \\ J_{21} & J_{22} & J_{23} \\ J_{31} & J_{32} & J_{33} \end{bmatrix}$$

$$= \left[\begin{array}{ccc|cc|cc} \frac{\partial \mathrm{F}_1}{\partial \dot{m}_1} & \frac{\partial \mathrm{F}_1}{\partial \dot{m}_2} & \frac{\partial \mathrm{F}_1}{\partial \dot{m}_3} & \frac{\partial \mathrm{F}_1}{\partial \boldsymbol{T}'_{s1}} & \frac{\partial \mathrm{F}_1}{\partial \boldsymbol{T}'_{s2}} & \frac{\partial \mathrm{F}_1}{\partial \boldsymbol{T}'_{r1}} & \frac{\partial \mathrm{F}_1}{\partial \boldsymbol{T}'_{r2}} \\ \frac{\partial \mathrm{F}_2}{\partial \dot{m}_1} & \frac{\partial \mathrm{F}_2}{\partial \dot{m}_2} & \frac{\partial \mathrm{F}_2}{\partial \dot{m}_3} & \frac{\partial \mathrm{F}_2}{\partial \boldsymbol{T}'_{s1}} & \frac{\partial \mathrm{F}_2}{\partial \boldsymbol{T}'_{s2}} & \frac{\partial \mathrm{F}_2}{\partial \boldsymbol{T}'_{r1}} & \frac{\partial \mathrm{F}_2}{\partial \boldsymbol{T}'_{r2}} \\ \frac{\partial \mathrm{F}_3}{\partial \dot{m}_1} & \frac{\partial \mathrm{F}_3}{\partial \dot{m}_2} & \frac{\partial \mathrm{F}_3}{\partial \dot{m}_3} & \frac{\partial \mathrm{F}_3}{\partial \boldsymbol{T}'_{s1}} & \frac{\partial \mathrm{F}_3}{\partial \boldsymbol{T}'_{s2}} & \frac{\partial \mathrm{F}_3}{\partial \boldsymbol{T}'_{r1}} & \frac{\partial \mathrm{F}_3}{\partial \boldsymbol{T}'_{r2}} \\ \hline \frac{\partial \mathrm{F}_4}{\partial \dot{m}_1} & \frac{\partial \mathrm{F}_4}{\partial \dot{m}_2} & \frac{\partial \mathrm{F}_4}{\partial \dot{m}_3} & \frac{\partial \mathrm{F}_4}{\partial \boldsymbol{T}'_{s1}} & \frac{\partial \mathrm{F}_4}{\partial \boldsymbol{T}'_{s2}} & \frac{\partial \mathrm{F}_4}{\partial \boldsymbol{T}'_{r1}} & \frac{\partial \mathrm{F}_4}{\partial \boldsymbol{T}'_{r2}} \\ \frac{\partial \mathrm{F}_5}{\partial \dot{m}_1} & \frac{\partial \mathrm{F}_5}{\partial \dot{m}_2} & \frac{\partial \mathrm{F}_5}{\partial \dot{m}_3} & \frac{\partial \mathrm{F}_5}{\partial \boldsymbol{T}'_{s1}} & \frac{\partial \mathrm{F}_5}{\partial \boldsymbol{T}'_{s2}} & \frac{\partial \mathrm{F}_5}{\partial \boldsymbol{T}'_{r1}} & \frac{\partial \mathrm{F}_5}{\partial \boldsymbol{T}'_{r2}} \\ \hline \frac{\partial \mathrm{F}_6}{\partial \dot{m}_1} & \frac{\partial \mathrm{F}_6}{\partial \dot{m}_2} & \frac{\partial \mathrm{F}_6}{\partial \dot{m}_3} & \frac{\partial \mathrm{F}_6}{\partial \boldsymbol{T}'_{s1}} & \frac{\partial \mathrm{F}_6}{\partial \boldsymbol{T}'_{s2}} & \frac{\partial \mathrm{F}_6}{\partial \boldsymbol{T}'_{r1}} & \frac{\partial \mathrm{F}_6}{\partial \boldsymbol{T}'_{r2}} \\ \frac{\partial \mathrm{F}_7}{\partial \dot{m}_1} & \frac{\partial \mathrm{F}_7}{\partial \dot{m}_2} & \frac{\partial \mathrm{F}_7}{\partial \dot{m}_3} & \frac{\partial \mathrm{F}_7}{\partial \boldsymbol{T}'_{s1}} & \frac{\partial \mathrm{F}_7}{\partial \boldsymbol{T}'_{s1}} & \frac{\partial \mathrm{F}_7}{\partial \boldsymbol{T}'_{r1}} & \frac{\partial \mathrm{F}_7}{\partial \boldsymbol{T}'_{r2}} \end{array}\right] \tag{2.52}$$

Following equation (2.47), $\boldsymbol{J}_{11}$ is expressed as

$$\boldsymbol{J}_{11} = \begin{bmatrix} C_p(T'_{s1} - T'_{o1}) & -C_p(T'_{s1} - T'_{o1}) & 0 \\ 0 & C_p(T'_{s2} - T'_{o2}) & C_p(T'_{s2} - T'_{o2}) \\ 2K_1|\dot{m}_1| & 2K_2|\dot{m}_2| & -2K_3|\dot{m}_3| \end{bmatrix} \tag{2.53}$$

Following equation (2.48), $\boldsymbol{J}_{12}$ is expressed as

$$\boldsymbol{J}_{12} = \begin{bmatrix} C_p(\dot{m}_1 - \dot{m}_2) & 0 \\ 0 & C_p(\dot{m}_2 + \dot{m}_3) \end{bmatrix} \tag{2.54}$$

Following equation (2.49), $\boldsymbol{J}_{22}$ and $\boldsymbol{J}_{33}$ are equal to the matrix of coefficients for the supply and return networks in the thermal model, which are shown in equation (2.34) and equation (2.39).

$$\begin{aligned} \boldsymbol{J}_{22} &= \boldsymbol{A}_s = \begin{bmatrix} 1 & 0 \\ -\dot{m}_2\Psi_2 & \dot{m}_{q2} \end{bmatrix} \\ \boldsymbol{J}_{33} &= \boldsymbol{A}_r = \begin{bmatrix} \dot{m}_1 & -\dot{m}_2\Psi_2 \\ 0 & 1 \end{bmatrix} \end{aligned} \tag{2.55}$$

The nonzero elements of the off-diagonal submatrices J_{21} and J_{31} in the Jacobian matrix are the derivatives of the mixture temperatures mismatches to the mass flow rates $\dot{\boldsymbol{m}}$. Thus, they are usually very small relative to the elements of the diagonal submatrices J_{11}, J_{22} and J_{33}. These are explained with the example as follows:

Following equations (2.51) and (2.52)

$$\begin{aligned} \boldsymbol{J}_{21} &= \frac{\partial \Delta \boldsymbol{T}'_s}{\partial \dot{\boldsymbol{m}}} = \begin{bmatrix} 0 & 0 & 0 \\ 0 & -T'_{s1}\Psi_2 + T'_{s2} & -T'_{s3}\Psi_3 + T'_{s2} \end{bmatrix} \\ \boldsymbol{J}_{31} &= \frac{\partial \Delta \boldsymbol{T}'_r}{\partial \dot{\boldsymbol{m}}} = \begin{bmatrix} T'_{r1} - T'_{o1} & -T'_{r1}\Psi_2 + T'_{o1} & 0 \\ 0 & 0 & 0 \end{bmatrix} \end{aligned} \tag{2.56}$$

Since Ψ is a coefficient that relates to the temperature drop along a pipe shown in equation (2.33), the value of Ψ is usually near to 1. The nonzero terms of $\boldsymbol{J}_{21}$ and $\boldsymbol{J}_{31}$ are the forms of $(-T'_{si}\Psi_k + T'_{sj})$ and $\left(-T'_{rj}\Psi_k + T'_{oj}\right)$, where *i, j, k* are the index of nodes. Thus, $\boldsymbol{J}_{21}$ and $\boldsymbol{J}_{31}$ are approximate to zero.

Assuming initial condition as, $\boldsymbol{x}^{(0)} = \begin{bmatrix} \dot{m}_1 \\ \dot{m}_2 \\ \dot{m}_3 \\ T'_{s1} \\ T'_{s2} \\ T'_{r1} \\ T'_{r2} \end{bmatrix} = \begin{bmatrix} 1 \\ 1 \\ 1 \\ 100 - 10 \\ 100 - 10 \\ 50 - 10 \\ 50 - 10 \end{bmatrix}$.

For the first iteration,

$$\Delta \boldsymbol{F}^{(0)} = \begin{bmatrix} -0.300 \\ 0.118 \\ 0.009 \\ 1.705 \\ 4.251 \\ 0.758 \\ 0 \end{bmatrix},$$

Following equation (2.43),

$$\boldsymbol{x}^{(1)} = \boldsymbol{x}^{(0)} - \left(\boldsymbol{J}^{(0)}\right)^{-1} \Delta \boldsymbol{F}^{(0)} = \begin{bmatrix} 1.762 \\ 0.327 \\ 1.226 \\ 88.295 \\ 87.038 \\ 39.242 \\ 40.000 \end{bmatrix}.$$

The procedure is repeated until the maximum element in the mismatches $|\Delta \boldsymbol{F}|$ becomes less than the tolerance $\boldsymbol{\varepsilon}$ = 10^{-3}. After 5 iterations, the converged results are shown in Table 2.3. The results of the decomposed and integrated calculations are very close. The small differences are due to the simplification of the integrated Jacobian matrix in the integrated hydraulic-thermal calculation and the different stopping criteria of two calculations.

Table 2.3: Results of the decomposed and integrated hydraulic-thermal calculations

Decomposed hydraulic and thermal calculation	$\dot{m}_1 = 1.6420, \dot{m}_2 = 0.1767, \dot{m}_3 = 1.3451.$ $T_{s1,load}$ = 98.9576, $T_{s2,load}$ = 97.1401. $T_{r1,load}$ = 49.5583, $T_{r2,load}$ = 50, $T_{r1,source}$ = 49.1251.
Integrated hydraulic-thermal calculation	$\dot{m}_1 = 1.6420, \dot{m}_2 = 0.1767, \dot{m}_3 = 1.3451.$ $T_{s1,load}$ = 98.9575, $T_{s2,load}$ = 97.1400. $T_{r1,load}$ = 49.5583, $T_{r2,load}$ = 50, $T_{r1,source}$ = 49.1251.

2.6 Summary

Hydraulic-thermal model was developed to investigate the performance of a district heating network. The objective of the hydraulic-thermal model was to determine the mass flow rates within each pipe and the

load supply temperatures and the source return temperatures. It was assumed that the supply temperatures of the source and the return temperatures of the load are specified; the injected mass flow rates or the heat power supplied or consumed at all the nodes except one are specified.

The individual hydraulic and thermal models in district heating networks were modelled. In the hydraulic model, the network description was based on a graph-theoretical method and the Newton-Raphson method was used to solve the hydraulic equations for looped networks. In the thermal model, the mixture temperatures at nodes were considered and a matrix formulation of the thermal model was implemented.

Conventionally, the decomposed hydraulic-thermal calculation was through an iterative procedure between the individual hydraulic and thermal models. In this thesis, an integrated hydraulic-thermal calculation was developed, in which the hydraulic and thermal models were combined in a single system of equations solved by the Newton-Raphson method. The results of two calculations were very close and the results were validated using SINCAL with the same values at 10^{-3} precision.

Chapter 3 - Combined Analysis of Electricity and Heat Networks

3.1 Introduction

3.1.1 Combined Electricity and District Heating Networks

A schematic for combined electricity and district heating networks is shown in Figure 3.1. The electricity and heat networks are linked through the coupling components (e.g., CHP units, heat pumps, electric boilers and circulation pumps), which are represented as the Sources in Figure 3.1. These coupling components allow flows of energy between the two networks. The CHP units generate electricity and heat simultaneously; heat pumps and electric boilers convert electricity to heat; circulation pumps consume electricity to circulate water in the district heating network. The coupling components are generalised as an electrical and heat interface with adjustable heat-to-power ratio. These coupling components increase the flexibility of the electricity and heat supply systems for facilitating the integration of intermittent renewable energy.

An illustration of the energy flow of a CHP and heat pump composite supply system is shown in Figure 3.2.

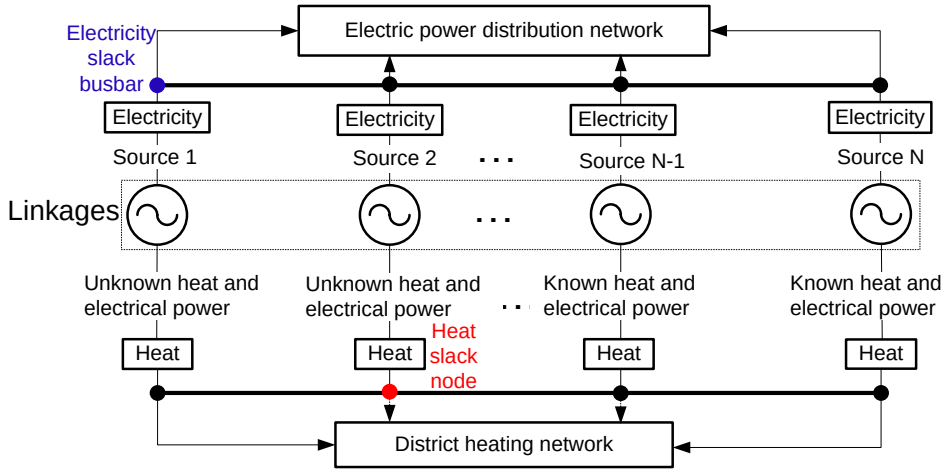

Figure 3.1: Schematic diagram of the combined electricity and district heating networks in islanded mode

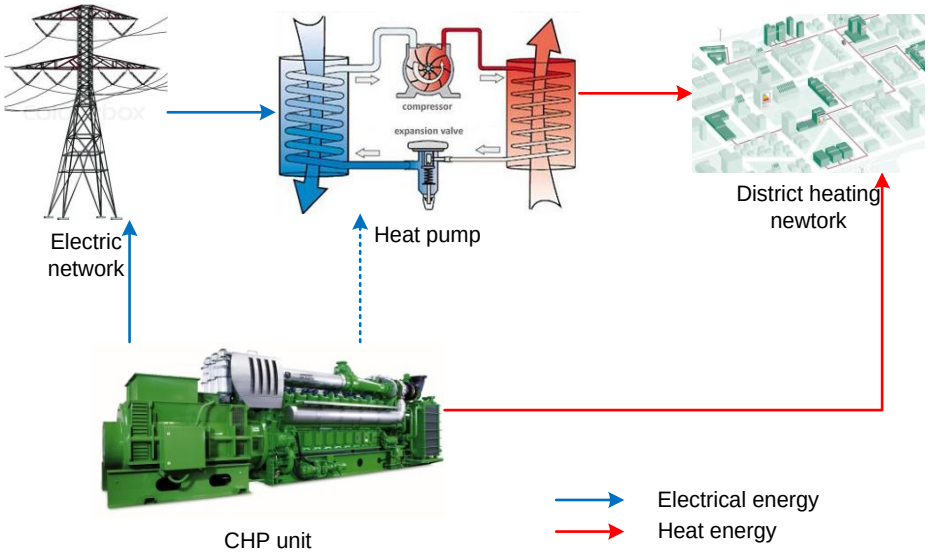

Figure 3.2: Energy flow of a CHP and heat pump composite supply system (picture sources: ARUP DENet and GE's Jenbacher Gas Engines)

Conventional electrical power flow calculations use a single slack busbar. While in the integrated power flow of the combined networks, one electrical slack busbar and one heat slack node are used.

- In the case of islanded operation of the electrical network, CHP units are chosen as providing the slack busbar and slack node which are shown as Source 1 and Source 2 in Figure 3.1.
- In grid-connected mode as shown in Figure 3.3, the electricity slack busbar is chosen as the connection to the grid and so there is no heat

generated at the electricity slack busbar. Therefore, the grid-connected mode can be considered as a simplified special case of islanded operation.

Other than the CHP unit providing the electricity slack busbar, CHP units with adjustable real power output and voltage magnitude are classified as PV busbars; the other CHP units such as micro-CHP are classified as PQ busbars.

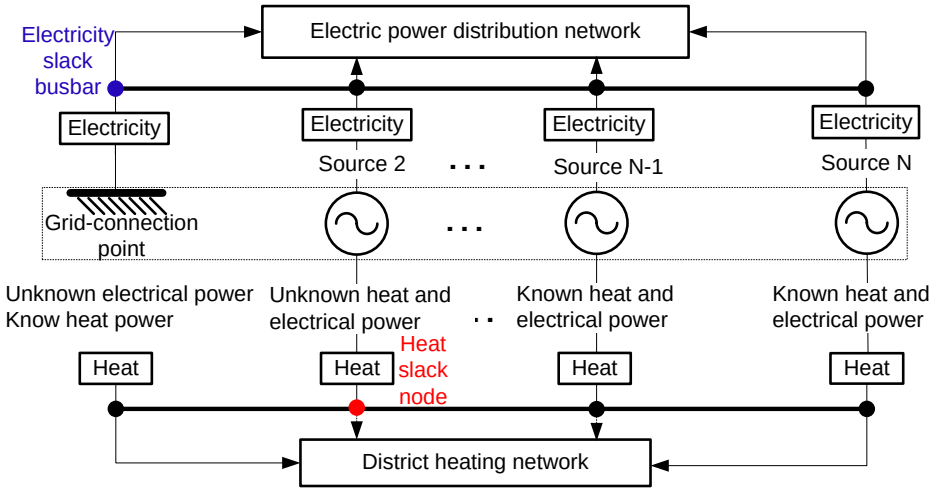

Figure 3.3: Schematic diagram of the combined electricity and district heating networks in grid-connected mode

The CHP units and other coupling components allow flows of energy between the two networks. In islanded mode, the heat power generated by Source 2 (at the electricity slack busbar) is determined by the electrical power generated from this unit. Similarly, the electrical power generated from Source 1 (at the heat slack node) is a function of the heat network. Neither the heat network nor the electricity network can be calculated without taking into account the other network. It is assumed that the heat and electrical power generated by the CHP units is fully utilised without heat dumping.

Two calculation techniques were developed to calculate the operating points of the electricity and heat networks as follows. The schematics of the two calculation techniques are shown in Figure 3.4, where $\boldsymbol{x}^{(i)}$ is the vector of unknown state variables at the ith iteration.

- In the decomposed electrical-hydraulic-thermal calculation, the independent hydraulic equations and thermal equations and electrical power flow equations were calculated sequentially and linked through the coupling components. This is based on the decomposed hydraulic-thermal calculation of district heating networks in Chapter 2. This sequential procedure is iterated at each time step until the solution converges to an acceptable tolerance (Figure 3.4a.i). Grid-connected operation is a special case of the sequential method (Figure 3.4a.ii). Here only one calculation is taken between the independent hydraulic calculation and thermal calculation and electrical power flow calculation.
- In the integrated electrical-hydraulic-thermal calculation, the electrical power flow equations, the hydraulic equations, and the thermal equations were combined and solved simultaneously as an integrated whole (Figure 3.4b). This is based on the integrated hydraulic-thermal calculation of district heating networks in Chapter 2.

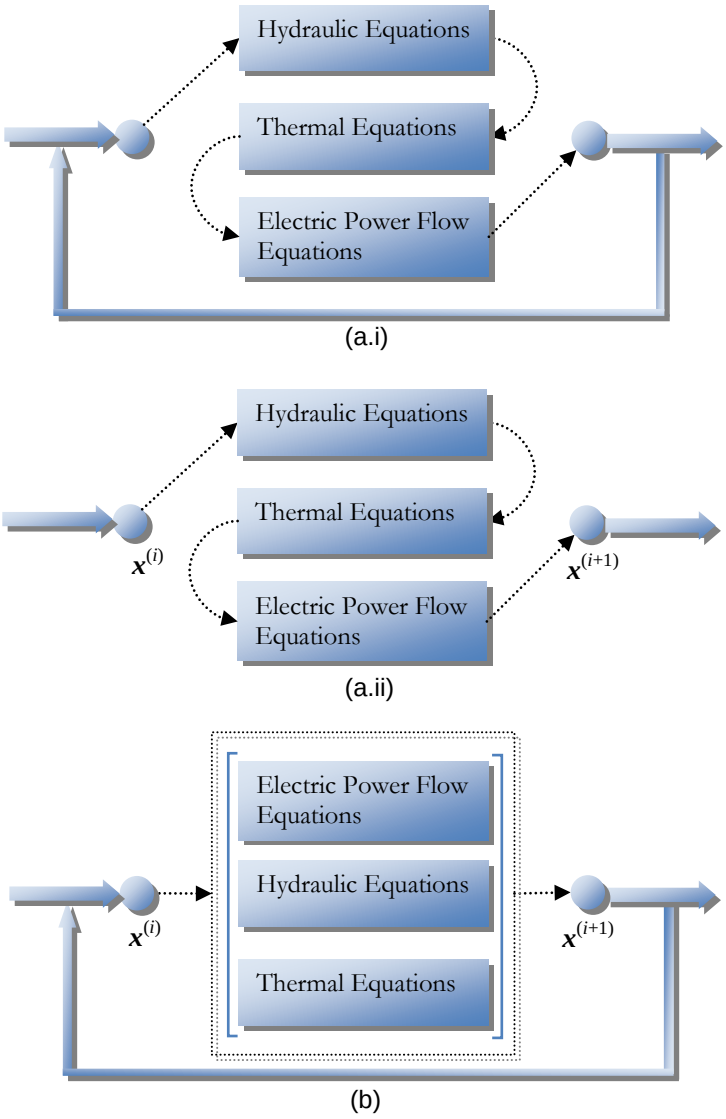

Figure 3.4: Schematics of the decomposed electrical-hydraulic-thermal calculation (a.i) in grid-connected mode and (a.ii) islanded mode and (b) the integrated electrical-hydraulic-thermal calculation

The structure of the integrated electrical-hydraulic-thermal calculation is shown in Figure 3.5. The hydraulic and thermal model equations are linked through the mass flow rates. The electrical power flow equations and hydraulic-thermal model equations are linked through the coupling components. The equations of the integrated electrical-hydraulic-thermal model are derived from the equations of the electrical power flow, the hydraulic model, the thermal model and the coupling components model.

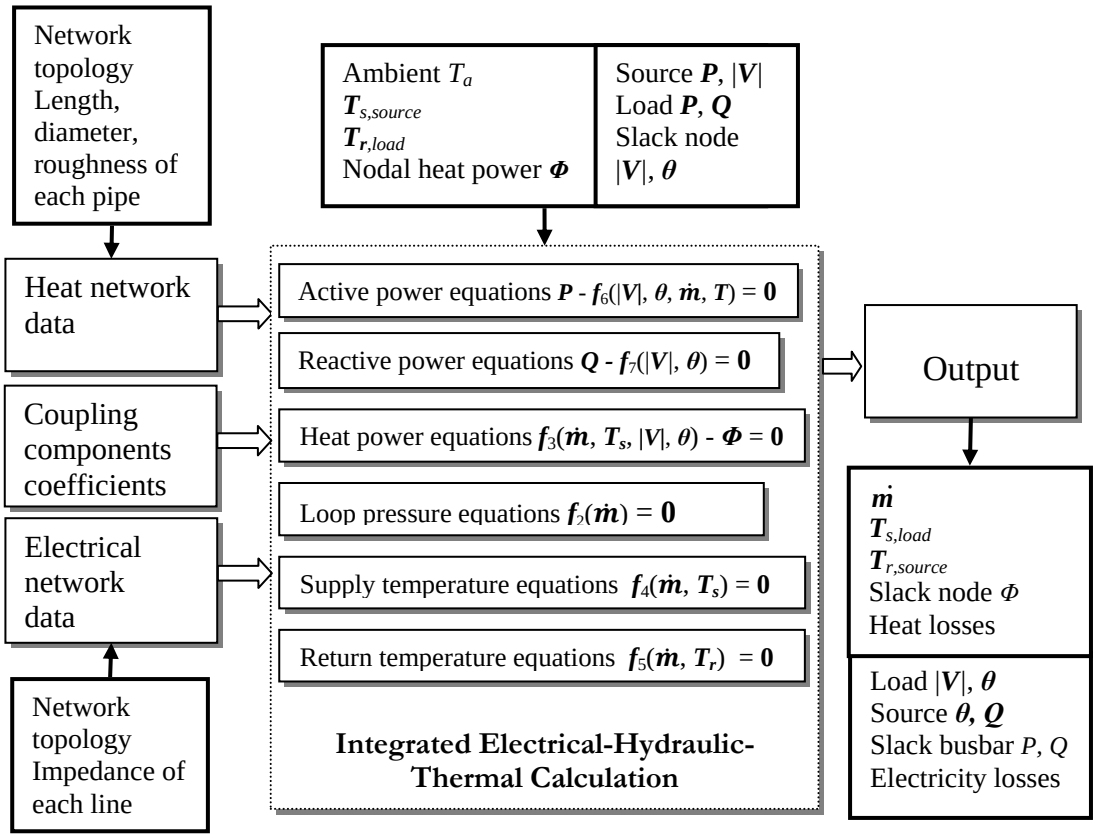

Figure 3.5: Structure of the integrated electrical-hydraulic-thermal calculation technique

The result of the electrical power flow is used to further calculate the current in each branch. Similarly, for the thermal power flow, the additional calculation is nodal mass flow rates based on calculated supply and return temperatures and known nodal heat power.

In the integrated hydraulic-thermal method, nodal mass flow rates were eliminated. In the integrated electrical-hydraulic-thermal method, electrical or heat power of coupling components were eliminated. Thus, the integrated method reduces dimensionality.

3.1.2 Known Variables and Unknown Variables

The power flow formulation of a district heating network is similar to that of an electrical network. The AC electrical power flow model for electrical networks is well established [8, 86]. An integrated hydraulic-thermal calculation technique of district heating networks, the so-called thermal power flow has been described in Chapter 2. Based on these two power flows, an integrated electrical-hydraulic-thermal calculation technique,

the so-called integrated power flow was developed in this Chapter using the Newton-Raphson method. In the integrated power flow, the known and unknown variables of the electricity and heat networks and the coupling components are shown in Table 3.1.

Table 3.1: Known and unknown variables of the electricity and heat networks and the coupling components

	Variables	Known	Unknown
Electricity networks	voltage angle θ	at the slack busbar	at all busbars except the slack busbar
	active power P	at all busbars except the slack busbar	at the slack busbar
	voltage magnitude $\|V\|$	at each source busbar	at each load busbar
	reactive power Q	at each load busbar	at each source busbar
Heat networks	pressure head H	at one node	at all nodes except the one node
	heat power Φ	at all nodes except the slack busbar	at the slack node
	supply temperature T_s	at each source node	at each load node
	return temperature T_r	at each load node (before mixing)	at each source node
	mass flow rate $\dot{m}$		within each pipe
Coupling components	electrical power P_{CHP}, P_{hp} heat power Φ_{CHP}, Φ_{hp}	heat-to-power ratio of CHP units; efficiencies of heat pumps and circulation pumps; fraction of electrical power from CHP units modulated to drive heat pumps	heat and electrical power from CHP units and heat pumps

3.1.3 Analogues of Electrical and Thermal Power Flows

From Table 3.1, the analogues of the known variables in electricity and heat networks are shown in Table 3.2. Consequently, the analogues of three types of busbars and nodes in the electrical and thermal power

flows are shown in Table 3.3. Each type of busbar and node is classified according to two known quantities.

Table 3.2: Analogues of the known variables in electricity and heat networks

Busbar (Node)	**Electricity Networks**	**District Heating Networks**
slack busbar (node)	voltage angle θ	pressure head H
all busbars except the slack busbar (node)	active power P	heat power Φ
source busbar (node)	voltage magnitude $\|V\|$	supply temperature T_s
load busbar (node)	reactive power Q	return temperature T_r

Table 3.3: Analogues of busbar and node types in electrical and thermal power flows

Electrical power flow	P Q busbar	P V busbar	V θ busbar
Thermal power flow	Φ T_r node	Φ T_s node	T_s H node

3.2 Coupling Components Model

The electricity and heat networks are linked through the coupling components (CHP units, heat pumps, electric boilers and circulation pumps). From the modelling point of view, heat pumps or electric boilers are equivalent to CHP units with negative electrical power output; electrical power generators are equivalent to CHP units with zero heat output. These components are generalised as an electrical and heat interface with adjustable heat-to-power ratio. The heat and electrical power outputs of the interface are described by their equivalent heat-to-power ratios as was introduced by Mancarella [62].

3.2.1 CHP Units

Three types of CHP units are discussed: gas turbines, internal combustion reciprocating engines and steam turbine CHP units.

For CHP units using gas turbines or internal combustion reciprocating engines, then the relation between heat and electrical power generation is simplified as equation (3.1) and the schematic is shown in Figure 3.7 (a). It can be seen that the heat-to-power ratio is constant [19, 87].

$$c_m = \frac{\emptyset_{CHP}}{P_{CHP}} \tag{3.1}$$

where P_{CHP} (MW_e) is the electrical power output and Φ_{CHP} (MW_{th}) is the useful heat output of CHP units. The outputs are varied by the fuel input rate. c_m is the heat-to-power ratio [88].

Steam turbine CHP units may be divided into: condensing units and back-pressure units [89, 90]. In the condensing units, no heat is used for industrial processes or district heating purposes. In the back-pressure units, the remaining heat after the turbine can be used for heating purposes with the temperature and pressure of the exhaust steam being higher than that of condensing units [91]. In an extraction steam turbine as shown in Figure 3.6, some steam is extracted at an intermediate pressure for the supply of useful heat [26]. Extraction units may vary from full condensing to full extraction mode by changing the extraction ratio and thus possess the ability to adjust the ratio between useful heat extracted and electrical power generation [19, 26, 91, 92]. A fraction of extraction of 1 denotes full extraction mode and 0 denotes full condensing mode.

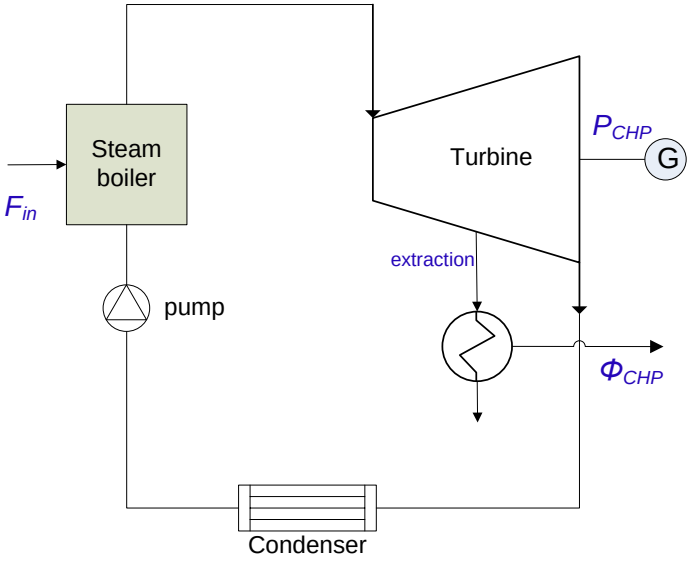

Figure 3.6: Schematic of condensing steam turbines with extraction [19, 89, 90]

The relation between heat and electrical power generation of a CHP unit is represented by the working area [88]. The working area of the extraction unit is a polygon, defined by four lines sketched as shown in Figure 3.7 (b) [93]. The two lines OC and AB define the lower and upper limits of electrical power generation corresponding to any given heat generation. In the Figure 3.7 (b) [93],

- a point on the line OC represents the operation of partially loaded back-pressure turbine;
- point C represents the operation of a fully loaded back-pressure turbine;
- point B represents the operation of a fully loaded extraction turbine with maximum useful heat extracted;
- a point on the line AB represents the operation of a partially loaded extraction turbine.

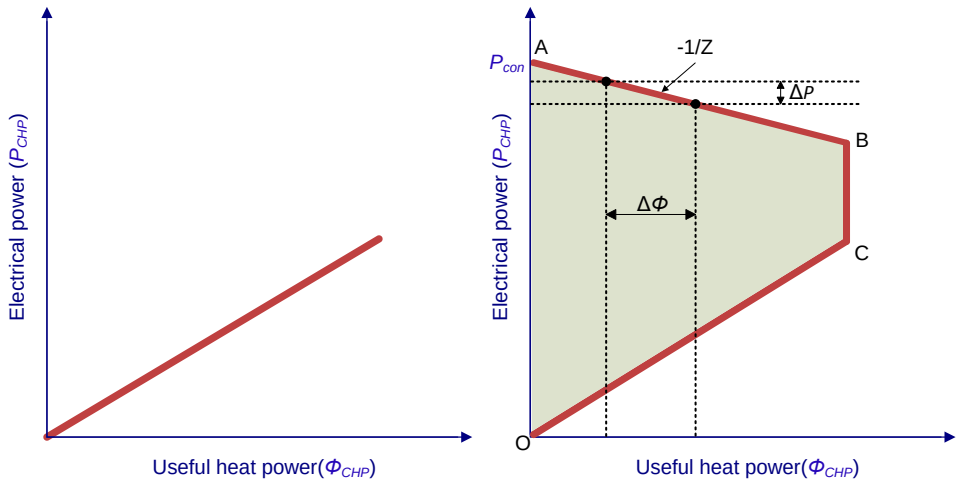

(a) (b)

Figure 3.7: The relation between heat and electrical power generation of CHP units: (a) gas turbines or internal combustion engines and (b) extraction steam turbines [93]

For the steady state analysis in this thesis, the relation between heat and electrical power generation of the extraction unit is chosen as the line AB shown in Figure 3.7 (b). For a given fuel consumption, the electrical power efficiency will decline as steam extraction increases [94]. The relation is described using equation (3.2)

$$Z = \frac{\Delta \emptyset}{\Delta P} = \frac{\emptyset_{CHP} - 0}{P_{con} - P_{CHP}} \tag{3.2}$$

where Z is the ratio that describes the trade-off between heat supplied to site and electrical power (Z = 3.9 ~ 8.1) [94]. $\Delta\emptyset$ is the increased heat recovery and ΔP is the reduced electrical power output. P_{CHP} (MW_e) is the electrical power output and Φ_{CHP} (MW_{th}) is the useful heat output of extraction units. They are shown in the Figure 3.6. P_{con} (MW_e) is the electrical power generation of the extraction unit in full condensing mode, shown in Figure 3.7 (b).

$$P_{con} = \eta_e F_{in} \tag{3.3}$$

where η_e is the electrical efficiency of the extraction unit in full condensing mode; F_{in} (MW) is the fuel input rate which is held constant in this thesis.

Following equation (3.2), (-1/Z) represents the slope of the line AB and P_{con} represents the intercept value in Figure 3.7 (b).

Extraction steam turbines allow a wide range of heat-to-power ratios which are varied by the extraction ratio. In islanded mode, a gas turbine and an extraction turbine CHP units are chosen as providing the slack busbar and slack node. Since two CHP units with contrary properties that slope upwards and downwards are more likely to be able to meet both electricity and heat demands. It is assumed that the heat and electrical power generated by the CHP units is fully utilised without heat dumping.

3.2.2 Heat Pumps

Heat pumps use a small quantity of electricity to leverage heat from the surroundings to higher temperatures, using a compressor just like a refrigerator [22, 32]. Heat pumps are more energy efficient than gas boilers, typically producing three units of heat for every unit of electricity [22]. On the other hand, heat pumps have higher investment costs and also use more expensive fuel [60]. There are two types of heat pumps: air source and ground source heat pumps. The efficiency of a heat pump is modelled as

$$COP = \frac{\emptyset_{hp}}{P_{hp}} \tag{3.4}$$

where the coefficient of performance (COP) is the ratio of heat power supplied $\emptyset_{hp}$ (MW_{th}) to electrical power consumed P_{hp} (MW_e). The COP of a heat pump varies according to the magnitude of the temperature difference between the heat source and the heat load [33].

3.2.3 Electric Boilers

Electric boilers consume electricity to generate heat. The efficiency of an electric boiler is calculated as

$$\eta_b = \frac{\emptyset_b}{P_b} \tag{3.5}$$

where η_b represents the efficiency of an electric boiler; P_b (MW_e) and Φ_b (MW_{th}) are the electrical power consumed and the heat power supplied.

3.2.4 Circulation Pumps

A circulation pump is located at the heat plant to create and maintain pressure difference between supply and return lines. The pressure difference of a pump at a supply must be high enough to ensure that the node farthest away from the pump still has a sufficient minimum pressure difference to allow the water to pass from the supply line through the heat exchanger into the return line [13, 19, 95]. The consumed electrical power by a circulation pump is calculated as

$$P_p = \frac{\dot{m}_p g H_p}{10^6 \eta_p} \tag{3.6}$$

where P_p is the electrical power consumed (MW_e) by a circulation pump; $\dot{m}_p$ is the mass flow rate (kg/s) through the pump; η_p is the efficiency of the pump; H_p is the pump head (m) of the network. The pump head is selected to overcome the flow resistance in the supply and return pipes and also the head differential in the customer installation that is hydraulically the furthest from the delivery point [14]. The pump head is calculated as [11, 14]

$$H = 2 \sum_{i \in \ell} h_{fi} + H_c \tag{3.7}$$

where H_c is the minimum allowable head differential (m); h_f is the head losses (m) within a pipe; ℓ is a set which includes all the pipes in the critical route with the largest pressure drop in the network.

3.2.5 Combined Coupling Components

A CHP and heat pump composite supply system is modelled. Heat pumps are connected to the CHP units in cascade and fed by cogenerated electrical power, shown in Figure 3.8. It is assumed that the heat pumps can be operated at partial load. The modelling of the

composite supply system is similar to that of CHP units. The heat and electrical power outputs of the composite supply system are described by an equivalent heat-to-power ratio as was introduced by Mancarella [62].

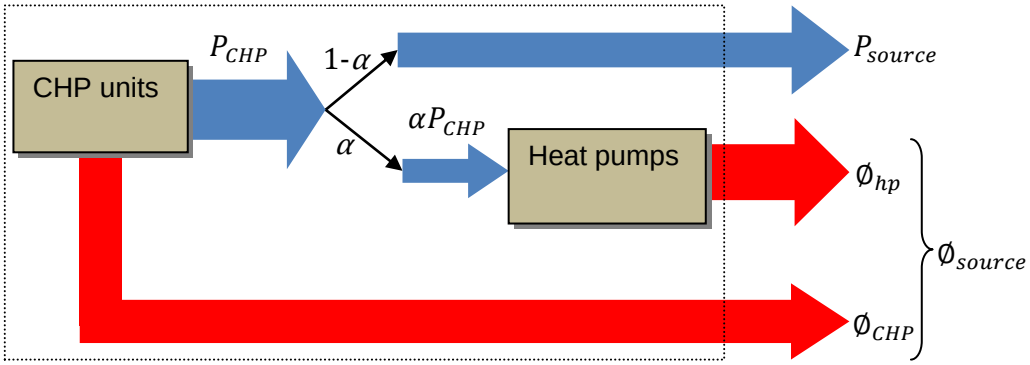

Figure 3.8: A CHP and heat pump composite supply system

For a CHP and heat pump composite supply system shown in Figure 3.8, the heat and electrical power outputs of the composite supply system are

$$\begin{aligned} \emptyset_{source} &= \emptyset_{CHP} + \emptyset_{hp} = \emptyset_{CHP} + \alpha P_{CHP} COP \\ P_{source} &= (1-\alpha) P_{CHP} \end{aligned} \tag{3.8}$$

where P_{source} (MW_e) is the electrical power output of the composite supply system and $\emptyset_{source}$ (MW_{th}) is the useful heat output; α is the percentage of a fraction of electrical power from the CHP units modulated to drive the heat pumps.

Hence, the equivalent heat-to-power ratio c'_m is calculated as

$$c'_m = \frac{\emptyset_{source}}{P_{source}} = \frac{\emptyset_{CHP} + \alpha P_{CHP} COP}{(1-\alpha) P_{CHP}} \tag{3.9}$$

Equations (3.8) and (3.9) illustrate that feeding the heat pumps with cogenerated electrical power brings about a net increase in heat production at the cost of net electrical power production [62].

For different types of CHP units, the relation between the heat and electrical power generation of the composite supply system is described as follows

- For CHP units using gas turbines or internal combustion reciprocating engines, substituting $\emptyset_{CHP}$ from equation (3.1) into equation (3.9), yields

$$c'_m = \frac{\emptyset_{source}}{P_{source}} = \frac{c_m + \alpha\ COP}{1 - \alpha} \tag{3.10}$$

- For CHP units using extraction steam turbines, substituting $\emptyset_{CHP}$ from equation (3.2) into equation (3.8), yields

$$\emptyset_{source} = Z(\eta_e F_{in} - P_{CHP}) + \alpha P_{CHP} COP \tag{3.11}$$

  Thus, rearranging the variable P_{CHP} to be on one side of equation (3.11), yields

$$P_{CHP} = \frac{\emptyset_{source} - Z\eta_e F_{in}}{\alpha COP - Z} \tag{3.12}$$

  Thus, substituting equation (3.12) into equation (3.8), yields

$$\begin{aligned} P_{source} &= (1 - \alpha) P_{CHP} \\ &= \frac{1 - \alpha}{\alpha COP - Z} (\emptyset_{source} - Z\eta_e F_{in}) \end{aligned} \tag{3.13}$$

Furthermore, if the circulation pump at a CHP unit is taken into account, P_{source} in equation (3.8) is written as

$$P_{source} = (1 - \alpha) P_{CHP} - P_p \tag{3.14}$$

where P_p is the consumed electrical power (MW_e) by a circulation pump and is calculated using equation (3.6).

3.3 Electrical Power Flow Analysis

Since the thermal power flow has been described in Chapter 2, this section focuses on the electrical power flow. The AC electrical power flow model for electrical networks is well established [8, 86]. Given a power system described by an admittance matrix, and given a subset of

voltage magnitudes, voltage angles and real and reactive power injections, the electrical power flow determines the other voltage magnitudes and angles and real and reactive power injections.

The voltage *V* at busbar *i* is given in polar coordinates by

$$V_i = |V_i|\angle\theta_i = |V_i|\, e^{j\theta_i} = |V_i|(\cos\theta_i + j\sin\theta_i) \tag{3.15}$$

where *j* is the imaginary unit.

The current injected into the network at busbar *i* is given by

$$I_i = \sum_{n=1}^{N} Y_{in} V_n \tag{3.16}$$

where *N* is the number of busbars in the electricity network; ***Y*** is the admittance matrix that relates current injections at a busbar to the busbar voltages. Current injections may be either positive (into the busbar) or negative (out of the busbar).

Thus, the calculated complex power injected at busbar *i* is

$$S_i = P_i + jQ_i = V_i I_i^{*} = V_i \sum_{n=1}^{N} (Y_{in} V_n)^{*} \tag{3.17}$$

Equation (3.17) constitutes the polar form of the electrical power flow equations.

The specified complex power being injected into the network at busbar *i* is the complex power difference between the source and the load.

$$S_i^{sp} = S_{i,source} - S_{i,load} \tag{3.18}$$

Following equations (3.17) and (3.18), the electrical complex power mismatches ΔS_i injected at busbar *i* are denoted as the specified value S_i^{sp} minus the calculated value S_i.

$$\Delta S_i = S_i^{sp} - S_i = S_i^{sp} - V_i \sum_{n=1}^{N} (Y_{in} V_n)^* \tag{3.19}$$

where $V_i = |V_i| e^{j\theta_i}$, j is the imaginary unit.

Following equation (3.19), the diagonal and off-diagonal elements are calculated as [96]

$$\boldsymbol{J_{S_\theta}} = \frac{\partial \Delta S_i}{\partial \theta_k} = \begin{cases} jV_i Y_{ik}^* V_k^* & k \neq i \\ jV_i Y_{ii}^* V_i^* - jS_i & k = i \end{cases} \tag{3.20}$$

$$\boldsymbol{J_{S_V}} = \frac{\partial \Delta S_i}{\partial |V_k|} = \begin{cases} -V_i Y_{ik}^* e^{-j\theta_k} & k \neq i \\ -V_i Y_{ii}^* e^{-j\theta_i} - S_i/|V_i| & k = i \end{cases} \tag{3.21}$$

Thus, the electricity Jacobian matrix is constituted as

$$\boldsymbol{J}_e = \begin{bmatrix} Real(\boldsymbol{J_{S_\theta}}) & Real(\boldsymbol{J_{S_V}}) \\ Imag(\boldsymbol{J_{S_\theta}}) & Imag(\boldsymbol{J_{S_V}}) \end{bmatrix} \tag{3.22}$$

where *Real* represents the real part of a complex expression and *Imag* represents the imaginary part of a complex expression.

Hence, the iterative form of the Newton-Raphson method is

$$\begin{bmatrix} \boldsymbol{\theta} \\ |\boldsymbol{V}| \end{bmatrix}^{(i+1)} = \begin{bmatrix} \boldsymbol{\theta} \\ |\boldsymbol{V}| \end{bmatrix}^{(i)} - \boldsymbol{J}_e^{-1} \begin{bmatrix} \Delta \boldsymbol{P} \\ \Delta \boldsymbol{Q} \end{bmatrix} \tag{3.23}$$

where $\boldsymbol{\theta}$ is the vector of voltage angles at non-reference busbars; $|\boldsymbol{V}|$ is the vector of voltage magnitudes at PQ busbars; $\Delta \boldsymbol{P}$ is the vector of active power at non-reference busbars; and $\Delta \boldsymbol{Q}$ is the vector of reactive power at PQ busbars.

3.4 Combined Analysis

A combined analysis was developed to investigate the performance of electricity and heat networks. This is based on the hydraulic-thermal model of heat networks described in Section 2.5 and the electrical power flow model in Section 3.3.

For the heat network, the analysis determines the mass flow rates within each pipe and the supply temperatures at each load and the return temperatures at each node. For the electricity network, the analysis determines the voltage magnitude at each load and the voltage angle at each busbar.

Two approaches for the combined analysis of electricity and heat networks are described:

- Decomposed electrical-hydraulic-thermal calculation technique
- Integrated electrical-hydraulic-thermal calculation technique

Three combinations of coupling mechanisms are made in each calculation:

a) **CHP only**: In this case, the electricity and heat networks are linked by the CHP units only.

b) **CHP and circulation pump**: Here, in addition to the CHP units, the circulation pump at each CHP unit has been taken into account.

c) **CHP, circulation pump and heat pump**: Here, in addition to the CHP units and their circulation pumps, a heat pump is connected to a CHP unit in cascade and fed by cogenerated electricity, shown in Figure 3.8.

For the power flow analysis, the electrical power at each busbar is specified except that of the slack busbar; the heat power is specified at each node except that of the slack node. Thus, the linkages between electrical and heat networks are through the generation components (CHP units and heat pumps) at the slack busbar or node and the non-generation components (circulation pumps).

In *grid-connected mode*, the electricity and heat networks are linked by a CHP unit only (or a CHP unit with a heat pump) at the heat slack node and the circulation pumps at each CHP unit. Since any surplus or deficit in electrical power is supplied from the main grid and not from the CHP units, there is no linkage back from the electrical system to the heat system.

In *islanded mode*, the electricity and heat networks are linked by CHP units only (or CHP units with heat pumps) at the electrical slack busbar and the heat slack node and the circulation pumps at each CHP unit. There are thus bidirectional linkages between the electricity and heat networks. The adjustments of heat and electrical power generated from the sources at the slack nodes and busbars are computed during the solution process in a closed loop computation.

Therefore, there are more interactions between electricity and heat networks in islanded mode than grid-connected mode.

The assumptions for the example network shown in Figure 3.1 are as follows

1) Source 1 provides the heat slack node and Source 2 provides the electricity slack busbar;
    a. In *grid-connected mode*, Source 1 corresponds to a gas turbine CHP unit and Source 2 corresponds to the connection to the grid;
    b. In *islanded mode*, Source 1 corresponds to a steam turbine CHP unit and Source 2 corresponds to a gas turbine CHP unit;
2) The heat-to-power ratio of the gas turbine CHP unit is constant and the gas turbine CHP unit can be operated at partial load conditions to respond to electricity and heat load variation;
3) The fuel input rate of the steam turbine CHP unit is constant and the heat-to-power ratio of the steam turbine CHP unit can be modulated;
4) The heat power generated by CHP units is fully utilised, without the waste of useful cogenerated heat.

3.4.1 Decomposed Electrical-Hydraulic-Thermal Calculation

The decomposed electrical-hydraulic-thermal calculation is based on the decomposed hydraulic-thermal calculation in Section 2.5 and the electrical power flow calculation in Section 3.3. In *grid-connected mode*, the hydraulic-thermal model is solved first. Then these results are

transferred to the electricity network through the coupling components (CHP units, heat pumps, electric boilers and circulation pumps). Finally the electrical power flow model is solved.

In *grid-connected mode*, any surplus or deficit in electrical power is supplied from the main grid and there is no heat generated at the electricity slack busbar. Therefore only one calculation is performed by the independent hydraulic model and thermal model and electrical power flow model.

In *islanded mode*, the independent hydraulic and thermal model and electrical power flow model are solved sequentially. This sequential procedure is iterated until the solution converges to an acceptable tolerance. The flowchart of the decomposed electrical-hydraulic-thermal calculation is shown in Figure 3.9.

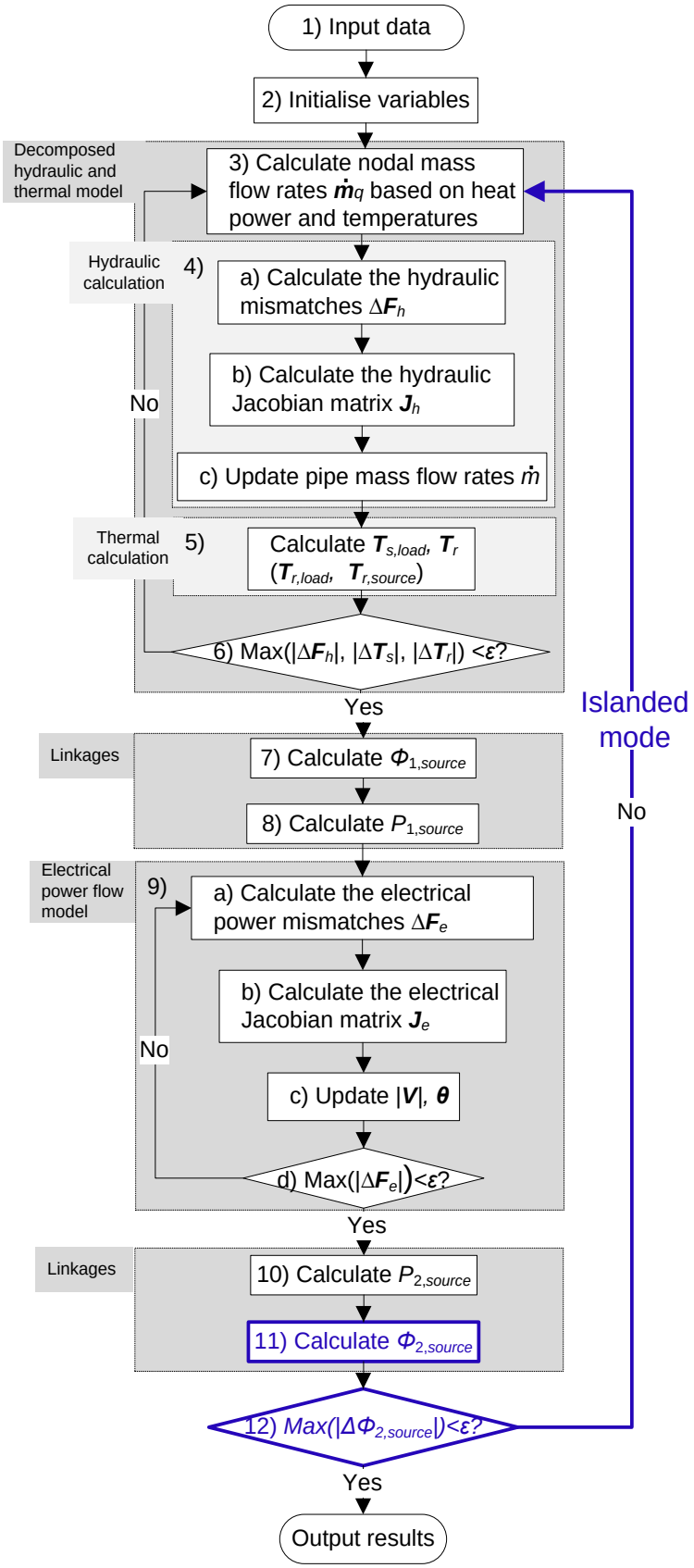

Figure 3.9: Flowchart of the decomposed electrical-hydraulic-thermal calculation (Both grid-connected mode and islanded mode are considered, and the islanded mode is highlighted in blue)

In the flowchart shown in Figure 3.9, the input data and the initialised variables are shown in Table 3.1. The input heat data are

- load return temperatures before mixing which is referred to as the outlet temperature ($\boldsymbol{T}_{o,load}$);
- source supply temperatures ($\boldsymbol{T}_{s,source}$);
- load and source heat power except the slack node.

The initialised heat variables are

- load supply temperatures $\boldsymbol{T}_{s,load}$;
- source return temperatures $\boldsymbol{T}_{r,source}$.

Based on these variables, the nodal mass flow rates $\dot{\boldsymbol{m}}_{\boldsymbol{q}}$ are calculated using the heat power equation (2.27) $\boldsymbol{\Phi} = C_p \dot{\boldsymbol{m}}_{\boldsymbol{q}} (\boldsymbol{T}_s - \boldsymbol{T}_r)$.

The heat power from Source 1 at the heat slack node is denoted as $\emptyset_{1,source}$. The electrical power from Source 1 is denoted as $P_{1,source}$. The heat power from Source 2 at the electricity slack busbar is denoted as $\emptyset_{2,source}$. The electrical power from Source 2 is denoted as $P_{2,source}$.

- $\boldsymbol{\Phi}_{1,source}$ is calculated from the results of the decomposed hydraulic and thermal calculation using the heat power equation (2.42)

$$\emptyset_{1,source} = C_p \boldsymbol{A}_{1,source} \dot{\boldsymbol{m}} \left(T_{s1,source} - T_{r1,source}\right) \tag{3.24}$$

  where $\boldsymbol{A}_{1,source}$ is a row of the network incidence matrix $\boldsymbol{A}$ that relates Source 1 at the heat slack node; $T_{s1,source}$ and $T_{r1,source}$ are the supply temperature and return temperature at Source 1.

- $P_{1,source}$ is determined by $\boldsymbol{\Phi}_{1,source}$ using equation (3.1) for a gas turbine and equation (3.2) for a steam turbine.

$$\begin{aligned} P_{1,source} &= P_{1,CHP} \\ &= \begin{cases} \emptyset_{1,source}/c_{m1}, & gas\ turbine \\ -\emptyset_{1,source}/\mathrm{Z} + \eta_e F_{in}, & steam\ turbine \end{cases} \end{aligned} \tag{3.25}$$

where c_{m1} is the heat-to-power ratio of the gas turbine CHP1; *Z* is the ratio that describes the trade-off between heat supplied to the site and the electrical power of the extraction steam turbine CHP1; η_e is the electrical efficiency of the unit in full condensing mode; F_{in} (MW) is the fuel input rate of the steam turbine unit, which is held constant in this thesis.

The total electrical power supplied from Source 1 is decreased by the pump electrical power consumption and thus equation (3.25) is

$$P_{1,source} = P_{1,CHP} - P_p \tag{3.26}$$

where P_p is the electrical power consumed (MW_e) by the pump and is calculated using equation (3.6).

- $P_{2,source}$ is calculated from the results of the electrical power flow calculation using equation (3.17)

$$P_{2,source} = P_{2,CHP} = Re\left\{V_{2,source}\sum_{k=1}^{N}(Y_{ik}V_k)^*\right\} \tag{3.27}$$

where *Re* represents the real part of a complex expression.

The electrical power generated from Source 2 at the electrical slack busbar is increased by considering the pump electrical power consumption and thus equation (3.29) is

$$P_{2,source} = P_{2,CHP} + P_p \tag{3.28}$$

- In islanded mode, $\Phi_{2,source}$ is determined by $P_{2,source}$ using equation (3.1) for a gas turbine

$$\emptyset_{2,source} = c_{m2}P_{2,source} \tag{3.29}$$

where c_{m2} is the heat-to-power ratio of the CHP unit at Source 2.

3.4.2 Integrated Electrical-Hydraulic-Thermal Calculation

In the integrated electrical-hydraulic-thermal calculation, the electrical power flow equations, the hydraulic equations and the thermal equations were combined to form a single system of equations and solved simultaneously as an integrated whole using the Newton-Raphson method. The structure of the calculation technique is shown in Figure 3.5 and the flowchart is shown in Figure 3.10. During each iteration of the integrated electrical-hydraulic-thermal calculation, the network incidence matrix $\boldsymbol{A}$ and the loop incidence matrix $\boldsymbol{B}$ are updated according to the signs of calculated pipe mass flow rates.

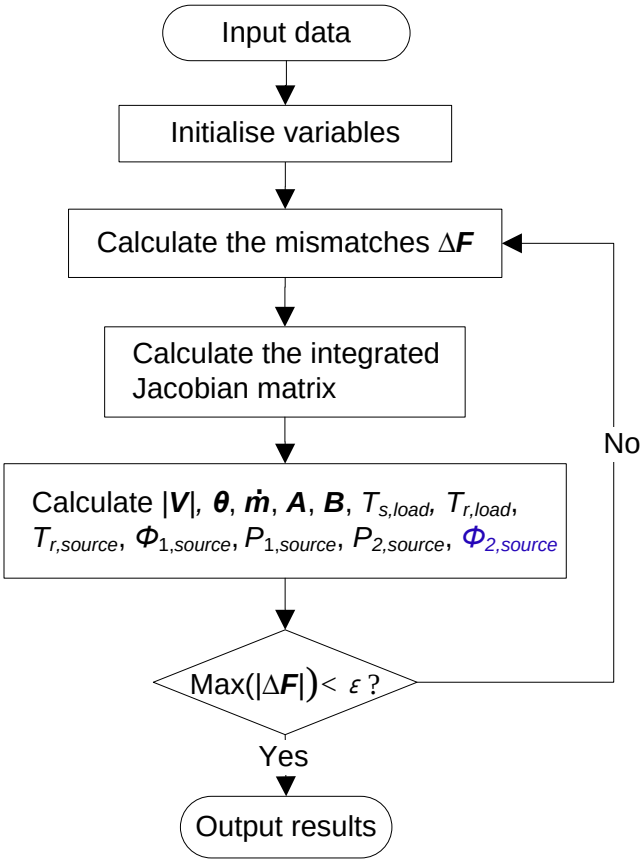

Figure 3.10: Flowchart of the integrated electrical-hydraulic-thermal calculation (Both grid-connected mode and islanded mode are considered, and the islanded mode is highlighted in blue)

In *grid-connected mode*, any surplus or deficit in electrical power is supplied from the main grid and there is no heat generated at the electricity slack busbar. Thus, the derivative of the heat power mismatches with respect to the electrical variables is zero, which means

the lower off-diagonal submatrix of the integrated Jacobian matrix is zero.

While in *islanded mode*, the heat generated at the electricity slack busbar ($\boldsymbol{\Phi}_{2,source}$) is a function of the electricity network, which means the lower off-diagonal submatrix of the integrated Jacobian matrix is nonzero.

The iterative form of the Newton-Raphson method is

$$\boldsymbol{x}^{(i+1)} = \boldsymbol{x}^{(i)} - \boldsymbol{J}^{-1}\Delta\boldsymbol{F} \tag{3.30}$$

where i is the iteration number; $\boldsymbol{x}$ is the vector of state variables as shown in equation (3.31); $\Delta\boldsymbol{F}$ is the vector of total mismatches as shown in equation (3.32); and $\boldsymbol{J}$ is the Jacobian matrix as shown in equation (3.33).

$$\boldsymbol{x} = \begin{bmatrix} \boldsymbol{\theta} \\ |\boldsymbol{V}| \\ \dot{\boldsymbol{m}} \\ \boldsymbol{T}'_{s,load} \\ \boldsymbol{T}'_{r,load} \end{bmatrix} \tag{3.31}$$

Following the structure of the integrated electrical-hydraulic-thermal calculation as shown in Figure 3.5, $\Delta\boldsymbol{F}$ is expressed as

$$\Delta\boldsymbol{F} = \begin{bmatrix} \Delta\boldsymbol{P} \\ \Delta\boldsymbol{Q} \\ \Delta\boldsymbol{\Phi} \\ \Delta\boldsymbol{p} \\ \Delta\boldsymbol{T}'_s \\ \Delta\boldsymbol{T}'_r \end{bmatrix} = \begin{bmatrix} \boldsymbol{P}^{sp} - Real\{\boldsymbol{V}(\boldsymbol{YV})^*\} \\ \boldsymbol{Q}^{sp} - Imag\{\boldsymbol{V}(\boldsymbol{YV})^*\} \\ C_p \boldsymbol{A}\,\dot{\boldsymbol{m}}(\boldsymbol{T}_s - \boldsymbol{T}_o) - \boldsymbol{\Phi}^{sp} \\ \boldsymbol{B}\,\boldsymbol{K}\,\dot{\boldsymbol{m}}|\dot{\boldsymbol{m}}| - \boldsymbol{0} \\ \boldsymbol{C}_s\boldsymbol{T}'_{s,load} - \boldsymbol{b}_s \\ \boldsymbol{C}_r\boldsymbol{T}'_{r,load} - \boldsymbol{b}_r \end{bmatrix} \begin{matrix} \leftarrow \text{Active power mismatches} \\ \leftarrow \text{Reactive power mismatches} \\ \leftarrow \text{Heat power mismatches} \\ \leftarrow \text{Loop pressure mismatches} \\ \leftarrow \text{Supply temperature mismatches} \\ \leftarrow \text{Return temperature mismatches} \end{matrix} \tag{3.32}$$

where *Real* represents the real part of a complex expression and *Imag* represents the imaginary part of a complex expression. The superscript *sp* represents *specified*.

Conventionally, for electrical power flow analysis, the vector $\boldsymbol{P}^{sp}$ in the active power mismatches is specified. While for the integrated electrical-hydraulic-thermal calculation, in the mismatches $\Delta\boldsymbol{F}$ in equation (3.32),

the element $P_{1,source}$ of the vector $\boldsymbol{P}^{sp}$ is determined from the heat power generated at the heat slack node and it is expressed as a function of the heat network. $P_{1,source}$ was described in Section 3.4.1. Thus, the derivative of the electrical power mismatches ($\Delta\boldsymbol{P}$) with respect to the heat variables ($\dot{\boldsymbol{m}}$) is nonzero ($\frac{\partial P_{1,source}}{\partial \dot{\boldsymbol{m}}}$).

Conventionally, for hydraulic and thermal analysis, the vector $\boldsymbol{\Phi}^{sp}$ in the heat power mismatches is specified. While for the integrated calculation in *islanded mode*, the element $\emptyset_{2,source}$ of the vector $\boldsymbol{\Phi}^{sp}$ is expressed as a function of the electricity network. $\emptyset_{2,source}$ was described in Section 3.4.1. Thus, the derivative of the heat power mismatches ($\Delta\boldsymbol{\Phi}$) with respect to the electrical variables ($\boldsymbol{\theta}, |\boldsymbol{V}|$) is nonzero.

The integrated Jacobian matrix $\boldsymbol{J}$ is derived from the mismatches $\Delta\boldsymbol{F}$. It consists of four submatrices: electricity submatrix $\boldsymbol{J}_e$, electricity to heat submatrix $\boldsymbol{J}_{eh}$, heat to electricity submatrix $\boldsymbol{J}_{he}$ and heat submatrix $\boldsymbol{J}_h$.

$$\boldsymbol{J} = \begin{bmatrix} \boldsymbol{J}_e & \boldsymbol{J}_{eh} \\ \boldsymbol{J}_{he} & \boldsymbol{J}_h \end{bmatrix} = \begin{bmatrix} \frac{\partial \Delta P}{\partial \theta} & \frac{\partial \Delta P}{\partial |V|} & \frac{\partial \Delta P}{\partial \dot{m}} & \frac{\partial \Delta P}{\partial T} \\ \frac{\partial \Delta Q}{\partial \theta} & \frac{\partial \Delta Q}{\partial |V|} & \frac{\partial \Delta Q}{\partial \dot{m}} & \frac{\partial \Delta Q}{\partial T} \\ \frac{\partial \Delta \emptyset}{\partial \theta} & \frac{\partial \Delta \emptyset}{\partial |V|} & \frac{\partial \Delta \emptyset}{\partial \dot{m}} & \frac{\partial \Delta \emptyset}{\partial T} \\ \frac{\partial \Delta T}{\partial \theta} & \frac{\partial \Delta T}{\partial |V|} & \frac{\partial \Delta T}{\partial \dot{m}} & \frac{\partial \Delta T}{\partial T} \end{bmatrix} \tag{3.33}$$

where the shaded block matrices are nonzero and the others are zero. The off-diagonal submatrix highlighted in blue is zero in grid-connected mode and nonzero in islanded mode.

For $\boldsymbol{J}_{eh}$, the vector of the nonzero elements $\frac{\partial P_{1,source}}{\partial \dot{\boldsymbol{m}}}$ is calculated using equations (3.24) and (3.25)

$$\begin{aligned} &\frac{\partial P_{1,source}}{\partial \dot{\boldsymbol{m}}} = \frac{\partial P_{1,CHP}}{\partial \dot{\boldsymbol{m}}} \\ &= \begin{cases} C_p \boldsymbol{A}_{1,source}\left(T_{s1,source} - T_{r1,source}\right)/c_{m1}\,, gas\ turbine \\ -C_p \boldsymbol{A}_{1,source}\left(T_{s1,source} - T_{r1,source}\right)/\mathrm{Z}\,, steam\ turbine \end{cases} \end{aligned} \tag{3.34}$$

where $\boldsymbol{A}_{1,source}$ is a row of the network incidence matrix $\boldsymbol{A}$ that relates to Source 1 at the heat slack node. In the return network, the term $T_{r1,source}$ is expressed as a function of the pipe mass flow rates $\dot{\boldsymbol{m}}$ and the load return temperatures $\boldsymbol{T}'_{r,load}$. For simplicity, the derivatives of the term $T_{r1,source}$ with respect to $\dot{\boldsymbol{m}}$ and $\boldsymbol{T}'_{r,load}$ are very small and are neglected.

In the case of circulation pumps, the derivative of the term P_p (the electrical power consumed by the pumps) with respect to $\dot{\boldsymbol{m}}$ in equations (3.25) and (3.26) is very small and is neglected.

For $\boldsymbol{J}_{he}$, in grid-connected mode, the heat power is not a function of the electricity network thus $\boldsymbol{J}_{he} = \boldsymbol{0}$. In islanded mode, $\boldsymbol{J}_{he}$ is nonzero and the vector of the nonzero elements is calculated using equations (3.27) and (3.29)

$$\begin{aligned}&\left[\frac{\partial \emptyset_{2,source}}{\partial \theta_k} \quad \frac{\partial \emptyset_{2,source}}{\partial |V_k|}\right] \\ &= c_{m2}\left[Re\left(jV_i Y_{ik}^* V_k^*\right) \quad Re\left(-V_i Y_{ik}^* e^{-j\theta_k}\right)\right]\end{aligned} \tag{3.35}$$

where the subscript i represents Source 2 at the electricity slack busbar.

CHP, circulation pump and heat pump

In addition to the CHP units and their circulation pumps, a heat pump is connected to a CHP unit in cascade and fed by cogenerated electricity. Thus, Source 1 corresponds to a CHP unit with a heat pump in the example network shown in Figure 3.1. The assumptions are that the heat pump can be operated at partial load conditions to respond to heat load variation and the COP of the heat pump is constant.

Equation (3.25) yields

$$P_{1,source} = \begin{cases} \emptyset_{1,source}/c'_{m1} - P_p, & gas\ turbine \\ \dfrac{1-\alpha}{\alpha COP - Z}\left(\emptyset_{1,source} - Z\eta_e F_{in}\right) - P_p, & steam\ turbine \end{cases} \tag{3.36}$$

where the equivalent heat-to-power ratio c'_{m1} of Source 1 is calculated using equation (3.10). For a steam turbine $P_{1,source}$ is calculated using equation (3.13).

Hence, following equation (3.36), the vector of the nonzero elements of the Jacobian submatrix $\boldsymbol{J}_{eh}$ is expressed as

$$\frac{\partial P_{1,source}}{\partial \dot{\boldsymbol{m}}} = \begin{cases} C_p \boldsymbol{A}_n \left(T_{s1,source} - T_{r1,source}\right)/c'_{m1}, gas\ turbine \\ \dfrac{1-\alpha}{\alpha COP - Z} C_p \boldsymbol{A}_n \left(T_{s1,source} - T_{r1,source}\right), steam\ turbine \end{cases} \quad (3.37)$$

3.5 Examples

3.5.1 Decomposed Electrical-Hydraulic-Thermal Calculation

a) Grid-connected mode

A simple example is used to illustrate the decomposed electrical-hydraulic-thermal calculation in *grid-connected mode*, Figure 3.11. The subscript '*e*' represents nodal electrical variables and '*h*' represents nodal heat variables. From Table 3.1, the known and unknown variables are shown in Table 3.4. The parameters of the two networks are in the Appendix C.

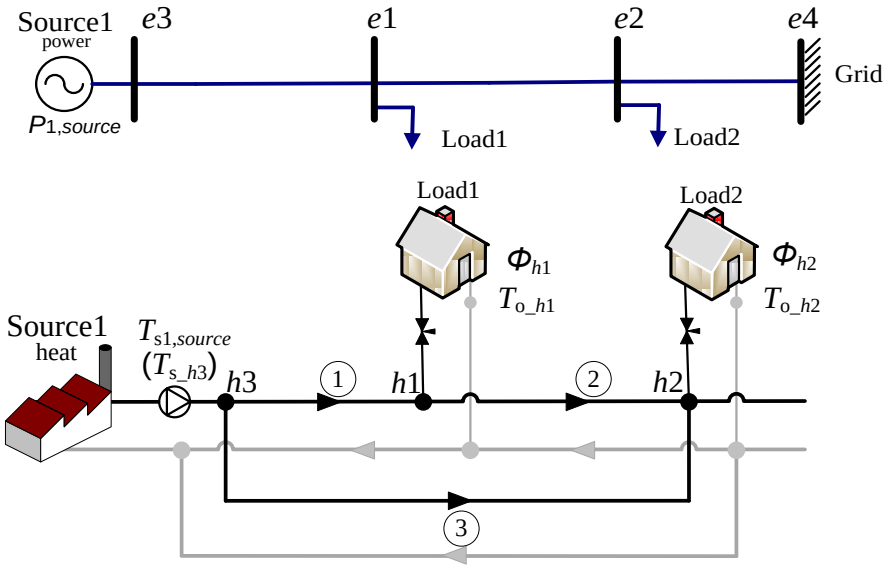

Figure 3.11: A simple grid-connected electricity network and a district heating network (The numbering sequence starts with the loads, followed by the sources and the last element is the slack busbar or node)

Table 3.4: Known variables and unknown variables of electricity and heat networks

	Variables	Known	Unknown
Electricity network	voltage angle θ	θ_{e4}	θ_{e1}, θ_{e2}, θ_{e3}
	active power P	P_{e1}, P_{e2}	$P_{e3}(P_{1,source})$, $P_{e4}(P_{grid})$
	voltage magnitude $\|V\|$	$\|V_{e3}\|(\|V_{1,source}\|)$, $\|V_{e4}\|(\|V_{grid}\|)$	$\|V_{e1}\|$, $\|V_{e2}\|$
	reactive power Q	Q_{e1}, Q_{e2}	Q_{e3}, Q_{e4}
Heat network	pressure head difference H	H_{h2}	H_{h1}, H_{h3}
	heat power Φ	Φ_{h1}, Φ_{h2}	$\Phi_{h3}(\Phi_{1,source})$
	supply temperature T_s	$T_{s\_h3}(T_{s1,source})$	T_{s_h1}, T_{s_h2}
	return temperature T_r	T_{o_h1}, T_{o_h2}	T_{r_h1}, T_{r_h2}, $T_{r\_h3}(T_{r1,source})$
	pipe mass flow rate $\dot{m}$		$\dot{m}_1, \dot{m}_2, \dot{m}_3$

In Table 3.4, H represents the pressure head difference between the supply and return nodes.

In this example, Source 1 refers to the coupling components (CHP units, heat pumps and circulation pumps) that link the electricity and heat networks.

Following equations (3.25), (3.26) and (3.36), $P_{1,source}$ is expressed as

$$P_{1,source} = \begin{cases} \emptyset_{1,source}/c_{m1}\,, & CHP\ only \\ \emptyset_{1,source}/c_{m1} - P_p\,, & CHP + pump \\ \emptyset_{1,source}/c'_{m1} - P_p, & CHP + pump + heat\ pump \end{cases} \tag{3.38}$$

where c_{m1} is the heat-to-power ratio of the gas turbine CHP1. P_p is the electrical power consumed (MW_e) by the pump and is calculated using equation (3.6). c'_{m1} is the equivalent heat-to-power ratio of a composite CHP and heat pump system and is calculated using equation (3.10).

For the heat supply network as shown in Figure 3.11, the network incidence matrix ***A*** and the loop incidence matrix ***B*** are:

$$\boldsymbol{A} = \begin{array}{c} \\ \text{Node No.} \end{array} \begin{array}{c} \begin{array}{ccc} \text{Pipe No.} & & \\ 1 & 2 & 3 \end{array} \\ \begin{array}{c} 1 \\ 2 \end{array} \begin{bmatrix} 1 & -1 & 0 \\ 0 & 1 & 1 \end{bmatrix} \end{array} \qquad \boldsymbol{B} = \begin{array}{c} \\ \text{Loop No.} \end{array} \begin{array}{c} \begin{array}{ccc} \text{Pipe No.} & & \\ 1 & 2 & 3 \end{array} \\ 1 \begin{bmatrix} 1 & 1 & -1 \end{bmatrix} \end{array}$$

Following Figure 3.9, for the example networks in grid-connected mode, steps 1) – 10) used to solve the example networks linked by a CHP unit only are as follows

1) The calculation starts with the known heat and electrical variables as shown in Table 3.5. The known heat variables are labelled in Figure 3.11.

Table 3.5: Known variables for the example networks

Known heat variables
• Heat power of each heat load: $\Phi_{h1} = \Phi_{h2}$ = 0.3MW$_{th}$ • Supply temperature of Source 1: $T_{s1,source}$ = 100°C • Outlet temperature (return temperature before mixing) of each heat load: $T_{o\_h1} = T_{o\_h2}$ = 50°C
Known electrical variables
• Active power of each electrical load: $P_{e1} = P_{e2}$ = 0.15MW$_e$ • Power factor of each electrical load: *p.f.* = 0.95, thus $Q_{e1} = Q_{e2}$ = 0.0493MVar • Voltage magnitude of Source 1 and Grid: $\|V_{1,source}\| = \|V_{e3}\|$ = 1.05*p.u.*, $\|V_{grid}\| = \|V_{e4}\|$ = 1.02*p.u.* • Voltage angle of Grid: $\theta_{grid} = \theta_{e4}$ = 0°

2) Assume the initial conditions for the heat and electricity networks are as follows:

Heat:

$$T_{s\_h1}^{(0)} = T_{s\_h2}^{(0)} = 100°\text{C},\ \dot{\boldsymbol{m}}^{(0)} = \begin{bmatrix} \dot{m}_1^{(0)} \\ \dot{m}_2^{(0)} \\ \dot{m}_3^{(0)} \end{bmatrix} = \begin{bmatrix} 1 \\ 1 \\ 1 \end{bmatrix}.$$

Electricity:

$$\begin{bmatrix} \theta_{e1}^{(0)} & \theta_{e2}^{(0)} & \theta_{e3}^{(0)} & \left|V_{e1}^{(0)}\right| & \left|V_{e2}^{(0)}\right| \end{bmatrix}^T = [0 \quad 0 \quad 0 \quad 1 \quad 1]^T.$$

3) Calculate the nodal mass flow rates $\dot{\boldsymbol{m}}_q$ using the heat power equation (2.27). For the first iteration

$$\dot{m}_{q\_h1}^{(1)} = \frac{\emptyset_{h1}}{C_p\left(T_{s\_h1}^{(0)} - T_{o\_h1}\right)} = \frac{0.3}{4.218 \times 10^{-3} \times (100 - 50)} = 1.4347 kg/s$$

$$\dot{m}_{q\_h2}^{(1)} = \frac{\emptyset_{h2}}{C_p\left(T_{s\_h2}^{(0)} - T_{o\_h2}\right)} = \frac{0.3}{4.218 \times 10^{-3} \times (100 - 50)} = 1.4347 kg/s$$

4) Hydraulic calculation

Update the pipe mass flow rates $\dot{\boldsymbol{m}}$ based on $\dot{\boldsymbol{m}}_q$ using the hydraulic model.

a) Calculate the hydraulic mismatches $\Delta \boldsymbol{F}_h$ using the flow continuity equation (2.3) and the loop pressure equation (2.8)

$$\Delta \boldsymbol{F}_h = \begin{bmatrix} \boldsymbol{A}\,\dot{\boldsymbol{m}} - \dot{\boldsymbol{m}}_q \\ \boldsymbol{B}\boldsymbol{K}\dot{\boldsymbol{m}}|\dot{\boldsymbol{m}}| \end{bmatrix} = \begin{bmatrix} \dot{m}_1 - \dot{m}_2 - \dot{m}_{q\_h1} \\ \dot{m}_2 + \dot{m}_3 - \dot{m}_{q\_h2} \\ K_1\dot{m}_1|\dot{m}_1| + K_2\dot{m}_2|\dot{m}_2| - K_3\dot{m}_3|\dot{m}_3| \end{bmatrix}$$

For the first iteration

$$\Delta \boldsymbol{F}_h^{(1)} = \begin{bmatrix} -1.4347 \\ 0.5653 \\ 0.0090 \end{bmatrix}$$

b) Hence, the hydraulic Jacobian matrix $\boldsymbol{J}_h$ is

$$\therefore\ \boldsymbol{J}_h = \begin{bmatrix} \boldsymbol{A} \\ \boldsymbol{2BK}\,|\dot{\boldsymbol{m}}| \end{bmatrix} = \begin{bmatrix} 1 & -1 & 0 \\ 0 & 1 & 1 \\ 2K_1|\dot{m}_1| & 2K_2|\dot{m}_2| & -2K_3|\dot{m}_3| \end{bmatrix}$$

For the first iteration

$$\boldsymbol{J}_h^{(1)} = \begin{bmatrix} -1 & -1 & 0 \\ 0 & 1 & 1 \\ 0.0358 & 0.0358 & -0.0537 \end{bmatrix}$$

c) Update the pipe mass flow rates $\dot{\boldsymbol{m}}$

$$\dot{\boldsymbol{m}}^{(1)} = \dot{\boldsymbol{m}}^{(0)} - \left(\boldsymbol{J}_h^{(1)}\right)^{-1} \Delta \boldsymbol{F}_h^{(1)} = \begin{bmatrix} 1.7111 \\ 0.2764 \\ 1.1583 \end{bmatrix}$$

5) Thermal calculation

Calculate the nodal temperatures using the temperature drop equation (2.29) and the temperature mixing equation (2.30).

a) Calculate $T_{s\_h1}^{(1)}, T_{s\_h2}^{(1)}$ based on $\dot{\boldsymbol{m}}^{(1)}$ and the known $T_{s1,source}(T_{s\_h3})$.

$$\begin{cases} T'_{s\_h1} = T'_{s\_h3}\Psi_{h1} \\ (\dot{m}_2 + \dot{m}_3)T'_{s\_h2} = \dot{m}_2\left(T'_{s\_h1}\Psi_{h2}\right) + \dot{m}_3\left(T'_{s\_h3}\Psi_{h3}\right) \end{cases}$$

$$\Rightarrow \begin{bmatrix} T_{s\_h1}^{(1)} \\ T_{s\_h2}^{(1)} \end{bmatrix} = \begin{bmatrix} 98.9994 \\ 96.8828 \end{bmatrix}$$

where $T'_s = T_s - T_a$, $\Psi = e^{-\frac{\lambda L}{C_p \dot{m}}}$.

b) Calculate $T_{r\_h1}^{(1)}, T_{r\_h2}^{(1)}$ based on $\dot{\boldsymbol{m}}^{(1)}$ and the known T_{o_h1}, T_{o_h2}.

$$\begin{cases} \dot{m}_1 T'_{r\_h1} = \dot{m}_2 T'_{r\_h2}\Psi_{h2} + (\dot{m}_1 - \dot{m}_2)T'_{o\_h1} \\ T'_{r\_h2} = T'_{o\_h2} \end{cases} \Rightarrow \begin{bmatrix} T_{r\_h1}^{(1)} \\ T_{r\_h2}^{(1)} \end{bmatrix}$$

$$= \begin{bmatrix} 49.5679 \\ 50.0000 \end{bmatrix}$$

c) Calculate $T_{r1,source}^{(1)}(T_{r\_h3}^{(1)})$ based on $\dot{\boldsymbol{m}}^{(1)}$ and $T_{r\_h1}^{(1)}, T_{r\_h2}^{(1)}$.

$$(\dot{m}_1 + \dot{m}_3)T'_{r\_h3} = \dot{m}_1\left(T'_{r\_h1}\Psi_{h1}\right) + \dot{m}_3\left(T'_{r\_h1}\Psi_{h3}\right)$$

$$\Rightarrow T_{r1,source}^{(1)} = T_{r\_h3}^{(1)} = 49.3397$$

6) The procedure of this decomposed hydraulic-thermal calculation is repeated from step 3) until the maximal $|\Delta \boldsymbol{F}_h|$, $|\Delta \boldsymbol{T}_s|$ and $|\Delta \boldsymbol{T}_r|$ become less than $\boldsymbol{\varepsilon} = 10^{-3}$.

   After 4 iterations, the converged results of the variables (pipe mass flow rates and temperatures) of the heat network are:

$$\begin{bmatrix} \dot{m}_1 \\ \dot{m}_2 \\ \dot{m}_3 \end{bmatrix} = \begin{bmatrix} 1.6420 \\ 0.1767 \\ 1.3451 \end{bmatrix}, \begin{bmatrix} T_{s\_h1} \\ T_{s\_h2} \\ T_{r\_h1} \\ T_{r\_h2} \\ T_{r1,source} \end{bmatrix} = \begin{bmatrix} 98.9576 \\ 97.1401 \\ 49.5583 \\ 50.0000 \\ 49.1251 \end{bmatrix}.$$

7) Calculate the heat power $\emptyset_{1,source}$ generated from Source 1.

   - Firstly, calculating $\dot{m}_{q1,source}$ based on $\dot{\boldsymbol{m}}$ from Step 6)

$$\dot{m}_{q1,source} = \dot{m}_1 + \dot{m}_3 = 1.6420 + 1.3451 = 2.9871 kg/s$$

   - Then, substituting $\dot{m}_{q1,source}$ and $T_{r1,source}$ from Step 6) into the heat power equation (2.27) to obtain

$$\begin{aligned} \emptyset_{1,source} &= C_p \dot{m}_{q1,source}\left(T_{s1,source} - T_{r1,source}\right) \\ &= 4.182 \times 10^{-3} \times 2.9871 \times (100 - 49.1251) \\ &= 0.6355 MW_{th} \end{aligned}$$

   Thus, the heat power losses in the heat network are: $\emptyset_{loss} = 0.0355 MW_{th}$.

8) Calculate the electrical power generated from Source 1 using equation (3.38), $P_{1,source} = \emptyset_{1,source}/c_{m1} = 0.6355/1.3 = 0.4889 MW_e$.

9) Electrical power flow calculation
a) Calculate the electrical mismatches $\Delta \boldsymbol{F}_e^{(1)}$. For the first iteration,

$$\Delta \boldsymbol{F}_e^{(1)} = \begin{bmatrix} P_{e1} - Re\{V_{e1}(Y_{e11}V_{e1} + Y_{e12}V_{e2} + Y_{e13}V_{e3})^*\} \\ P_{e2} - Re\{V_{e2}(Y_{e12}V_{e1} + Y_{e22}V_{e2} + Y_{e24}V_{e4})^*\} \\ P_{1,source} - Re\{V_{e3}(Y_{e13}V_{e1} + Y_{e33}V_{e3})^*\} \\ Q_{e1} - Im\{V_{e1}(Y_{e11}V_{e1} + Y_{e12}V_{e2} + Y_{e13}V_{e3})^*\} \\ Q_{e2} - Im\{V_{e2}(Y_{e12}V_{e1} + Y_{e22}V_{e2} + Y_{e24}V_{e4})^*\} \end{bmatrix}$$

$$= \begin{bmatrix} -0.0135 \\ -0.0954 \\ 0.3455 \\ 0.1899 \\ 0.0464 \end{bmatrix}$$

b) Hence, the electrical Jacobian matrix $\boldsymbol{J}_e^{(1)}$ is:

$\boldsymbol{J}_e^{(1)} =$

$$\begin{bmatrix} 9.8056 & -4.7832 & -5.0224 & 5.3231 & -2.7298 \\ -4.7832 & 9.6621 & 0.0000 & -2.7298 & 5.4050 \\ -5.0224 & 0.0000 & 5.0224 & -2.8663 & 0.0000 \\ -5.5961 & 2.7298 & 2.8663 & 9.3273 & -4.7832 \\ 2.7298 & -5.5142 & 0.0000 & -4.7832 & 9.4708 \end{bmatrix}$$

c) Update the state variables (voltage magnitudes and angles)

$$\begin{bmatrix} \boldsymbol{\theta} \\ |\boldsymbol{V}| \end{bmatrix}^{(1)} = \begin{bmatrix} \boldsymbol{\theta} \\ |\boldsymbol{V}| \end{bmatrix}^{(0)} - \left(\boldsymbol{J}_{\boldsymbol{e}}^{(1)}\right)^{-1} \Delta \boldsymbol{F}_e^{(1)} = \begin{bmatrix} 6.2584 \\ 2.5531 \\ 10.8359 \\ 1.0194 \\ 1.0092 \end{bmatrix}$$

d) After 3 iterations, the converged results of the state variables (voltage magnitudes and angles) of the electricity network are:

$$\begin{bmatrix} \theta_{e1} \\ \theta_{e2} \\ \theta_{e3} \\ |V_{e1}| \\ |V_{e2}| \end{bmatrix} = \begin{bmatrix} 5.6833 \\ 2.2959 \\ 9.9627 \\ 1.0150 \\ 1.0056 \end{bmatrix}$$

where the unit of voltage angle is ‘deg’ and the unit of voltage magnitude is *p.u*.

The results of the electrical power flow calculation is validated using IPSA and MATLAB toolbox MATPOWER [96, 97].

10) Calculate the electrical power generated from Grid, $P_{grid} = -0.1543 MW_e$.

Thus, the electrical power losses in the electricity network are: $P_{loss} = 0.0346MW_e$.

Steps 11) and 12) in Figure 3.9 are only applicable to the example in islanded mode, which will be discussed in the next section.

In the case of different coupling components, step 8) varies as follows

- **CHP and circulation pump**

  Following equation (3.38)

  $$P_{1,source} = \emptyset_{1,source}/c_{m1} - P_p = 0.6355/1.3 - 0.0045 = 0.4844MW_e$$

  where the electrical power consumed by the pump P_p is calculated using equation (3.6)

  $$P_p = \frac{\dot{m}_{q1,source} g H_p}{10^6 \eta_p} = \frac{2.9871 \times 9.81 \times 100.0959}{10^6 \times 0.65} = 0.0045MW_e$$

  where the pump head H_p is calculated using equation (3.7)

  $$H_p = 2\sum_{i\in\ell} h_{fi} + H_c = 2(K_1\dot{m}_1^2 + K_2\dot{m}_2^2) + H_{h2}$$
  $$= 2 \times (0.0473 + 0.0007) + 100 = 100.0959m$$

  where H_c is the minimum allowable head differential (m) which refers to H_{h2} in the network shown in Figure 3.11.

- **CHP, circulation pump and heat pump**

  Following equation (3.38)

  $$P_{1,source} = \emptyset_{1,source}/c'_{m1} - P_p = 0.6355/4.1667 - 0.0045 = 0.1480MW_e$$

  where the equivalent heat-to-power ratio c'_{m1} of a composite CHP and heat pump system is calculated using equation (3.10).

  $$c'_{m1} = \frac{c_{m1} + \alpha \cdot COP}{1 - \alpha} = \frac{1.3 + 0.4 \cdot 3}{1 - 0.4} = 4.1667$$

  where α is the percentage of a fraction of electrical power from the CHP unit modulated to drive the heat pump.

In all three cases, the results of the variables (pipe mass flow rates and temperatures) of the heat network are the same. The results of the

variables (voltage magnitudes and angles, electrical power and losses) of the electricity network are as shown in Table 3.6.

Table 3.6: Results of the decomposed electrical-hydraulic-thermal calculation

Variables	Decomposed calculation		
	CHP only	CHP+ pump	CHP+ pump + heat pump
θ_{e1}	5.6833	5.5877	-1.8469
θ_{e2}	2.2959	2.2485	-1.4584
θ_{e3}	9.9627	9.8211	-1.1908
$\|V_{e1}\|$	1.0150	1.0151	1.0189
$\|V_{e2}\|$	1.0056	1.0057	1.0087
$P_{1,source}(MW_e)$	0.4889	0.4844	0.1480
$P_{grid}(MW_e)$	-0.1543	-0.1506	0.1576
$P_{loss}(MW_e)$	0.0346	0.0338	0.0056

In cases 'CHP only' and 'CHP+pump', the results show that active power from the CHP unit is exported to Grid. In the case 'CHP+pump+heat pump', 40% of the electrical power from the CHP unit at Source 1 is modulated to drive the heat pump. Thus the net electrical power supplied from Source 1 to the loads is reduced, and more electrical power is imported from Grid. As a result of this change in the electrical power flow, the voltage angles drop in the case 'CHP+pump+heat pump' as shown in Table 3.6.

b) Islanded mode

A simple islanded electricity network and a district heating network are used to illustrate the use of the model in *islanded mode*, Figure 3.12. Source 1 provides the heat slack node and Source 2 provides the electricity slack busbar. Source 1 corresponds to an extraction steam turbine CHP unit and Source 2 corresponds to a gas turbine CHP unit. Following Table 3.1, the known and unknown variables are shown in Table 3.7. The parameters of the two networks are in the Appendix C.

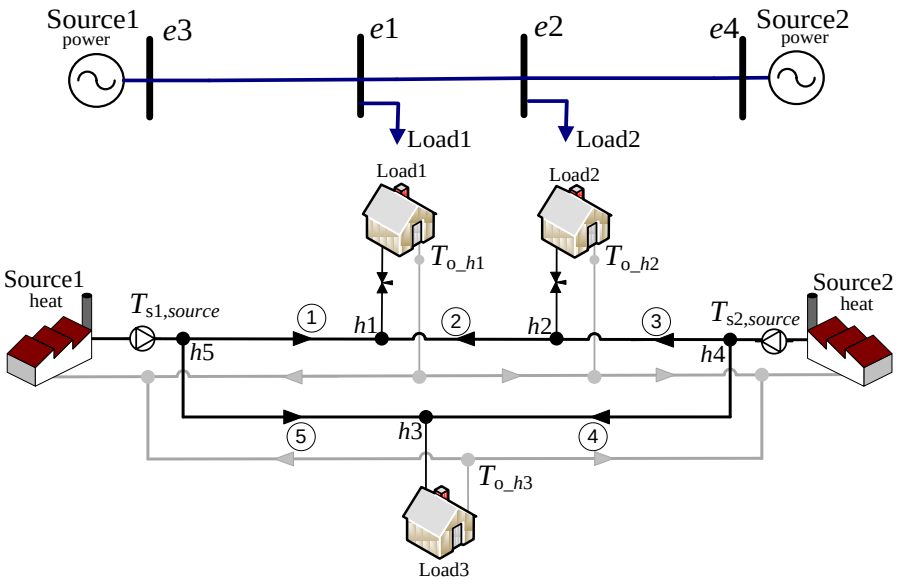

Figure 3.12: A simple islanded electricity network and a district heating network

(The numbering sequence starts with the loads, followed by the sources and the last element is the slack busbar or node)

Table 3.7: Known variables and unknown variables of electricity and heat networks

	Variables	**Known**	**Unknown**
Electricity network	voltage angle θ	θ_{e4}	θ_{e1}, θ_{e2}, θ_{e3}
	active power P	P_{e1}, P_{e2}	$P_{e3}(P_{1,source})$, $P_{e4}(P_{2,source})$
	voltage magnitude $\|V\|$	$\|V_{e3}\|(\|V_{1,source}\|)$, $\|V_{e4}\|(\|V_{2,source}\|)$	$\|V_{e1}\|$, $\|V_{e2}\|$
	reactive power Q	Q_{e1}, Q_{e2}	Q_{e3}, Q_{e4}
Heat network	pressure head H	H_{h2}	H_{h1}, H_{h3}, H_{h4}, H_{h5}
	heat power Φ	Φ_{h1}, Φ_{h2}, Φ_{h3}	$\Phi_{h4}(\Phi_{1,source})$, $\Phi_{h5}(\Phi_{2,source})$
	supply temperature T_s	$T_{s\_h4}(T_{s1,source})$, $T_{s\_h5}(T_{s2,source})$	T_{s_h1}, T_{s_h2}, T_{s_h3}
	return temperature T_r	T_{o_h1}, T_{o_h2}, T_{o_h3}	T_{r_h1}, T_{r_h2}, T_{r_h3}, $T_{r\_h4}(T_{r1,source})$, $T_{r\_h5}(T_{r2,source})$
	mass flow rate $\dot{m}$		$\dot{m}_1, \dot{m}_2, \dot{m}_3, \dot{m}_4, \dot{m}_5$

In this example, Source 1 and Source 2 refer to the coupling components (CHP units, heat pumps and circulation pumps) that link the electricity and heat networks.

Following from equations (3.25), (3.26) and (3.36), for the extraction steam turbine CHP unit at Source 1, $P_{1,source}$ is expressed as

$$P_{1,source} = \begin{cases} -\emptyset_{1,source}/\mathrm{Z} + \eta_e F_{in}, & CHP\ only \\ -\emptyset_{1,source}/\mathrm{Z} + \eta_e F_{in} - P_p, & CHP + pump \\ \dfrac{1-\alpha}{\alpha COP - Z}\left(\emptyset_{1,source} - Z\eta_e F_{in}\right) - P_p, & CHP + pump \\ & +heat\ pump \end{cases} \quad (3.39)$$

In the case 'CHP+pump+heat pump', a heat pump is connected to the CHP unit at Source 1 in cascade and fed by cogenerated electricity.

Following from equations (3.25) and (3.26), for the gas turbine CHP unit at Source 2, $\emptyset_{2,source}$ is expressed as

$$\emptyset_{2,source} = \begin{cases} c_{m2}P_{2,source}, & CHP\ only \\ c_{m2}P_{2,source} - P_p, & CHP + pump \end{cases} \quad (3.40)$$

For the heat supply network shown in Figure 3.12, the network incidence matrix ***A*** and the loop incidence matrix ***B*** are

A =

Node No. \ Pipe No.	1	2	3	4	5
1	1	1	0	0	0
2	0	-1	1	0	0
3	0	0	0	1	1
4	0	0	-1	-1	0
5	-1	0	0	0	-1

B =

Loop No. \ Pipe No.	1	2	3	4	5
1	1	-1	-1	1	-1

The procedure used to illustrate the use of the model is through determining the heat and electrical power generated from Source 1 and Source 2 at each iteration, Figure 3.13. This Figure illustrates the steps 7, 8, 10, 11 in the flowchart as shown in Figure 3.9. In Figure 3.13, the

left line that slopes downward describes the performance curve of an extraction steam turbine CHP unit at Source 1 and the slope is equal to the negative of the Z ratio of Source 1 (-Z). The right line that slopes upward describes the performance curve of a gas turbine CHP unit at Source 2 and the slope is equal to the heat-to-power ratio of Source 2 (c_{m2}).

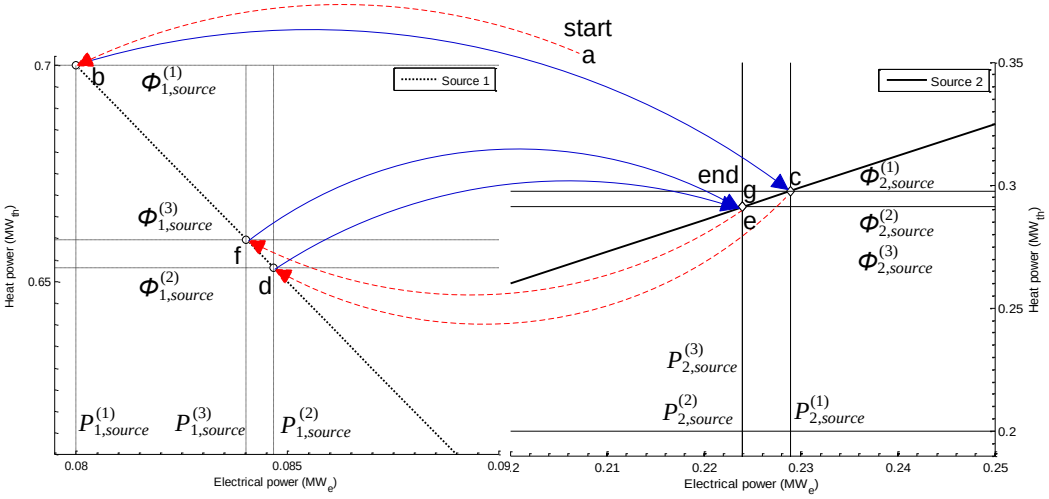

Figure 3.13: Procedure to calculate the electrical and heat power from both Source 1 and Source 2 that link electricity and heat networks

Following Figure 3.9, the steps used to solve the model for the example networks linked by a CHP unit only are as follows

1) Start with the known variables as shown in Table 3.7.
2) Assume the initial conditions for the heat and electricity networks are as follows:

   Heat:

   $$T^{(0)}_{s\_h1} = T^{(0)}_{s\_h2} = T^{(0)}_{s\_h3} = 100°\text{C},$$

   $$\dot{\boldsymbol{m}}^{(0)} = [1 \quad 1 \quad 1 \quad 1 \quad 1]^T.$$

   $$\emptyset^{(0)}_{2,source} = 0.2MW_{th}.$$

   Electricity:

   $$\left[\theta^{(0)}_{e1} \quad \theta^{(0)}_{e2} \quad \theta^{(0)}_{e3} \quad \left|V^{(0)}_{e1}\right| \quad \left|V^{(0)}_{e2}\right|\right]^T = [0 \quad 0 \quad 0 \quad 1 \quad 1]^T.$$

Iteration i = 1.

3-6) Solve the hydraulic and thermal model, represented in Figure 3.13 as the red dashed arrow a→b when i = 1.

7) Calculate $\emptyset_{1,source}^{(i)}$, represented in Figure 3.13 as a horizontal dotted line.

8) Calculate $P_{1,source}^{(i)}$, represented in Figure 3.13 as a vertical dotted line, according to the performance curve of Source 1 using equation (3.39).

9) Solve the electrical power flow model, represented in Figure 3.13 as the blue solid arrow b→c when i = 1.

10) Calculate $P_{2,source}^{(i)}$, represented in Figure 3.13 as a vertical solid line.

11) Calculate $\emptyset_{2,source}^{(i)}$, represented in Figure 3.13 as a horizontal solid line, according to the performance curve of Source 2 using equation (3.40).

12) This procedure is repeated from step 3 until $\Delta\emptyset_{2,source}^{(i)} = \emptyset_{2,source}^{(i)} - \emptyset_{2,source}^{(i-1)}$ becomes less than the tolerance ε. $i = i + 1$.

The number of iterations for the hydraulic and thermal model and the electrical power flow model is shown in Table 3.8. After 16 total iterations (3 + 3 + 4 + 2 + 3 + 1 = 16), the results converged.

Table 3.8: Number of iterations in the hydraulic and thermal and electrical models

Model	Hydraulic and thermal	Electrical	Hydraulic and thermal	Electrical	Hydraulic and thermal	Electrical
	a → b	b → c	c → d	d → e	e → f	f → g
No. of iterations	3	3	4	2	3	1

In the case of different coupling components, the results of the variables of the electricity and heat networks are shown in Table 3.9.

Table 3.9: Results of the decomposed electrical-hydraulic-thermal calculation

Variables	Decomposed calculation		
	CHP only	CHP+pump	CHP+pump +heat pump
$\|V_{e1}\|$	1.0186	1.0186	1.0183
$\|V_{e2}\|$	1.0083	1.0082	1.0079
θ_{e1}	-3.3541	-3.4494	-4.0351
θ_{e2}	-2.2118	-2.2595	-2.5522
θ_{e3}	-3.4214	-3.5624	-4.4287
$\dot{m}_1$	1.7705	1.7605	1.7083
$\dot{m}_2$	-0.3075	-0.2973	-0.2443
$\dot{m}_3$	1.2004	1.2104	1.2623
$\dot{m}_4$	0.1622	0.1840	0.2957
$\dot{m}_5$	1.3392	1.3176	1.2065
T_{s_h1}	99.0328	99.0273	98.9978
T_{s_h2}	97.5749	97.5812	97.6164
T_{s_h3}	97.7798	97.7728	97.7532
T_{r_h1}	49.5810	49.5790	49.5692
T_{r_h2}	50.0000	50.0000	50.0000
T_{r_h3}	50.0000	50.0000	50.0000
T_{r_h4}	48.9132	48.9343	49.0370
T_{r_h5}	49.2749	49.2678	49.2288
$\emptyset_{1,source}$	0.6597	0.6531	0.6189
$P_{1,source}$	0.0840	0.0847	0.0601
$\emptyset_{2,source}$	0.2920	0.2976	0.3319
$P_{2,source}$	0.2246	0.2310	0.2577
P_{loss}	0.0087	0.0111	0.0134
$\emptyset_{loss}$	0.0517	0.0506	0.0508

Based on Table 3.9, the bar chart in Figure 3.14 is used to show the heat and electrical power supplied from two sources. The electrical (heat) network losses are expressed as the differences between the sum of the electrical (heat) power of two sources and total electrical (heat) loads.

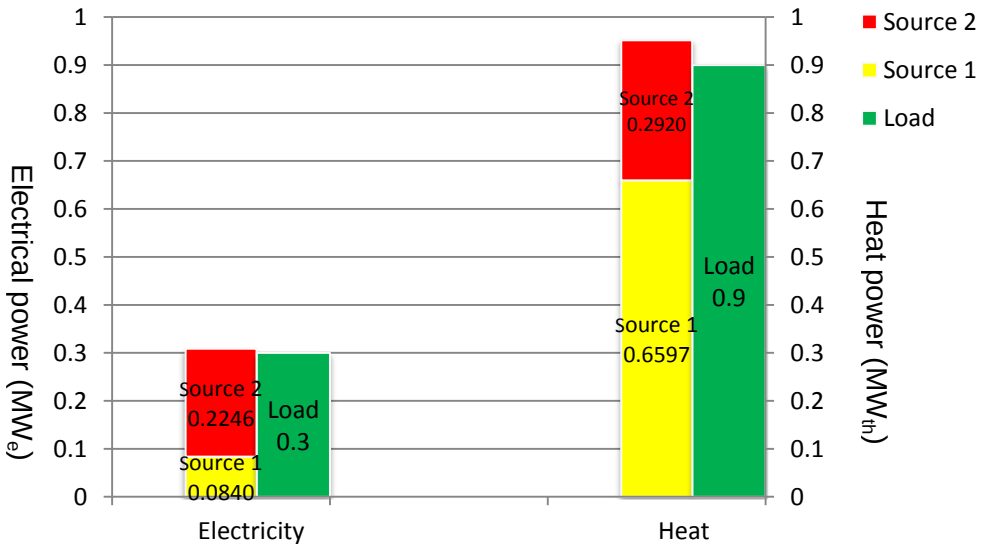

Figure 3.14: Electrical and heat power supplied from two sources

3.5.2 Integrated Electrical-Hydraulic-Thermal Calculation

a) Grid-connected mode

To illustrate the integrated electrical-hydraulic-thermal calculation in *grid-connected mode*, the model equations are applied to the electricity and heat networks shown in Figure 3.11.

Following equation (3.31), the state variables $\boldsymbol{x}$ are

$$\boldsymbol{x} = \begin{bmatrix} \theta_{e1} \\ \theta_{e2} \\ \theta_{e3} \\ |V_{e1}| \\ |V_{e2}| \\ \dot{m}_1 \\ \dot{m}_2 \\ \dot{m}_3 \\ T'_{s\_h1} \\ T'_{s\_h2} \\ T'_{r\_h1} \\ T'_{r\_h2} \end{bmatrix} \tag{3.41}$$

Following equation (3.32), the vector of total mismatches $\Delta \boldsymbol{F}$ for the electricity and heat networks shown in Figure 3.11 are

$$
\begin{aligned}
&\Delta \boldsymbol{F} \\
&= \begin{bmatrix}
\begin{bmatrix} P_{e1}^{sp} - Real\{V_{e1}(Y_{e11}V_{e1} + Y_{e12}V_{e2} + Y_{e13}V_{e3})^*\} \\ P_{e2}^{sp} - Real\{V_{e2}(Y_{e12}V_{e1} + Y_{e22}V_{e2} + Y_{e24}V_{e4})^*\} \\ P_{e3}^{sp} - Real\{V_{e3}(Y_{e13}V_{e1} + Y_{e33}V_{e3})^*\} \end{bmatrix} \\
\begin{bmatrix} Q_{e1}^{sp} - Imag\{V_{e1}(Y_{e11}V_{e1} + Y_{e12}V_{e2} + Y_{e13}V_{e3})^*\} \\ Q_{e2}^{sp} - Imag\{V_{e2}(Y_{e12}V_{e1} + Y_{e22}V_{e2} + Y_{e24}V_{e4})^*\} \end{bmatrix} \\
\begin{bmatrix} C_p \begin{bmatrix} 1 & -1 & 0 \\ 0 & 1 & 1 \end{bmatrix} \begin{bmatrix} \dot{m}_1 \\ \dot{m}_2 \\ \dot{m}_3 \end{bmatrix} \left(\begin{bmatrix} T'_{s\_h1} \\ T'_{s\_h2} \end{bmatrix} - \begin{bmatrix} T'_{o\_h1} \\ T'_{o\_h2} \end{bmatrix} \right) - \begin{bmatrix} \emptyset_{h1}^{sp} \\ \emptyset_{h2}^{sp} \end{bmatrix} \end{bmatrix} \\
[K_1\dot{m}_1|\dot{m}_1| + K_2\dot{m}_2|\dot{m}_2| - K_3\dot{m}_3|\dot{m}_3|] \\
\begin{bmatrix} 1 & 0 \\ -\dot{m}_2\Psi_2 & q_2 \end{bmatrix} \begin{bmatrix} T'_{s\_h1} \\ T'_{s\_h2} \end{bmatrix} - \begin{bmatrix} T'_{s\_h3}\Psi_1 \\ \dot{m}_3 T'_{s\_h3}\Psi_3 \end{bmatrix} \\
\begin{bmatrix} \dot{m}_1 & -\dot{m}_2\Psi_2 \\ 0 & 1 \end{bmatrix} \begin{bmatrix} T'_{r\_h1} \\ T'_{r\_h2} \end{bmatrix} - \begin{bmatrix} \dot{m}_{q1} T'_{o\_h1} \\ T'_{o\_h2} \end{bmatrix}
\end{bmatrix}
\end{aligned}
\tag{3.42}
$$

where *Real* represents the real part of a complex expression and *Imag* represents the imaginary part of a complex expression. Following equations (3.24), (3.25), (3.26) and (3.36), P_{e3}^{sp} in the 3rd row of $\Delta \boldsymbol{F}$ is a function of the heat network and is expressed as

$$
\begin{aligned}
&P_{e3}^{sp} \\
&= \begin{cases}
C_p \dot{m}_{q\_h3}\left(T'_{s\_h3} - T'_{r\_h3}\right)/c_{m1}\,, & CHP\ only \\
C_p \dot{m}_{q\_h3}\left(T'_{s\_h3} - T'_{r\_h3}\right)/c_{m1} - P_p\,, & CHP + pump \\
C_p \dot{m}_{q_{h3}}\left(T'_{s_{h3}} - T'_{r_{h3}}\right)/c'_{m1} - P_p, & CHP + pump \\
 & +heat\ pump
\end{cases}
\end{aligned}
\tag{3.43}
$$

The steps used to solve the integrated electrical-hydraulic-thermal calculation for the example networks shown in Figure 3.11 linked by a CHP unit only are as follows

a) Assume the initial condition as,

$$
\begin{aligned}
&\boldsymbol{x}^{(0)} \\
&= \left[\theta_{e1}^{(0)} \quad \theta_{e2}^{(0)} \quad \theta_{e3}^{(0)} \quad \left|V_{e1}^{(0)}\right| \quad \left|V_{e2}^{(0)}\right| \quad \dot{m}_1^{(0)} \quad \dot{m}_2^{(0)} \quad \dot{m}_3^{(0)} \quad T'^{(0)}_{s\_h1} \quad T'^{(0)}_{s\_h2} \quad T'^{(0)}_{o\_h1} \quad T'^{(0)}_{o\_h2}\right]^T \\
&= [0 \quad 0 \quad 0 \quad 1 \quad 1 \quad 1 \quad 1 \quad 1 \quad 90 \quad 90 \quad 40 \quad 40]^T
\end{aligned}
$$

b) Calculate the mismatches $\Delta \boldsymbol{F}$. For the first iteration,

$$
\Delta \boldsymbol{F}^{(1)} = [0.0135 \quad 0.0954 \quad -0.178 \quad -0.190 \quad -0.0464 \ \ldots
$$

$$-0.300 \quad 0.118 \quad 0.009 \quad 1.705 \quad 4.251 \quad 0.758 \quad 0]^T,$$

c) Hence, the Jacobian matrix $\boldsymbol{J}$ is:

$\boldsymbol{J}^{(1)} =$

9.806	-4.783	-5.022	5.323	-2.730								
-4.783	9.662		-2.730	5.405								
-5.022		5.022	-2.866		-0.277		-0.277					
-5.596	2.730	2.866	9.327	-4.783								
2.730	-5.514		-4.783	9.471								
					0.209	-0.209						
						0.209	0.209		0.008			
					0.036	0.036	-0.054					
								1.000				
								-0.981	2.000			
										1.000	-0.981	
											1.000	

d) Update the state variables. For the first iteration,

$$\boldsymbol{x}^{(1)} = x^{(0)} - \left(\boldsymbol{J}^{(1)}\right)^{-1}\Delta\boldsymbol{F}^{(1)}$$

$$= [0.151 \quad 0.065 \quad 0.251 \quad 1.019 \quad 1.009 \cdots$$

$$1.762 \quad 0.327 \quad 1.226 \quad 88.295 \quad 87.038 \quad 39.242 \quad 40.000]^T.$$

e) The procedure is repeated until the maximum absolute value of elements in the mismatches $|\Delta\boldsymbol{F}|$ becomes less than the tolerance $\boldsymbol{\varepsilon}$ = 10^{-3}.

After 5 iterations, the converged results of the variables of the networks are:

$$\begin{bmatrix} \dot{m}_1 \\ \dot{m}_2 \\ \dot{m}_3 \\ T_{s\_h1} \\ T_{s\_h2} \\ T_{r\_h1} \\ T_{r\_h2} \end{bmatrix} = \begin{bmatrix} 1.6420 \\ 0.1767 \\ 1.3451 \\ 98.9575 \\ 97.1400 \\ 49.5583 \\ 50.0000 \end{bmatrix}, \begin{bmatrix} \theta_{e1} \\ \theta_{e2} \\ \theta_{e3} \\ |V_{e1}| \\ |V_{e2}| \end{bmatrix} = \begin{bmatrix} 5.6831 \\ 2.2958 \\ 9.9625 \\ 1.0150 \\ 1.0056 \end{bmatrix}$$

$T_{r1,source} = 49.1252.$

$\emptyset_{1,source} = 0.6355 MW_{th}.$

In the case of different coupling components, the results of the variables (pipe mass flow rates and temperatures) of the heat network are the same. The results of the variables (voltage magnitudes and angles, electrical power and losses) of the electricity network are as shown in Table 3.10.

Table 3.10: Results of the integrated electrical-hydraulic-thermal calculation

Variables	Integrated calculation		
	CHP only	CHP + pump	CHP + pump + heat pump
θ_{e1}	5.6831	5.5875	-1.8469
θ_{e2}	2.2958	2.2484	-1.4584
θ_{e3}	9.9625	9.8210	-1.1909
$\lvert V_{e1}\rvert$	1.0150	1.0151	1.0189
$\lvert V_{e2}\rvert$	1.0056	1.0057	1.0087
$P_{1,source}(MW_e)$	0.4889	0.4843	0.1480
$P_{grid}(MW_e)$	-0.1543	-0.1506	0.1576
$P_{loss}(MW_e)$	0.0346	0.0338	0.0056

b) Islanded mode

To illustrate the use of the model in *islanded mode*, the model equations are applied to the electricity and heat networks shown in Figure 3.12.

The procedure used to illustrate the example networks linked by a CHP unit only is shown in Figure 3.15. During each iteration, the electrical and heat power generated from two sources are obtained simultaneously, which are represented as the points on the performance curves (the left line that slopes downward and the right line that slopes upward) of two CHP units. Due to the scale of the graph, starting from the 6th points on two lines, the two points on two lines are then simultaneously moved to the next two points with the same index at each iteration. The iteration procedure is repeated until the maximum absolute value of elements in the mismatches $|\Delta \boldsymbol{F}|$ becomes less than the tolerance $\boldsymbol{\varepsilon} = 10^{-3}$. After **12** iterations, the results converged.

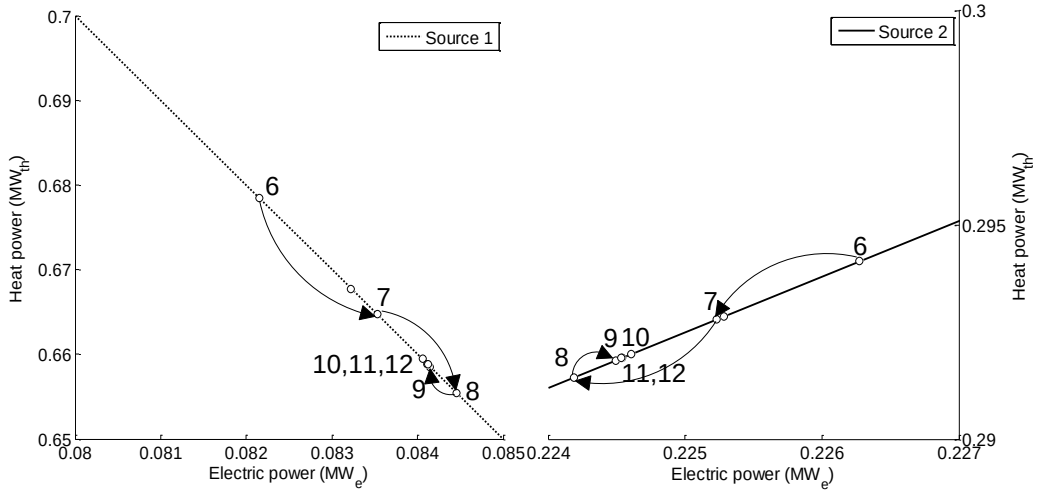

Figure 3.15: Procedure to calculate the electrical and heat power from both Source 1 and Source 2 that link electricity and heat networks

Following from equations (3.25), (3.26) and (3.36), for the extraction steam turbine CHP unit at Source 1, $P_{1,source}$ is expressed as

$$P_{1,source}^{sp} = \begin{cases} -\emptyset_{1,source}/\mathrm{Z} + \eta_e F_{in}, & CHP\ only \\ -\emptyset_{1,source}/\mathrm{Z} + \eta_e F_{in} - P_p, & CHP + pump \\ \dfrac{1-\alpha}{\alpha COP - Z}\left(\emptyset_{1,source} - Z\eta_e F_{in}\right) - P_p, & CHP + pump \\ & +heat\ pump \end{cases} \quad (3.44)$$

where $\emptyset_{1,source} = C_p \dot{m}_{q1,source}\left(T'_{s1,source} - T'_{r1,source}\right)$.

In the case 'CHP+pump+heat pump', a heat pump is connected to the CHP unit at Source 1 in cascade and fed by cogenerated electricity.

Following from equations (3.25) and (3.26), for the gas turbine CHP unit at Source 2, $\emptyset_{2,source}$ is expressed as

$$\emptyset_{2,source}^{sp} = \begin{cases} c_{m2} P_{2,source}, & CHP\ only \\ c_{m2} P_{2,source} - P_p, & CHP + pump \end{cases} \quad (3.45)$$

where $P_{2,source} = Re\left\{V_{2,source} \sum_{k=1}^{N} (Y_{ik} V_k)^*\right\}$.

In the case of different coupling components, the results of the variables of the electricity and heat networks are shown in Table 3.11.

Table 3.11: Results of the integrated electrical-hydraulic-thermal calculation

Variables	Integrated calculation		
	CHP only	CHP + pump	CHP + pump + heat pump
$\|V_{e1}\|$	1.0186	1.0186	1.0183
$\|V_{e2}\|$	1.0083	1.0082	1.0079
θ_{e1}	-3.3523	-3.4439	-4.0303
θ_{e2}	-2.2109	-2.2567	-2.5498
θ_{e3}	-3.4187	-3.5542	-4.4216
$\dot{m}_1$	1.7693	1.7571	1.7043
$\dot{m}_2$	-0.3063	-0.2939	-0.2401
$\dot{m}_3$	1.2016	1.2137	1.2663
$\dot{m}_4$	0.1648	0.1912	0.3042
$\dot{m}_5$	1.3367	1.3105	1.1981
T_{s_h1}	99.0321	99.0257	98.9953
T_{s_h2}	97.5757	97.5831	97.6195
T_{s_h3}	97.7787	97.7710	97.7522
T_{r_h1}	49.5807	49.5785	49.5684
T_{r_h2}	50.0000	50.0000	50.0000
T_{r_h3}	50.0000	50.0000	50.0000
T_{r_h4}	48.9160	48.9406	49.0449
T_{r_h5}	49.2740	49.2655	49.2253
$\emptyset_{1,source}$	0.6589	0.6509	0.6163
$P_{1,source}$	0.0841	0.0849	0.0603
$\emptyset_{2,source}$	0.2919	0.3000	0.3347
$P_{2,source}$	0.2245	0.2308	0.2575
P_{loss}	0.0087	0.0110	0.0134
$\emptyset_{loss}$	0.0508	0.0509	0.0510

The differences of the results of the cases ‘CHP only’ and ‘CHP+pump’ are not significant, which means the impact of the circulation pump to the interaction of two networks is small. In the case ‘CHP+pump+heat pump’, 40% of the electrical power from the CHP unit at Source 1 is modulated to drive the heat pump. Thus the net electrical power supplied from Source 1 to the loads is reduced, and more electrical power is supplied from Source 2. As a result of this change in the electrical power flow, the voltage angles drop in the case ‘CHP+pump+heat pump’ as shown in Table 3.11.

3.5.3 Comparison of Two Calculation Techniques

The comparison is based on the example networks in Figure 3.12. The slight differences of the results between the integrated electrical-hydraulic-thermal calculation and the decomposed electrical-hydraulic-thermal calculation are as shown in Table 3.12. Variables (θ_{e3}, $\dot{m}_4$, $\dot{m}_5$ and T_{r_h4}) have larger differences. The differences are because of the different stopping criteria of two calculations and the simplification of the integrated Jacobian matrix in the integrated calculation. It is shown that the solutions of two calculations are sufficiently accurate.

Table 3.12: Differences of the solutions between decomposed and integrated calculations

Variables	Differences between the decomposed calculation and integrated calculation		
	CHP only	CHP+pump	CHP+pump +heat pump
$\|V_{e1}\|$	0.0000	0.0000	0.0000
$\|V_{e2}\|$	0.0000	0.0000	0.0000
θ_{e1}	-0.0018	-0.0055	-0.0048
θ_{e2}	-0.0009	-0.0028	-0.0024
θ_{e3}	-0.0027	-0.0082	-0.0071
$\dot{m}_1$	0.0012	0.0034	0.0040
$\dot{m}_2$	-0.0012	-0.0034	-0.0042
$\dot{m}_3$	-0.0012	-0.0033	-0.0040
$\dot{m}_4$	-0.0026	-0.0072	-0.0085
$\dot{m}_5$	0.0025	0.0071	0.0084
T_{s_h1}	0.0007	0.0016	0.0025
T_{s_h2}	-0.0008	-0.0019	-0.0031
T_{s_h3}	0.0011	0.0018	0.0010
T_{r_h1}	0.0003	0.0005	0.0008
T_{r_h2}	0.0000	0.0000	0.0000
T_{r_h3}	0.0000	0.0000	0.0000
T_{r_h4}	-0.0028	-0.0063	-0.0079
T_{r_h5}	0.0009	0.0023	0.0035
$\emptyset_{1,source}$	0.0008	0.0022	0.0026
$P_{1,source}$	-0.0001	-0.0002	-0.0002
$\emptyset_{2,source}$	0.0001	-0.0024	-0.0028
$P_{2,source}$	0.0001	0.0002	0.0002
P_{loss}	0.0000	0.0001	0.0000
$\emptyset_{loss}$	0.0009	-0.0003	-0.0002

The convergence characteristics of two calculations are shown in Figure 3.16. The integrated electrical-hydraulic-thermal calculation was solved

in 12 iterations and the decomposed electrical-hydraulic-thermal calculation was solved in 16 iterations. The integrated calculation achieves fewer iterations than the decomposed calculation, because the set of equations is solved as a whole using the Newton-Raphson method, providing quadratic convergence with respect to time. However, the integrated calculation requires more computations per iteration than the decomposed calculation. In the decomposed calculation, the electrical power flow equations and the hydraulic and thermal model equations are solved individually, hence this method requires more iterations.

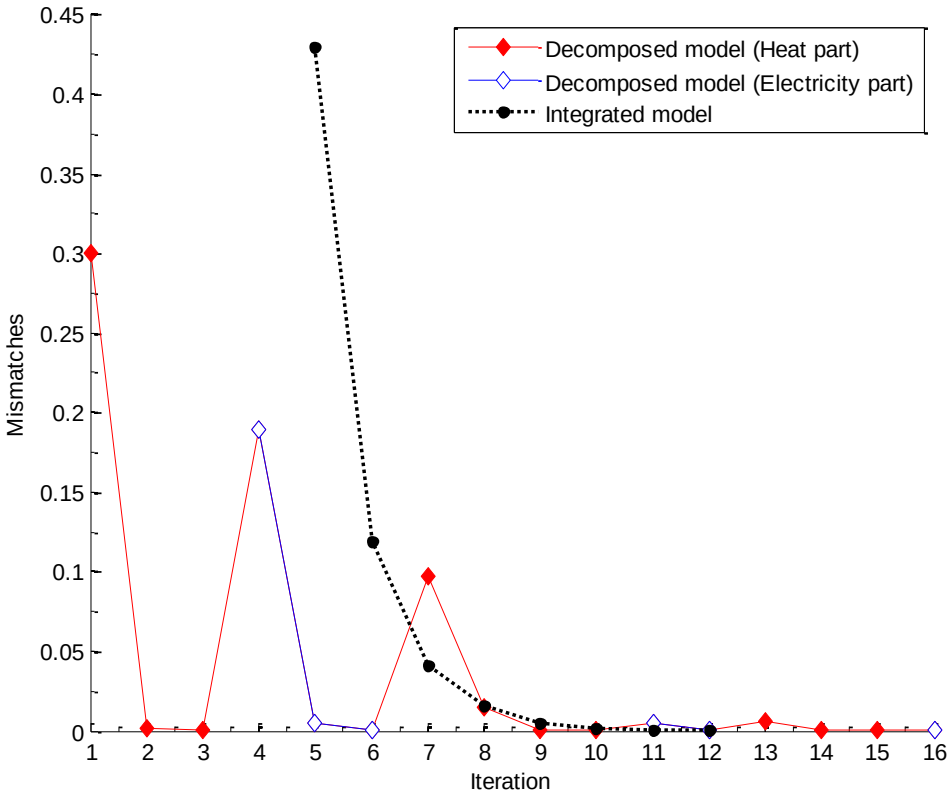

Figure 3.16: Convergence characteristics of the decomposed and integrated electrical-hydraulic-thermal calculations

3.6 Summary

The use of CHP units and heat pumps increases the linkages between electricity and heat networks. A combined analysis was developed to investigate the performance of electricity and heat networks as an integrated whole. This was based on a model of electrical power flow and hydraulic and thermal circuits together with their coupling components elements (CHP units, heat pumps, electric boilers and circulation pumps). The combined analysis took into account the flows of energy between the electricity and heat networks through the coupling components.

Two calculation techniques (decomposed and integrated electrical-hydraulic-thermal calculations) were developed. Three combinations of coupling mechanisms (CHP only; CHP and circulation pump; CHP, circulation pump and heat pump) were considered in each calculation. The calculations were demonstrated in grid-connected and islanded operation modes.

In grid-connected mode, any surplus or deficit in electrical power is supplied from the main grid and not from the CHP units, thus there is no linkage back from the electrical system to the heat system. While in islanded mode there are bidirectional linkages between the electricity and heat networks.

For the *decomposed electrical-hydraulic-thermal* calculation in grid-connected mode, the hydraulic and thermal model was solved first. Then these results were transferred to the electricity network through the coupling components. Finally the electrical power flow model was solved. In islanded mode, this sequential procedure was iterated until the solution converged to an acceptable tolerance.

For the *integrated electrical-hydraulic-thermal* calculation, the electrical power flow equations, the hydraulic equations and the thermal equations were combined to form a single system of equations and solved simultaneously as an integrated whole using the Newton-Raphson method.

Using the combined analysis, the variables of the electrical and heat networks were calculated. These included: heat and electrical power from the CHP units, mass flow rates, supply and return temperatures, voltage magnitudes and voltage angles, heat and electrical power losses.

The results of the decomposed and integrated calculations were very close to 10^{-3} precision. The real values were used in the calculation of heat networks and the per unit was used in the calculation of electrical networks. The convergence characteristics of two calculations were compared. The comparison showed that the integrated calculation requires fewer iterations than the decomposed calculation. In a simple example network, the *decomposed* calculation was solved in 16 iterations and the *integrated* calculation was solved in 12 iterations.

The combined analysis can be used for the design and operation of integrated heat and electricity systems for energy supply to buildings. This will increase the flexibility of the electricity and heat supply systems for facilitating the integration of intermittent renewable energy.

Chapter 4 - Case Study

4.1 Introduction

The linkage between the electricity and heat networks is formed by coupling components with unknown electrical and heat power. The coupling components can be CHP units, heat pumps and electric boilers. The schematic diagram for the linkages is shown in Figure 4.1. The electrical and heat power generated from all sources, except the slack busbar or node, are known, there is one linkage in grid-connected mode and two linkages in islanded mode through the slack busbar or node.

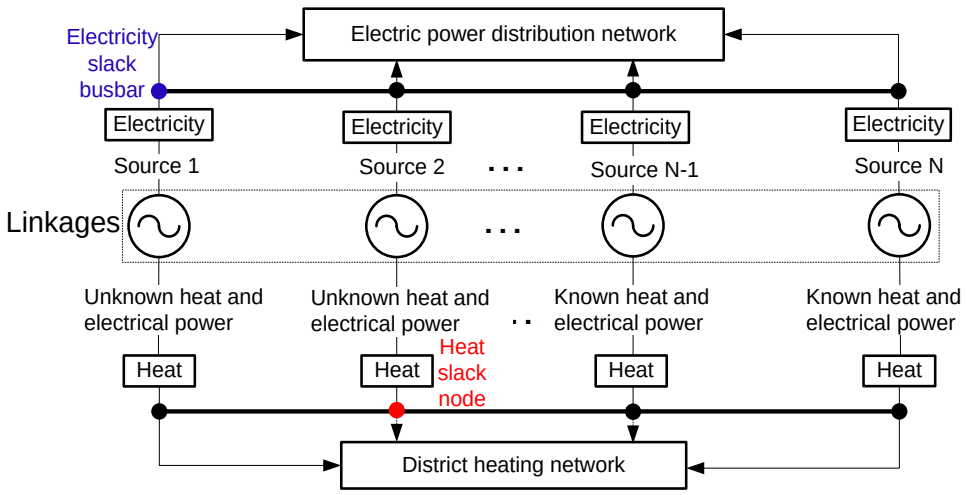

Figure 4.1: Linkages between electricity and district heating networks

To demonstrate the capabilities of the combined analysis, a case study was conducted. The decomposed and integrated calculation techniques were used to investigate the Barry Island electricity and district heating networks.

The Barry Island case study examines how electrical and heat demands in a self-sufficient system (no interconnection with external systems) are met using CHP units. The following variables of the electrical and heat networks are calculated:

- heat and electrical power supplied from CHP units,
- mass flow rates within each pipe, and supply and return temperatures at each node in the heat network,
- voltage magnitude at each load and voltage angle at each busbar in the electricity network.

4.2 Network Description

The Barry Island electricity and district heating networks are shown in Figure 4.2. The heat network is a low temperature looped pipe district heating network fed by three CHP units. The Barry Island district heating network was based on Reference [98], with more sources and looped network added. The electrical network parameters were from Reference [99].

Source 1 is a gas turbine CHP unit. Source 2 is an extraction steam turbine CHP unit. Source 3 is a reciprocating engine CHP unit. The capacities of the gas turbine and steam turbine CHP units are larger than the reciprocating engine CHP unit [100]. Therefore the gas turbine CHP unit at Source 1 is chosen as the electricity slack busbar and the steam turbine CHP unit at Source 2 is chosen as the heat slack node.

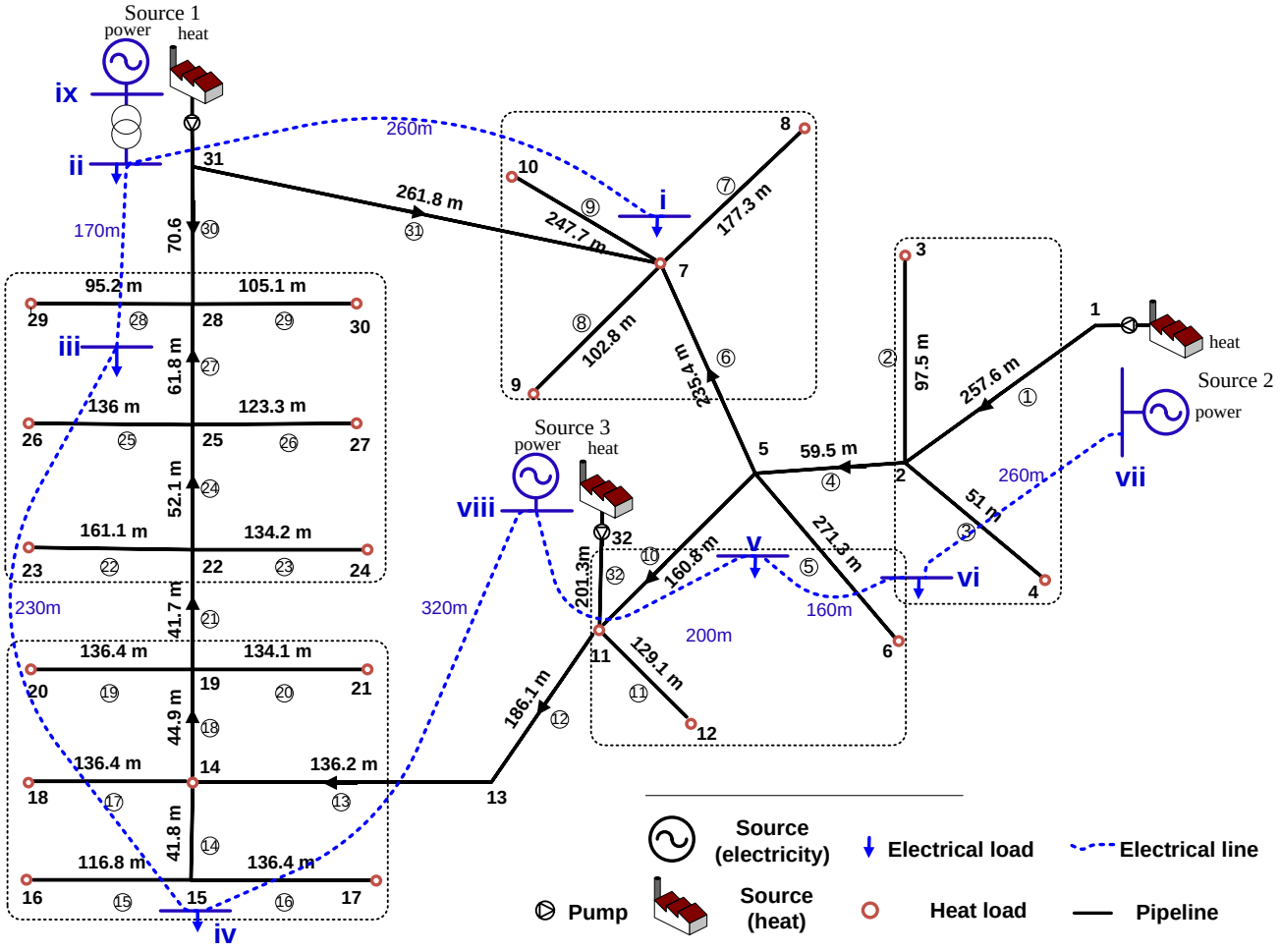

Figure 4.2: Schematic diagram of the electricity and district heating networks of the Barry Island case study

4.2.1 Electricity Network

The schematic diagram of the electric power distribution network is shown in Figure 4.3. The electrical power is supplied to 5 lumped electrical loads through a 11/0.433kV transformer at each feeder. Source 1 is connected to the 11kV distribution network through a 33/11.5kV transformer. Busbar ix is the slack busbar.

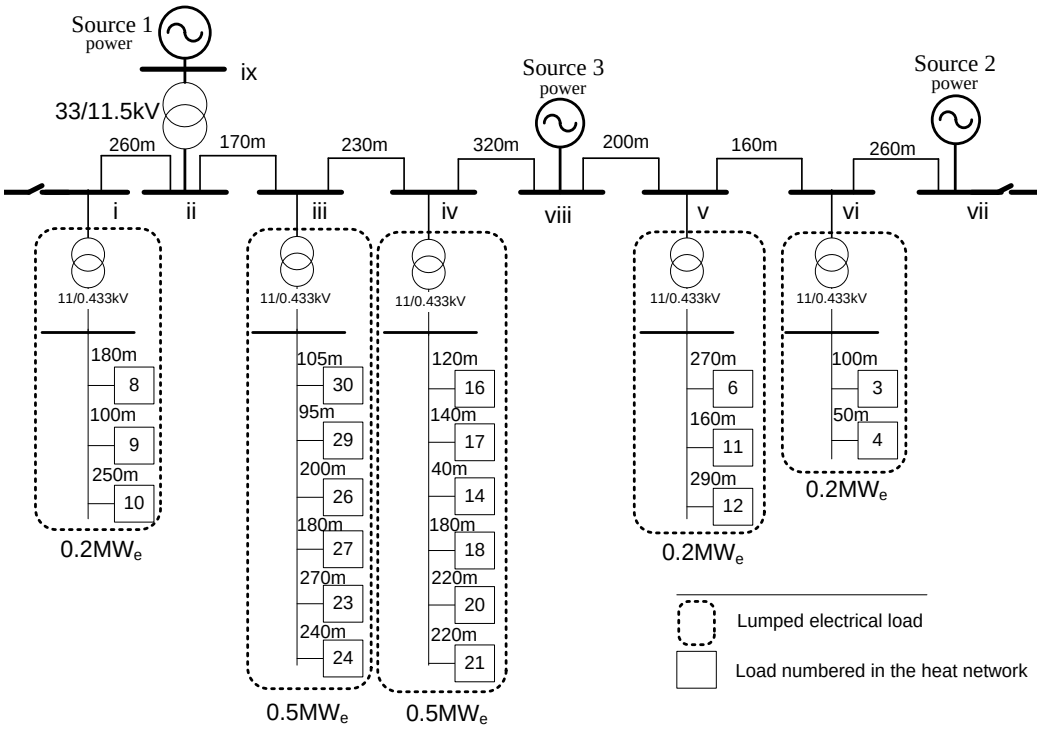

Figure 4.3: Schematic diagram of the electric power distribution network of the Barry Island case study

For the electricity network, the following assumptions were made:

- The base apparent power is 1MVA and base voltage is 11kV.
- The impedance of 185mm^2 Cable is 0.164 + j0.080Ω/km [99].
- 33/11.5kV 15MVA transformer has an impedance of 18% and X/R ratio of 15 [99].
- Active power of 5 lumped electrical loads at each load busbar:

  P_i = 0.2MW$_e$,

  P_{iii} = 0.5MW$_e$,

P_{iv} = 0.5MW_e,

P_v = 0.2MW_e,

P_{vi} = 0.2MW_e.

- Power factor of each electrical load: *p.f.* = 1.
- Voltage magnitude of each Source:

  $|V_{1,source}|$ = 1.02*p.u.*,

  $|V_{2,source}|$ = 1.05*p.u.*,

  $|V_{3,source}|$ = 1.05*p.u.*

- Voltage angle of Source 1: $\theta_{1,source}$ = 0°.

The input data of the units of the electrical system were converted into per unit:

- For the impedance of each cable:

  Taking the cable i-ii as an example, the length is 260m, thus the impedance of the cable is $Y_{12} = (0.164 + \mathrm{j}0.080) \times 260/1000 = 0.0426 + \mathrm{j}0.0208\Omega$.

  The base impedance is $Y_{base} = \frac{(11kV)^2}{1MVA} = 121\Omega$, thus the impedance of the cable is $Y_{12} = (0.0426 + \mathrm{j}0.0208)/121 = (3.5240 + \mathrm{j}1.7190) \times 10^{-4} p.u.$

- For the impedance of the 33/11.5kV transformer:

  The transformer is 15MVA and the system base apparent power is 1MVA, thus the reactance of the transformer is X_{trans} = 18%/15 = 0.012*p.u.*

  The X/R ratio is 15, thus the resistance of the transformer is R_{trans} = 0.012/15 = 0.0008*p.u.*

- For active power at each load busbar:

The base apparent power is 1MVA, thus

P_i = 0.2*p.u.*,

P_{iii} = 0.5*p.u.*,

P_{iv} = 0.5*p.u.*,

P_v = 0.2*p.u.*,

P_{vi} = 0.2*p.u.*

4.2.2 Heat Network

The schematic diagram of the heat network is shown in Figure 4.4. The pipe parameters are presented in the Appendix D.

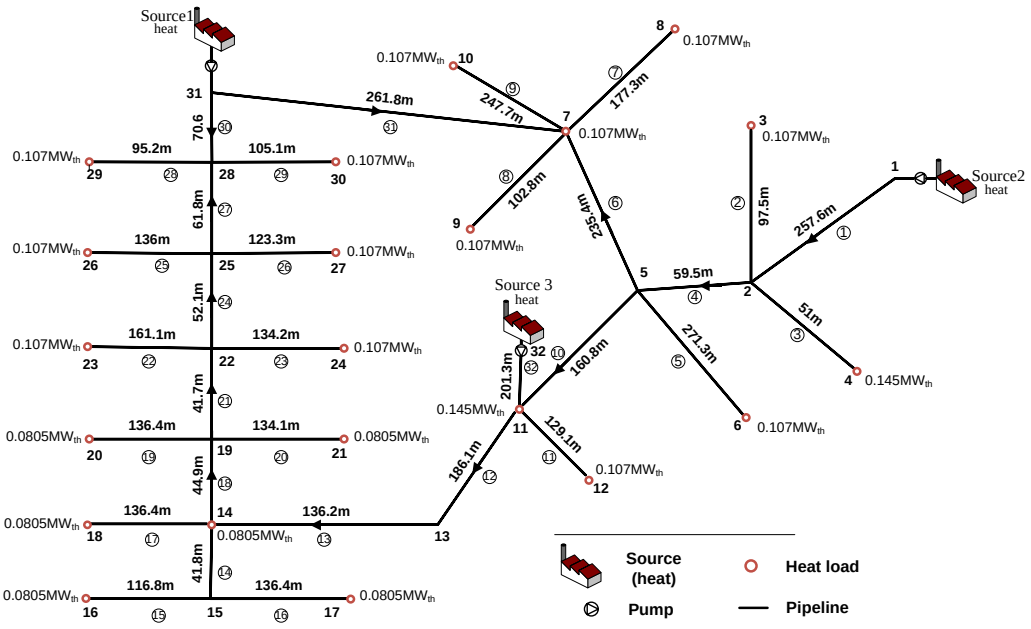

Figure 4.4: Schematic diagram of the heat network of the Barry Island case study

It was assumed that the heat power of the loads is known. The data of the heat power of the loads (MW_{th}) are shown in Figure 4.4. The total heat power of the loads is 2.164MW_{th}. Node 1, node 11 and node 31 correspond to three sources. Node 1 is the heat slack node.

It was assumed that:

- Supply temperature at each source: $T_{s,source}$ = 70°C.

- Outlet temperature (return temperature before mixing) at each heat load: $T_{o,load}$ = 30°C.

4.2.3 CHP Units

For the gas turbine CHP unit at Source 1, the relation between the heat and electrical power generation was calculated using the equation:

$$c_{m1} = \frac{\emptyset_{CHP1}}{P_{CHP1}} \tag{4.1}$$

where c_{m1} is the heat-to-power ratio, $c_{m1} = 1.3$ [89, 90]. Φ_{CHP1} (MW_{th}) is the useful heat output. P_{CHP1} (MW_e) is the electrical power output. Both variables are unknown in this case study.

For the extraction steam turbine CHP unit at Source 2, the Z ratio was used to calculate the heat output [94]:

$$Z_2 = \frac{\Delta\emptyset_2}{\Delta P_2} = \frac{\emptyset_{CHP2} - \emptyset_{con2}}{P_{con2} - P_{CHP2}} \tag{4.2}$$

where Z_2 is the Z ratio, $Z_2 = 8.1$ [94]. $\Delta\emptyset_2$ is the increased heat recovery and ΔP is reduced electrical power output. Φ_{CHP2} (MW_{th}) is the useful heat output. P_{CHP2} (MW_e) is the electrical power output. Both variables are unknown in this case study. P_{con2} is the electrical power generation of the extraction unit in full condensing mode. In this mode, the heat generation is zero, thus $\emptyset_{con2} = 0$. In this case study, $P_{con2} = 0.6MW_{th}$.

For the reciprocating engine CHP unit at Source 3, the relation between the heat and electrical power generation was calculated using the equation:

$$c_{m3} = \frac{\emptyset_{CHP3}}{P_{CHP3}} \tag{4.3}$$

where c_{m3} is the heat-to-power ratio, $c_{m3} = 1/0.79$ [90]. Φ_{CHP3} (MW_{th}) is the useful heat output. P_{CHP3} (MW_e) is the electrical power output.

4.3 Calculations

In the case study, the heat and electrical power generated from Source 1 and Source 2 are unknown. The heat and electrical power generated from non-slack Source 3 are known (Table 4.1). It is assumed that the electrical power generated from Source 3 is $P_{3,source} = 0.3MW_e$. Its calculated heat power is $\emptyset_{3,source} = c_{m3}P_{3,source} = 0.3797MW_{th}$.

Table 4.1: Heat and electrical power from three sources

	Source 1 (electricity slack busbar)	Source 2 (heat slack node)	Source 3 (non-slack)
Heat power	Unknown	Unknown	Known
Electrical power	Unknown	Unknown	Known
Heat-to-power ratio or Z ratio	Known	Known	Known

The number of the state variables for the case study is shown in Table 4.2.

- The number of voltage angles ($\boldsymbol{\theta}$) is equal to the number of busbars minus one.
- The number of voltage magnitude ($|\boldsymbol{V}|$) is equal to the number of load busbars.
- The number of mass flow rates ($\dot{\boldsymbol{m}}$) is equal to the number of pipes.
- The number of temperatures ($\boldsymbol{T}_{s,load}$ or $\boldsymbol{T}_{r,load}$) is equal to the number of load nodes.

Table 4.2: Number of the state variables for the case study

State variables	$\boldsymbol{\theta}$	$\|\boldsymbol{V}\|$	$\dot{\boldsymbol{m}}$	$\boldsymbol{T}_{s,load}$	$\boldsymbol{T}_{r,load}$	**Total**
Number	8	6	32	29	29	104

The following initial conditions for the heat and electricity networks were assumed:

Heat:

- Supply temperature at each heat load: $T_{s,load}^{(0)} = 70°\mathrm{C}$
- Mass flow rate within each pipe: $\dot{m}^{(0)} = 1kg/s$
- Heat power generated from Source 1: $\emptyset_{1,source}^{(0)} = 1.1MW_{th}$

Electricity:

- Voltage magnitude at each electrical load busbar: $\left|V^{(0)}\right| = 1.05p.u.$
- Voltage angle at each busbar except the slack busbar: $\theta^{(0)} = 0^{\circ}$

For the heat supply network as shown in Figure 4.4, the network incidence matrix **A** was created and is shown in the Appendix E.

The integrated and decomposed electrical-hydraulic-thermal calculations were used in this case study. The calculation techniques were the same as described in Chapter 3.

The steps used to solve the integrated calculation are as follows:

1) Initialise variables. Iteration *i* = 1.
2) Calculate the mismatches $\Delta\boldsymbol{F}^{(i)}$.
3) Calculate the Jacobian matrix $\boldsymbol{J}^{(i)}$.
4) Update the state variables using the equation $\boldsymbol{x}^{(i)} = \boldsymbol{x}^{(i-1)} - \left(\boldsymbol{J}^{(i)}\right)^{-1}\Delta\boldsymbol{F}^{(i)}$.
5) The procedure is repeated until the maximum absolute value of elements in the mismatches $|\Delta\boldsymbol{F}|$ becomes less than the tolerance $\boldsymbol{\varepsilon}$ = 10^{-3}. *i* = *i* + 1.

   After 16 iterations, the results converged.

The steps used to solve the decomposed calculation are as follows:

1) Initialise variables. Iteration i = 1.
2) Solve the hydraulic and thermal model to obtain pipe mass flow rates, supply and return temperatures.
3) Calculate $\emptyset_{2,source}^{(i)}$.
4) Calculate $P_{2,source}^{(i)}$.
5) Solve the electrical power flow model to obtain voltage magnitudes and voltage angles.
6) Calculate $P_{1,source}^{(i)}$.
7) Calculate $\emptyset_{1,source}^{(i)}$.
8) This procedure is repeated until $\Delta\emptyset_{1,source}^{(i)} = \emptyset_{1,source}^{(i)} - \emptyset_{1,source}^{(i-1)}$ becomes less than the tolerance $\varepsilon = 10^{-3}$. $i = i + 1$.

   After 33 total iterations, the results converged. The total iterations consist of the iterations of the electrical power flow model and the hydraulic and thermal model.

The results of the decomposed and integrated calculations were very close at 10^{-3} precision.

4.4 Results

The results of the calculation of the heat and electrical power from Source 1 and Source 2 are shown in Figure 4.5. The electrical and heat power network losses are the differences between the sum of the power supplied from three sources and the electrical and heat loads. The electrical power network loss is 0.0118MW_e (0.74%). The heat network loss is 0.0809MW_{th} (3.74%).

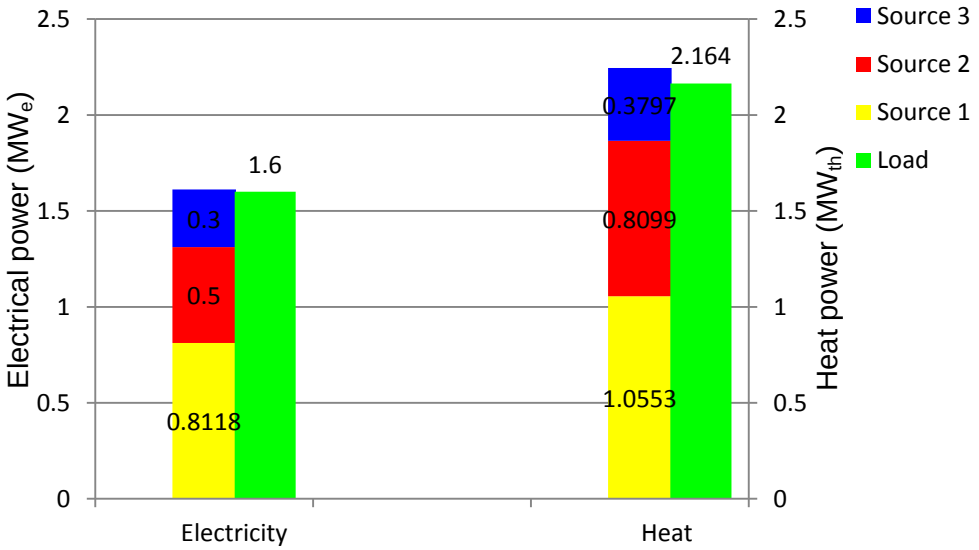

Figure 4.5: Heat and electrical power supplied from three sources

The results of the calculation of the pipe mass flow rates are shown in Figure 4.6. In the figure the main flow route 1 – 2 – 5 – 11 – 13 – 14 – 19 – 22 – 25 – 28 – 31 – 7 – 5 is indicated using bold lines. It is seen that in some pipes (⑥, ㉔ and ㉗) the flows are of opposite direction compared with the initial guess, as shown in Figure 4.4, and the mass flow rates are different. The mass flow rate within pipe ⑫ is increased due to the flow injection from Source 3. The mass flow rate at node 31 is the largest since the heat power generated in Source 1 is the largest.

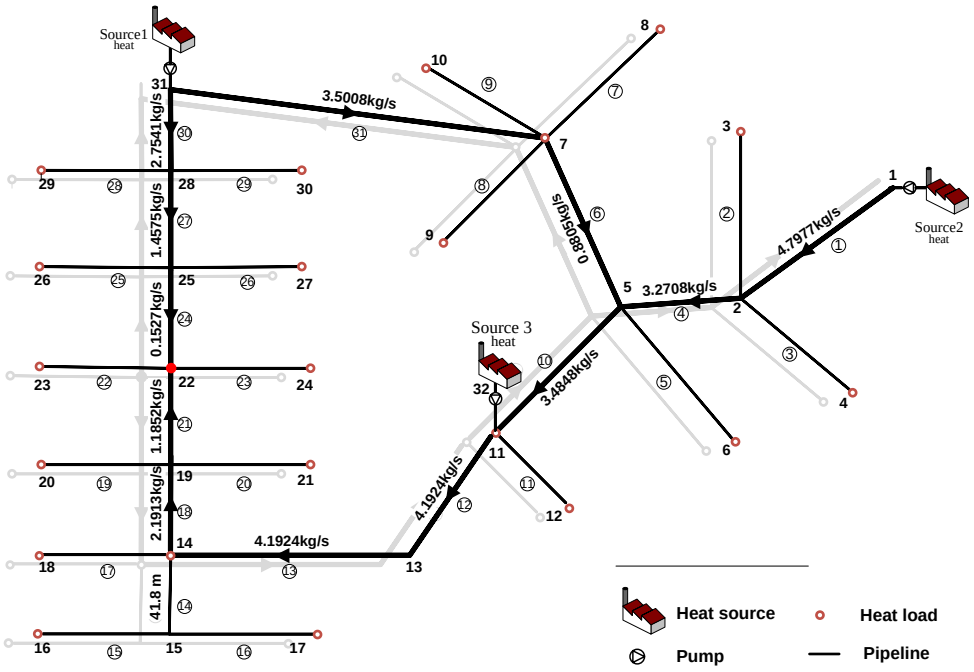

Figure 4.6: Results of the pipe mass flow rates (kg/s) in a flow route

The results of the calculation of the supply and return temperatures at each node in the main flow route: 1 – 2 – 5 – 11 – 13 – 14 – 19 – 22 – 25 – 28 – 31 – 7 – 5 are shown in Figure 4.7. Node 22 is the end of two flow streams from Source 1 and Source 2 in the supply network and the start of the two flow streams in the return network. The lowest supply temperature and the highest return temperature are at node 22, where two opposite flow streams meet.

In the main route of the supply network (Figure 4.6), the flows mix at nodes 5 and 22 only. The supply temperature from node 1 to node 22 reduces gradually because of the heat losses.

In the same route of the return network, the flow mixing occurs at each node except node 13. Due to the mixing and due to the assumption that the return temperature from the consumer is fixed, the return temperature from node 22 to node 1 decreases unevenly.

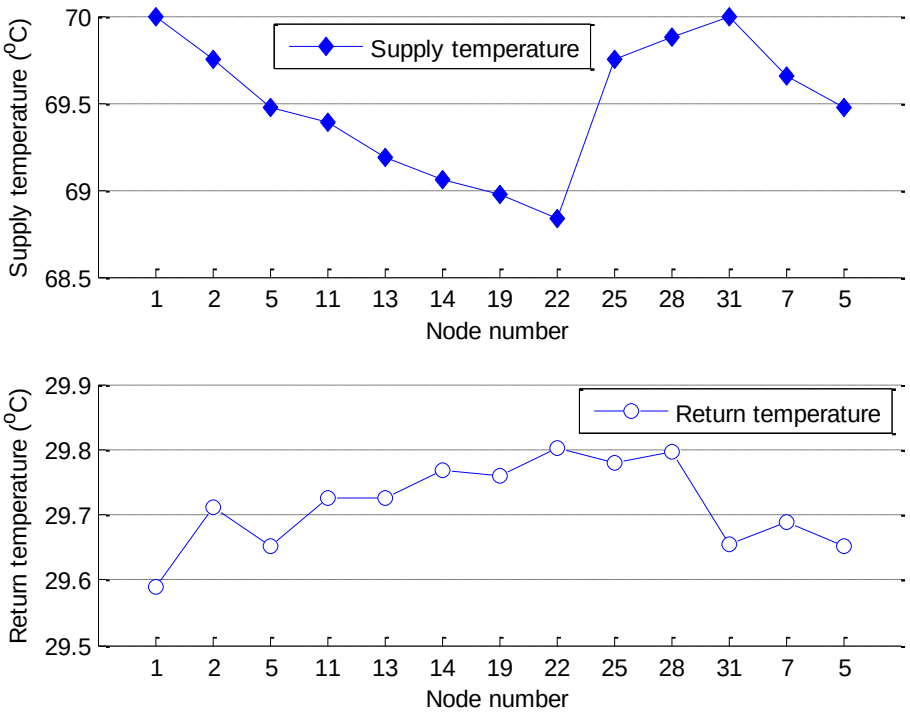

Figure 4.7: Results of the supply and return temperatures of the nodes in a flow route

The results of the calculation of the voltage magnitude and voltage angle at each busbar are as shown in Figure 4.8. The voltage angles at source busbars are lower than those of some load busbars.

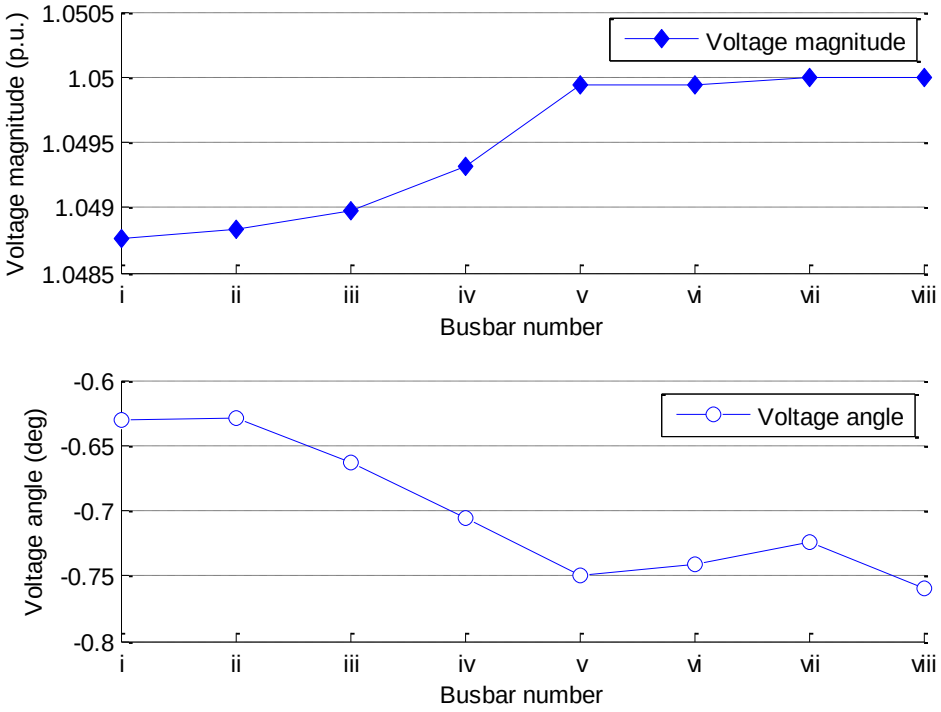

Figure 4.8: Results of the voltage magnitude and voltage angle at each busbar

To validate the results of the heat network analysis, the same heat network as shown in Figure 4.2 was built using commercial software SINCAL [67]. The heat power of the CHP unit at Source 1 is specified in SINCAL based on the calculated value from the combined analysis (Φ_{CHP1} = 1.0553MW$_{th}$). The results of the heat network obtained using the combined analysis are the same as that obtained by SINCAL at 10^{-3} precision.

To validate the results of the electricity network analysis, the same electricity network as shown in Figure 4.3, was built using commercial software IPSA [97]. The electrical power of the CHP unit at Source 2 is specified in IPSA based on the calculated value from the combined analysis (P_{CHP2} = 0.5000MW$_e$). The results of the electricity network obtained using the combined analysis are the same as that obtained by IPSA.

The results from the combined analysis, SINCAL and IPSA are shown in the Appendix F.

4.5 Convergence Characteristics

The convergence characteristics of calculations using two methods: decomposed and integrated calculations, are shown in Figure 4.9. It is seen that the integrated calculation requires fewer iterations than the decomposed calculation. The *decomposed* electrical-hydraulic-thermal calculation was solved in 33 iterations. The *integrated* electrical-hydraulic-thermal calculation was solved in 14 iterations.

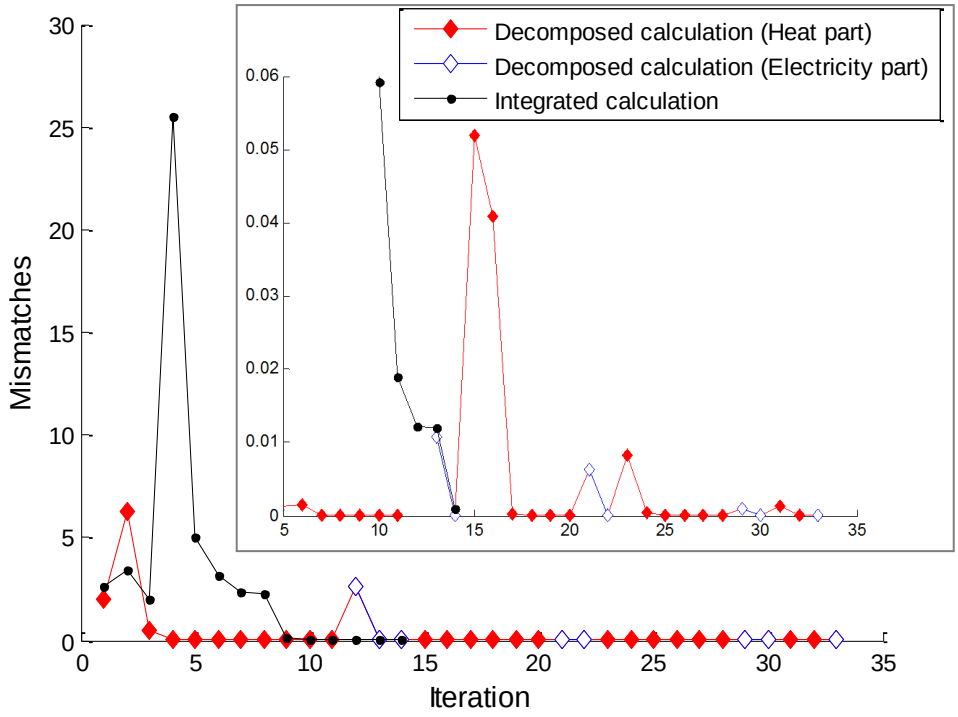

Figure 4.9: Convergence characteristics of the decomposed and integrated calculations

The reasons that the integrated calculation requires more iterations to converge than the conventional individual electrical power flow are as follows:

- The per unit was used in the electrical power flow model.

  Thus the differences between initial and actual values are small (less than 1) in the electrical power flow. In the hydraulic and thermal calculation, the actual values are used in the variables. Thus the differences between initial and actual values are larger. The stopping criterion for the supply temperature in the integrated

calculation is actually $1/70 \times 10^{-3}$ if the total stopping criteria is 10^{-3} and the base supply temperature is 70°C. In this case, the iterations of the integrated calculation are reduced to **11** iterations.

- Loops were considered in the hydraulic and thermal model.

  In 11 iterations there are 5 iterations where the largest mismatches are from the loop pressure equation. In the loop pressure equation, the friction factor is calculated using the implicit equation (2.11) and it is a function of mass flow rates.

4.6 Optimal Dispatch of Electricity Generation

As an addition to the power flow, the use of optimal dispatch was added to the combined analysis and was solved by the Newton-Raphson method. The optimal dispatch of combined heat and power without considering network losses was investigated by Guo et al [101]. For simplicity, the optimal dispatch of electricity generation only was considered in this section.

The Barry Island case study with optimal dispatch was investigated in this section. The heat and electrical power generated from Source 1 and Source 2 and non-slack Source 3 were unknown and their heat-to-power ratios were known (Table 4.3). Comparing to Section 4.3, it can be seen that one more variable was added. Thus, one more equation was added to solve the problem. This additional equation was formed using the equal-incremental-fuel-cost criterion [8, 86, 102].

Table 4.3: Heat and electrical power from three sources

	Source 1 (electricity slack busbar)	Source 2 (heat slack node)	Source 3 (non-slack)
Heat power	Unknown	Unknown	Unknown
Electrical power	Unknown	Unknown	Unknown
Heat-to-power ratio or Z ratio	Known	Known	Known

The equal-incremental-fuel-cost criterion states that for optimum economy the incremental fuel cost should be identical for all contributing turbine-generator sets [8, 86]. In this case study, the equal-incremental-fuel-cost criterion is applied to the electrical power of Source 2 and Source 3 ($P_{2,source}$ and $P_{3,source}$). The electrical power of Source 1 ($P_{1,source}$) is calculated from the heat power of Source 1 ($\emptyset_{1,source}$). These are illustrated as shown in Figure 4.10.

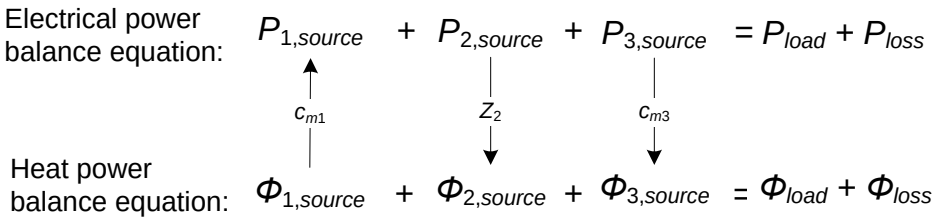

Figure 4.10: Illustration of optimal dispatch for combined electrical and heat power

It is assumed the fuel cost functions of Source 2 and Source 3 are:

$$f_{1,source} = a_1 P_{1,source}^2 + b_1 P_{1,source} + c_1$$
$$f_{2,source} = a_2 P_{2,source}^2 + b_2 P_{2,source} + c_2 \quad (4.4)$$
$$f_{3,source} = a_3 P_{3,source}^2 + b_3 P_{3,source} + c_3$$

Where $f_{i,source}$ is the fuel cost of Source i (£/h). a_i, b_i and c_i are constants. $i = 1,2,3$.

Source 2 and Source 3 are expressed in the equations using the equal-incremental-fuel-cost criterion:

$$\lambda = \frac{df_{2,source}}{dP_{2,source}} = \frac{df_{3,source}}{dP_{3,source}} \quad (4.5)$$

where λ is the incremental fuel cost.

The derivatives of equation (4.4) are:

$$\frac{df_{2,source}}{dP_{2,source}} = 2a_2 P_{2,source} + b_2$$
$$\frac{df_{3,source}}{dP_{3,source}} = 2a_3 P_{3,source} + b_3 \quad (4.6)$$

Hence, from equations (4.5) and (4.6), $P_{3,source}$ is given by:

$$P_{3,source} = \left(2a_2 P_{2,source} + b_2 - b_3\right)/(2a_3) \tag{4.7}$$

In this case, $P_{3,source}$ is expressed as a function of $P_{2,source}$.

The following text explains how equation (4.7) is added to the integrated and decomposed calculations.

a) Integrated electrical-hydraulic-thermal calculation

In the integrated calculation, all the equations were combined to form a single system of equations and solved simultaneously as an integrated whole using the Newton-Raphson method. The system of equations is shown as

$$\Delta \boldsymbol{F} = \begin{bmatrix} \Delta \boldsymbol{P} \\ \Delta \boldsymbol{Q} \\ \Delta \boldsymbol{\Phi} \\ \Delta \boldsymbol{p} \\ \Delta \boldsymbol{T}'_s \\ \Delta \boldsymbol{T}'_r \end{bmatrix} = \begin{bmatrix} \boldsymbol{P}^{sp}_{load} - Re\{\boldsymbol{V}(\boldsymbol{YV})^*\} \\ P^{sp}_{2,source} - Re\{V_{2,source}(\boldsymbol{YV})^*\} \\ P^{sp}_{3,source} - Re\{V_{3,source}(\boldsymbol{YV})^*\} \\ \boldsymbol{Q}^{sp} - Im\{\boldsymbol{V}(\boldsymbol{YV})^*\} \\ C_p \boldsymbol{A}\, \dot{\boldsymbol{m}}(\boldsymbol{T}_s - \boldsymbol{T}_o) - \boldsymbol{\Phi}^{sp}_{load} \\ C_p \boldsymbol{A}_1\, \dot{\boldsymbol{m}}(T_{s1} - T_{o1}) - \emptyset^{sp}_{1,source} \\ C_p \boldsymbol{A}_3\, \dot{\boldsymbol{m}}(T_{s3} - T_{o3}) - \emptyset^{sp}_{3,source} \\ \boldsymbol{B}\, \boldsymbol{K}\, \dot{\boldsymbol{m}}|\dot{\boldsymbol{m}}| - \boldsymbol{0} \\ \boldsymbol{C}_s \boldsymbol{T}'_{s,load} - \boldsymbol{b}_s \\ \boldsymbol{C}_r \boldsymbol{T}'_{r,load} - \boldsymbol{b}_r \end{bmatrix} \begin{matrix} \\ \\ \\ \\ \\ \\ \\ \\ \\ \\ \end{matrix} \begin{matrix} \\ \leftarrow \text{Active power mismatches} \\ \\ \leftarrow \text{Reactive power mismatches} \\ \\ \\ \leftarrow \text{Heat power mismatches} \\ \\ \leftarrow \text{Loop pressure mismatches} \\ \leftarrow \text{Supply temperature mismatches} \\ \leftarrow \text{Return temperature mismatches} \end{matrix} \tag{4.8}$$

Since Source 1 provides the electricity slack busbar, $P_{1,source}$ is unknown and there are no $P^{sp}_{1,source}$ in the mismatches in equation (4.8). Since Source 2 provides the heat slack node, $\emptyset_{2,source}$ is unknown and there are no $\emptyset^{sp}_{2,source}$ in the mismatches in equation (4.8). The shaded terms in equation (4.8) are the specified electrical and heat power and are expressed using equations (3.24)-(3.29) and equation (4.7)

$$\begin{aligned} P^{sp}_{3,source} &= \left(2a_2 P^{sp}_{2,source} + b_2 - b_3\right)/(2a_3) \\ \emptyset^{sp}_{3,source} &= c_{m3} P^{sp}_{3,source} \end{aligned} \tag{4.9}$$

where

$$\begin{aligned} P^{sp}_{2,source} &= -C_p \dot{m}_{q2,source}\left(T'_{s2,source} - T'_{r2,source}\right)/\mathrm{Z}_2 \\ &\quad + \eta_e F_{in} \\ \emptyset^{sp}_{1,source} &= c_{m1} \cdot Real\left\{V_{1,source} \sum_{k=1}^{N} (Y_{ik} V_k)^*\right\} \end{aligned} \tag{4.10}$$

This means the electrical power of Source 2 and Source 3 are expressed as functions of the variables of the heat network. The heat power of Source 1 is expressed as a function of the variables of the electricity network. Therefore, comparing to Chapter 3, the elements $\frac{\partial \Delta P_{3,source}}{\partial \dot{m}}$ in the electricity to heat Jacobian submatrix are nonzero.

b) Decomposed electrical-hydraulic-thermal calculation

The flowchart of the decomposed electrical-hydraulic-thermal calculation is illustrated through the linkages shown in Figure 4.11. The linkages are formed by three sources with unknown heat and electrical power.

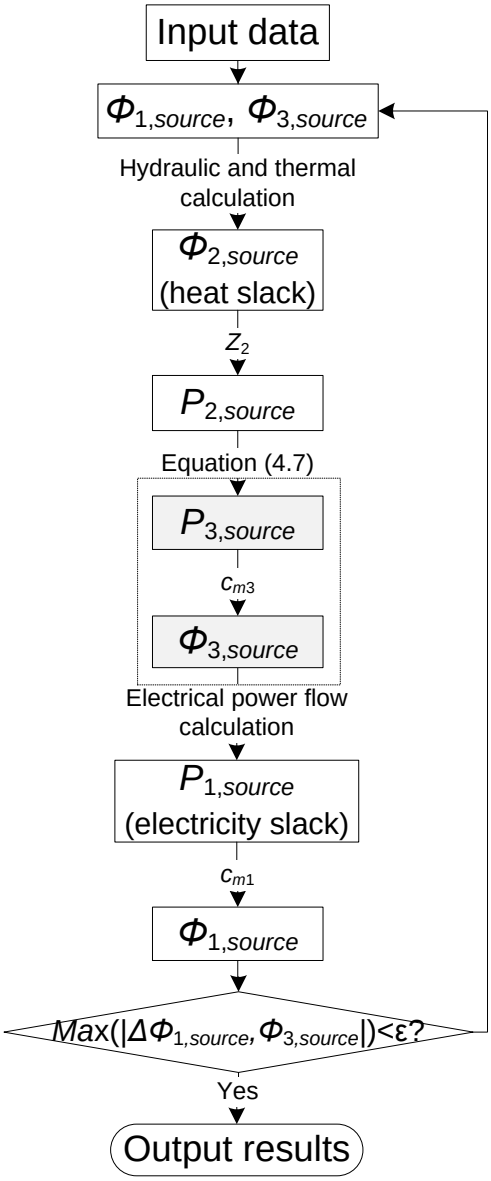

Figure 4.11: Flowchart of the decomposed electrical-hydraulic-thermal calculation

If the result of the electrical power generation of a source exceeds its generation upper or lower limit, then the lower or upper limit is the electrical power output from the source. For other sources, the same calculation process described in this section is performed again.

The cases with N (N ≥ 3) sources can be similarly implemented as that of $P_{3,source}$. The equal-incremental-fuel-cost criterion is then applied to the electrical power of N-1 sources.

It is assumed that in equation (4.4) $a_1 = 0.2, b_1 = 13,\ c_1 = 50, a_2 = 0.1, b_2 = 12.5,\ c_2 = 50,\ a_3 = 0.4, b_3 = 12, c_3 = 50$ [8]. By substituting these values in equations (4.4) – (4.7):

$$\begin{aligned} f_{1,source} &= 0.2P_{1,source}^2 + 13P_{1,source} + 50 \\ f_{2,source} &= 0.1P_{2,source}^2 + 12.5P_{2,source} + 50 \\ f_{3,source} &= 0.4P_{3,source}^2 + 12P_{3,source} + 50 \end{aligned} \tag{4.11}$$

$$\begin{aligned} \lambda &= \frac{df_{2,source}}{dP_{2,source}} = 0.2P_{2,source} + 12.5 \\ \lambda &= \frac{df_{3,source}}{dP_{3,source}} = 0.8P_{3,source} + 12 \end{aligned} \tag{4.12}$$

$$P_{3,source}^{sp} = \left(0.2P_{2,source}^{sp} + 0.5\right)/0.8 \tag{4.13}$$

The initial values were the same as those of the Barry Island case study in Section 4.3. In addition, initially assume $\emptyset_{3,source}^{(0)} = 0.4MW_{th}$.

Using the integrated electrical-hydraulic-thermal calculation technique, the model equations were solved in **15** iterations with the tolerance $\boldsymbol{\varepsilon}$ **=** 10^{-3}. Using the decomposed electrical-hydraulic-thermal calculation, the model equations were solved in **43** iterations with the tolerance $\boldsymbol{\varepsilon}$ **=** 10^{-3}. The results of the integrated and decomposed calculations were very close at 10^{-3} precision.

The results of the calculation of the heat and electrical power from Source 1, Source 2 and Source 3 are shown in Figure 4.12. The incremental fuel cost λ is 12.60£/MWh. The total cost of Source 1, Source 2 and Source 3 for supplying electricity over an hour is: $f_{2,source} + f_{3,source} = 54.75 + 56.25 + 59.22 = 170.22£/h$. Substituting the power flow results shown in Figure 4.5 into equation (4.11) of the cost function, the total cost is calculated as 170.60£/h. Comparing the two results, the results of optimal dispatch save 0.38£/h.

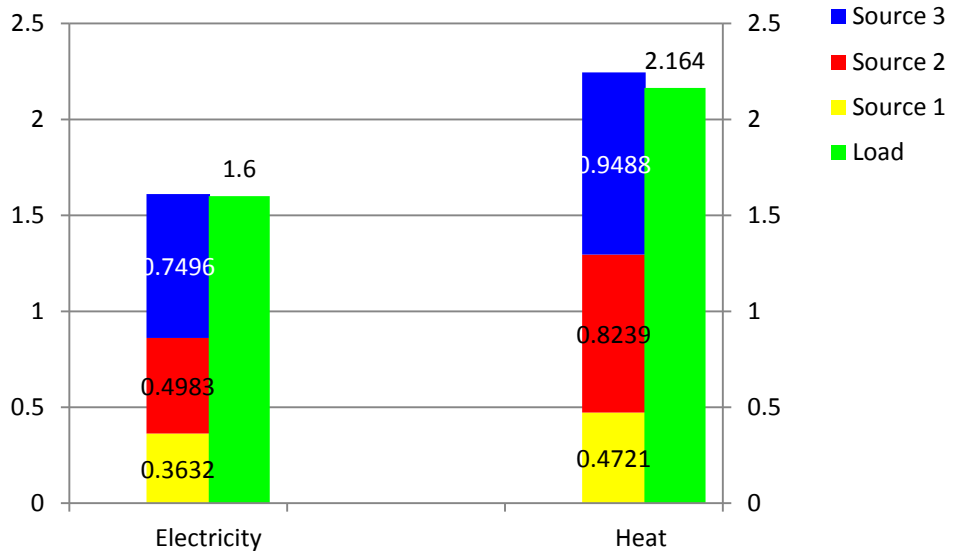

Figure 4.12: Heat and electrical power supplied from three sources

4.7 Summary

This chapter provided an engineering solution to the Barry Island case study. The case study examined how both electrical and heat demands in a self-sufficient system (no interconnection with external systems) were met using CHP units.

The combined analysis took into account the flows of energy between the electricity and heat networks through the CHP units. The combined analysis in the forms of the power flow and optimal dispatch was solved by the Newton-Raphson method. The variables of the electrical and heat networks were calculated. These included: heat and electrical power of

the CHP units, mass flow rates, supply and return temperatures, voltage magnitudes and voltage angles, heat and electrical power losses.

The combined analysis consisted of the decomposed and integrated calculation techniques. The comparison showed that the integrated calculation requires fewer iterations than the decomposed calculation.

Chapter 5 - Conclusions

5.1 Conclusions

The use of CHP units, heat pumps and electric boilers increases the linkages between electricity and heat networks. A combined analysis was developed to investigate the performance of electricity and heat networks as an integrated whole. This was based on a model of electrical power flow and hydraulic and thermal circuits together with their coupling components (CHP units, heat pumps, electric boilers and circulation pumps). The flows of energy between the electricity and heat networks through the coupling components were taken into account.

The combined analysis was used for the delivery of the electrical and heat energy from CHP units and heat pumps and other coupling components to the consumers through electrical and heat networks. It consisted of the *decomposed* and *integrated* electrical-hydraulic-thermal calculation techniques in the forms of the power flow and simple optimal dispatch. The *integrated* calculation required fewer iterations and the number of the iterations of the *decomposed* calculation increases with the size of the networks.

5.1.1 Analysis of District Heating Networks

Hydraulic-thermal model was developed to investigate the performance of a district heating network. The objective of the hydraulic-thermal model was to determine the mass flow rates within each pipe and the

load supply temperatures and the source return temperatures. It was assumed that the source supply temperatures and the load return temperatures were specified; the injected mass flow rates or the heat power supplied or consumed at all the nodes except one were specified.

The individual hydraulic and thermal models in district heating networks were modelled. In the hydraulic model, the network description was based on a graph-theoretical method. Two calculation methods were investigated for the hydraulic calculation of looped networks. The Newton-Raphson method considered all loops simultaneously. The Hardy-Cross method dealt with one loop at a time. The adjustments of the Hardy-Cross method used the main diagonal of the Jacobian matrix of the Newton-Raphson method. For the sake of combining with the thermal model and further combining with the electrical power flow, the Newton-Raphson method was used to solve the hydraulic equations. In the thermal model, the mixture temperatures at nodes were considered, and a matrix formulation of the thermal model was implemented.

Conventionally, the decomposed hydraulic-thermal calculation was through an iterative procedure between the individual hydraulic and thermal models. In this thesis, an integrated hydraulic-thermal calculation was developed, in which the hydraulic and thermal models were combined in a single system of equations solved by the Newton-Raphson method. It took into account the coupling between the individual hydraulic and thermal analyses. For instance, the thermal calculation cannot be performed without knowing the pipe mass flows, and the hydraulic calculation cannot be performed without knowing temperatures under the assumption that the nodal heat power is specified.

The results of the decomposed and integrated hydraulic-thermal calculations were very close to 10^{-3} precision. The results were validated using SINCAL with the same value at 10^{-3} precision.

5.1.2 Combined Analysis of Electricity and Heat Networks

Two calculation techniques (decomposed and integrated electrical-hydraulic-thermal calculations) were developed. Three combinations of coupling mechanisms (CHP only; CHP and circulation pump; CHP, circulation pump and heat pump) were considered in each calculation technique. The calculation techniques were demonstrated in the grid-connected and the islanded operation modes.

In the grid-connected mode, any surplus or deficit in electrical power is supplied from the main grid and not from the CHP units, thus there is no linkage back from the electrical system to the heat system. While in the islanded mode there are bidirectional linkages between the electricity and heat networks.

For the *decomposed electrical-hydraulic-thermal* calculation in the grid-connected mode, the hydraulic-thermal model was solved first. Then these results were transferred to the electricity network through the coupling components. Finally the electrical power flow model was solved. In the islanded mode, this sequential procedure was iterated until the solution converged within an acceptable tolerance.

For the *integrated electrical-hydraulic-thermal* calculation, the electrical power flow equations, the hydraulic equations and the thermal equations were combined to form a single system of equations and solved simultaneously as an integrated whole using the Newton-Raphson method.

The combined analysis has the ability to calculate the variables of the electrical and heat networks, which can be used for the design and operation of integrated heat and electricity systems. These variables included: heat and electrical power from the CHP units, mass flow rates, supply and return temperatures, voltage magnitudes and voltage angles, heat and electrical power losses. This was based on the assumptions that the source supply temperatures and the load return temperatures were specified; the injected nodal heat and electrical power supplied or

consumed at non-slack nodes or busbars were specified; and the voltage magnitudes at source busbars were specified.

The results of the *decomposed and integrated electrical-hydraulic-thermal* calculations were very close to 10^{-3} precision. The real values were used in the calculation of heat networks and the per unit was used in the calculation of electrical networks. The convergence characteristics of two calculations were compared. The comparison showed that the *integrated* calculation requires fewer iterations than the *decomposed* calculation. In a simple example network, the *decomposed* calculation was solved in 16 iterations and the *integrated* calculation was solved in 12 iterations.

5.1.3 Case Study

A case study of Barry Island was conducted. The heat network was a low temperature looped pipe district heating network with 32 nodes and fed by three CHP units. The electrical power from three CHP units was supplied to 5 lumped electrical loads. The case study examined how both electrical and heat demands in a self-sufficient system (no interconnection with external systems) were met using CHP units. To benefit from the efficient heat and electricity generation of CHP units, a solution was demonstrated to deliver the electrical and heat energy from the CHP units to the consumers through electrical and heat networks.

In this case study, the combined analysis consisted of the forms of the power flow and simple optimal dispatch. In the power flow, the *decomposed* calculation was solved in 33 iterations and the *integrated* calculation was solved in 14 iterations. In optimal dispatch, the *decomposed* calculation was solved in 43 iterations and the *integrated* calculation was solved in 15 iterations. Comparing to the simple example network, it can be seen that the *integrated* calculation requires fewer iterations and the number of the iterations of the *decomposed* calculation increases with the size of the networks.

The results of the *decomposed and integrated electrical-hydraulic-thermal* calculations were very close to 10^{-3} precision. The results of heat

variables were validated using SINCAL and the results of electrical variables were validated using IPSA. The comparison showed these results were very close to 10^{-3} precision.

The combined analysis can be used for the design and operation of integrated heat and electricity systems for energy supply to buildings. This will increase the flexibility of the electricity and heat supply systems for facilitating the integration of intermittent renewable energy.

5.2 Contributions of the Thesis

Contributions of the thesis are as follows:

- For the analysis of district heating networks, a power flow formulation analogous to the electrical power flow was described. Decomposed and integrated hydraulic-thermal calculation techniques were developed. In the integrated method, the Newton-Raphson method was employed to solve the hydraulic-thermal model.
- The coupling components model: three types of CHP units and a CHP and heat pump composite supply system were modelled. This provides linkages between electricity and heat networks.
- Two combined analysis methods were developed to investigate the performance of electricity and heat networks as an integrated whole. These two methods were the decomposed and integrated electrical-hydraulic-thermal calculation techniques in the forms of the power flow and simple optimal dispatch.
- The formulation of the integrated method reduces dimensionality. The comparison showed that the integrated method requires fewer iterations than the decomposed method.
- The models focused on network analysis. Variables (voltage, mass flow rates, temperature, electricity losses and heat losses) were calculated precisely for a network with arbitrary topology.

- An engineering solution was provided to the Barry Island case study.

5.3 Future Work

Recommendations for further work are as follows:

1) Applications of the combined analysis

- The impacts of the different penetration of CHP units and heat pumps on the electricity and heat networks may be investigated. For example, the generation capacity of the CHP units may range 0~100% of the total electricity supply.

- The impact of heat networks on electricity distribution networks and vice versa may be investigated. For example, the variations of heat demand to the operation of electrical networks.

- A consideration of local decentralised generation may be of interest, such as local heat pumps or electric boilers installed at consumers and interconnected to heat networks.

- An extension of optimal dispatch may be required. The fuel cost may be modelled as a function of both electrical and heat power.

2) Further development of the combined analysis

- The inclusion of thermal storage in a multi-time simulation may be conducted.

- The integration of more energy vectors may be considered, e.g., gas, cooling.

- An extension of the model to optimal power flow may be developed. The most energy efficient operating regime will be determined and energy losses, costs or gaseous emissions minimised.

Reference

[1] Department of Energy & Climate Change, "2011 UK greenhouse gas emissions: Final figures," 2013.

[2] Office of Public Sector Information, "Climate Change Act 2008," 2008.

[3] A. Simpson, "Briefing: Renewable Heat Incentive," *Friends of the Earth,* 2010.

[4] H. Lund, A. N. Andersen, P. A. Østergaard, B. V. Mathiesen, and D. Connolly, "From electricity smart grids to smart energy systems – A market operation based approach and understanding," *Energy,* vol. 42, pp. 96-102, 2012.

[5] Department of Energy and Climate Change, *The future of heating: Meeting the challenge*, March 2013.

[6] R. Platt, W. Cook, and A. Pendleton, "Green Streets, Strong Communities," *Institute for Public Policy Research,* 2011.

[7] M. Geidl and G. Andersson, "Optimal Power Flow of Multiple Energy Carriers," *Power Systems, IEEE Transactions on,* vol. 22, pp. 145-155, 2007.

[8] B. M. Weedy, B. J. Cory, N. Jenkins, J. B. Ekanayake, and G. Strbac, *Electric power systems 5th ed.*: Wiley, 2012.

[9] G. Harrison and R. Wallace, "Network integration of CHP: how to maximize access," *Cogeneration and On-Site Power Production,* vol. 5, pp. 69-76, 2004.

[10] CHPA, "Integrated Energy: The role of CHP and district heating in our energy future," *The Combined Heat and Power Association (CHPA),* 2010.

[11] H. Zhao, "Analysis, modelling and operational optimization of district heating systems," PhD Thesis, Technical University of Denmark, 1995.

[12] G. Davies and P. Woods, "The Potential and Costs of District Heating Networks," 2009.

[13] J. Kunz, P. Haldi, and G. Sarlos, "Dynamic behavior of district heating systems," Begell House Publishers, 1994.

[14] B. Skagestad and P. Mildenstein, "District Heating and Cooling Connection Handbook," International Energy Agency, IEA.

[15] P. Johansson, "Buildings and District Heating - Contributions to Development and Assessments of Efficient Technology," *PhD thesis, Dept. of Energy Sciences, Faculty of Engineering, Lund University,* 2011.

[16] *Heat and the City*. Available: http://www.heatandthecity.org.uk/ [Accessed: 07.03.2013]

[17] CHPA, "The role of CHP and district heating in our energy future," ed: The Combined Heat and Power Association (CHPA), 2010.

[18] G. Strbac, N. Jenkins, and T. Green, "Future network technologies," *Report to DTI,* 2006.

[19] CIBSE, "Guide to Community Heating and CHP (Good practice guide (GPG) 234) " the Chartered Institution of building services engineer (CIBSE).

[20] BERR, "Heat Call for Evidence," *Deparment for Business Enterprise & Regulatory Reform,* Jan 2008.

[21] Department of Energy & Climate Change, *Strategic Framework for Low Carbon Heat in the UK: Summary of Responses*, 2012.

[22] HM Government, "The Carbon Plan: Delivering our low carbon future," 2011.
[23] R. Wiltshire, "The UK potential for community heating with combined heat and power," *Building Research Establishment. Watford, UK, BRE,* 2003.
[24] F.Starr, "Future Challenges for CHP in the UK and Continental Europe," Claverton2010.
[25] S. Kelly and M. G. Pollitt, "Making Combined Heat and Power District Heating (CHP-DH) networks in the United Kingdom economically viable: a comparative approach," *University of Cambridge, Faculty of Economics,* 2009.
[26] N. Jenkins, G. Strbac, and J. Ekanayake, *Distributed Generation*: The Institution of Engineering and Technology, 2010.
[27] P. Woods. (2012). *The Case for District Heating – a flexible energy system*. Available: http://cardiff.ac.uk/ugc/flexible-energy-delivery-system-seminar-series-for-postgraduates-and-researchers [Accessed: 05.10.2012]
[28] LCICG, *Technology Innovation Needs Assessment (TINA) Heat Summary Report*: Low Carbon Innovation Coordination Group, September 2012.
[29] P. Woods, "Comparing CHP/DH with other technologies," *CIBSE Seminar,* 2011.
[30] Department of Energy & Climate Change, "Heat and Energy Saving Strategy Consultation " 2009.
[31] DECC and DCLG, " Warm Homes, Greener Homes: A Strategy for Household Energy Management Supporting Paper VIII, An Enabling Framework for District Heating and Cooling," *Department of Energy & Climate Change,* 2010.
[32] Postnote, "Renewable Heating," *The Parliamentary Office of Science and Technology,* 2010.
[33] Committee on Climate Change, "The Fourth Carbon Budget - Reducing emissions through the 2020s," 2010.
[34] A. Molyneaux, G. Leyland, and D. Favrat, "Environomic multi-objective optimisation of a district heating network considering centralized and decentralized heat pumps," *Energy,* vol. 35, pp. 751-758, 2010.
[35] *CHP Focus*. Available: http://chp.decc.gov.uk/cms/
[36] IEA, "Technology Roadmap Energy-efficient Buildings: Heating and Cooling Equipment," *International Energy Agency,* 2011.
[37] DESIRE. *Dissemination Strategy on Electricity Balancing for Large Scale Integration of Renewable Energy* Available: http://desire.iwes.fraunhofer.de/home.htm [Accessed: 21.06.2011]
[38] W. C. Turkenburg, D. J. Arent, R. Bertani, A. Faaij, M. Hand, W. Krewitt, E. D. Larson, J. Lund, M. Mehos, T. Merrigan, C. Mitchell, J. R. Moreira, W. Sinke, V. Sonntag-O'Brien, B. Thresher, W. van Sark, E. Usher, and E. Usher, "Chapter 11 - Renewable Energy," in *Global Energy Assessment - Toward a Sustainable Future*, ed Cambridge University Press, Cambridge, UK and New York, NY, USA and the International Institute for Applied Systems Analysis, Laxenburg, Austria, 2012, pp. 761-900.
[39] *E.ON starts construction of power-to-gas pilot plant in Germany*. Available: http://www.eon.com/en/media/news/press-releases/2012/8/21/eon-startsconstruction-of-power-to-gas-pilot-plant-in-germany.html?fromSearchResult=true [Accessed: 07.11.2012]

[40] *E.ON launches project unique in Europe to store heat from renewable energy sources*. Available: http://www.eon.com/en/media/news/press-releases/2011/7/1/e-dot-on-launches-project-unique-in-europe-to-store-heat-from-renewable-energy-sources.html?fromSearchResult=true [Accessed: 07.11.2012]

[41] M. Geidl, "Integrated modeling and optimization of multi-carrier energy systems," *PhD Thesis, the Swiss Federal Institute of Technology (ETH),* 2007.

[42] P. Mancarella, "Smart Multi-Energy Grids: Concepts, Benefits and Challenges " *IEEE PES General Meeting 2012,* 2012.

[43] G. Chicco and P. Mancarella, "Distributed multi-generation: A comprehensive view," *Renewable and Sustainable Energy Reviews,* vol. 13, pp. 535-551, 2009.

[44] P. Mancarella, "MES (multi-energy systems): An overview of concepts and evaluation models," *Energy,* vol. 65, pp. 1-17, 2014.

[45] P. Mancarella and G. Chicco, *"Distributed Multi-Generation: energy models and analyses"*: Nova Publisher, New York, 2009.

[46] R. Knight. (2012). *Smart Systems in the UK context – an ETI view*. Available: http://eti.co.uk/downloads/related_documents/Smart_Cities_Richard_Knight_17th_April_2012.pdf [Accessed: 20.09.2012]

[47] F. Kienzle, P. Favre-Perrod, M. Arnold, and G. Andersson, "Multi-energy delivery infrastructures for the future," in *Infrastructure Systems and Services: Building Networks for a Brighter Future (INFRA), 2008 First International Conference on*, 2008, pp. 1-5.

[48] P. Mancarella, "Multi-energy Systems: The Smart Grid beyond Electricity," *LBL, Berkeley,* 2012.

[49] P. Mancarella, "Distributed Multi-Generation Options to Increase Environmental Efficiency in Smart Cities " *IEEE PES General Meeting 2012,* 2012.

[50] A. Seungwon, L. Qing, and T. W. Gedra, "Natural gas and electricity optimal power flow," *Transmission and Distribution Conference and Exposition, IEEE PES,* vol. 1, pp. 138-143, 2003.

[51] M. Chaudry, N. Jenkins, and G. Strbac, "Multi-time period combined gas and electricity network optimisation," *Electric Power Systems Research,* vol. 78, pp. 1265-1279, 2008.

[52] M. Qadrdan, M. Chaudry, J. Wu, N. Jenkins, and J. Ekanayake, "Impact of a large penetration of wind generation on the GB gas network," *Energy Policy,* vol. 38, pp. 5684-5695, 2010.

[53] A. Martinez-Mares and C. R. Fuerte-Esquivel, "A Unified Gas and Power Flow Analysis in Natural Gas and Electricity Coupled Networks," *Power Systems, IEEE Transactions on,* vol. 27, pp. 2156-2166, 2012.

[54] R. Rubio-Barros, D. Ojeda-Esteybar, and A. Vargas, "Energy Carrier Networks: Interactions and Integrated Operational Planning Handbook of Networks in Power Systems II," A. Sorokin, S. Rebennack, P. M. Pardalos, N. A. Iliadis, and M. V. F. Pereira, Eds., ed: Springer Berlin Heidelberg, 2012, pp. 117-167.

[55] P. Favre-Perrod, "Hybrid energy transmission for multi-energy networks," PhD Thesis, ETH, 2008.

[56] B. Awad, M. Chaudry, J. Wu, and N. Jenkins, "Integrated optimal power flow for electric power and heat in a microgrid," Prague, 2009.

[57] M. T. Rees, J. Wu, B. Awad, J. Ekanayake, and N. Jenkins, "A modular approach to integrated energy distribution system analysis," *17th Power Systems Computation Conference, Stockholm Sweden,* 2011.

[58] M. T. Rees, J. Wu, B. Awad, J. Ekanayake, and N. Jenkins, "A total energy approach to integrated community infrastructure design," *Power and Energy Society General Meeting, 2011 IEEE,* 2011.
[59] H. Lund and E. Münster, "Integrated energy systems and local energy markets," *Energy Policy,* vol. 34, pp. 1152-1160, 2006.
[60] P. Meibom, J. Kiviluoma, R. Barth, H. Brand, C. Weber, and H. V. Larsen, "Value of electric heat boilers and heat pumps for wind power integration," *Wind Energy,* vol. 10, pp. 321-337, 2007.
[61] G. Chicco and P. Mancarella, "Evaluation of multi-generation alternatives: an approach based on load transformations," in *Power and Energy Society General Meeting - Conversion and Delivery of Electrical Energy in the 21st Century, 2008 IEEE*, 2008, pp. 1-6.
[62] M. Pierluigi, "Cogeneration systems with electric heat pumps: Energy-shifting properties and equivalent plant modelling," *Energy Conversion and Management,* vol. 50, pp. 1991-1999, 2009.
[63] R. Sansom, "The impact of future heat demand pathways on the economics of low carbon heating systems," *BIEE Conference,* 2012.
[64] J. Arran and J. Slowe, "2050 Pathways for Domestic Heat Final Report " *Delta Energy & Environment Ltd,* 2012.
[65] J. Speirs, R. Gross, S. Deshmukh, P. Heptonstall, L. Munuera, M. Leach, and J. Torriti, "Heat delivery in a low carbon economy," *BIEE Conference,* 2010.
[66] P. Dodd, "Delivering the low carbon energy jigsaw. Will the technology and incentive pieces fit," 2012.
[67] Siemens, "PSS Sincal 7.0 heating Manual," 2010.
[68] M. Fedorov, "Parallel Implementation of a Steady State Thermal and Hydraulic Analysis of Pipe Networks in OpenMP," in *Parallel Processing and Applied Mathematics*. vol. 6068, R. Wyrzykowski, J. Dongarra, K. Karczewski, and J. Wasniewski, Eds., ed: Springer Berlin / Heidelberg, 2010, pp. 360-369.
[69] B. E. Larock, R. W. Jeppson, and G. Z. Watters, *Hydraulics of pipeline systems*: CRC, 2000.
[70] A. Osiadacz, *Simulation and analysis of gas networks*: Gulf Pub. Co., 1987.
[71] 7-Technologies, "TERMIS Help Manual," 2009.
[72] A. Benonysson, "Dynamic Modelling and Operational Optimization of District Heating Systems," PhD Thesis. Laboratory of Heating and Air Conditioning. Technical University of Denmark, 1991.
[73] I. Ben Hassine and U. Eicker, "Impact of load structure variation and solar thermal energy integration on an existing district heating network," *Applied Thermal Engineering,* 2012.
[74] G. P. Henze and A. G. Floss, "Evaluation of temperature degradation in hydraulic flow networks," *Energy and Buildings,* vol. 43, pp. 1820-1828, 2011.
[75] D. Clamond, "Efficient resolution of the Colebrook equation," *Industrial & Engineering Chemistry Research,* vol. 48, pp. 3665-3671, 2009.
[76] W. H. Press, S. A. Teukolsky, W. T. Vetterling, and B. P. Flannery, "Numerical Recipes 3rd Edition: The Art of Scientific Computing " *Cambridge University Press,* 2007.
[77] MathWorld. *Newton's Method*. Available: http://mathworld.wolfram.com/NewtonsMethod.html [Accessed: 01.05.2010]

[78] T. Altman and P. F. Boulos, "Convergence of Newton method in nonlinear network analysis," *Mathematical and Computer Modelling,* vol. 21, pp. 35-41, 1995.

[79] K. C. B. Steer, A. Wirth, and S. K. Halgamuge, "Control period selection for improved operating performance in district heating networks," *Energy and Buildings,* vol. 43, pp. 605-613, 2011.

[80] J. Byun, Y. Choi, J. Shin, M. Park, and D. Kwak, "Study on the Development of an Optimal Heat Supply Control Algorithm for Group Energy Apartment Buildings According to the Variation of Outdoor Air Temperature," *Energies,* vol. 5, pp. 1686-1704, 2012.

[81] B. Bøhm and P. O. Danig, "Monitoring the energy consumption in a district heated apartment building in Copenhagen, with specific interest in the thermodynamic performance," *Energy and Buildings,* vol. 36, pp. 229-236, 2004.

[82] L. Saarinen, "Modelling and control of a district heating system," *Uppsala University, Department of Information Technology,* p. 12, 2008.

[83] B. Bøhm, S. Ha, W. Kim, B. Kim, T. Koljonen, H. Larsen, M. Lucht, Y. Park, K. Sipila, and M. Wigbels, *Simple models for operational optimisation*: Department of Mechanical Engineering, Technical University of Denmark, 2002.

[84] J. M. Coulson, J. F. Richardson, and R. K. Sinnott, "Coulson & Richardson's Chemical Engineering. Volume 1: Fluid Flow, Heat Transfer & Mass Transfer," *Butterworth-Heinemann Ltd,* p. 501, 1999.

[85] J. McCalley. *Power System Analysis I (Fall 2006) Course*. Available: www.ee.iastate.edu/~jdm/EE456/FastPowerFlow.doc [Accessed: 08.11.2012]

[86] J. J. Grainger and W. D. Stevenson, *Power system analysis*: McGraw-Hill (New York), 1994.

[87] J. Kalina and J. Skorek, "CHP plants for distributed generation–equipment sizing and system performance evaluation," *Proceeding of ECOS,* 2002.

[88] C. Sondergren and H. F. Ravn, "A method to perform probabilistic production simulation involving combined heat and power units," *Power Systems, IEEE Transactions on,* vol. 11, pp. 1031-1036, 1996.

[89] L. Goldstein, *Gas-fired distributed energy resource technology characterizations*: National Renewable Energy Laboratory, 2003.

[90] EPA, *Catalog of CHP Technologies*: U.S. Environmental Protection Agency (EPA) Combined Heat and Power Partnership, 2008.

[91] EURELECTRIC, "European Combined Heat & Power: A Technical Analysis of Possible Definition of the Concept of "Quality CHP"," *Union of the Electricity Industry – EURELECTRIC,* 2002.

[92] H. Palsson, "Methods for planning and operating decentralized combined heat and power plants," Technical University of Denmark, 2000.

[93] H. V. Larsen, H. Pálsson, and H. F. Ravn, "Probabilistic production simulation including combined heat and power plants," *Electric Power Systems Research,* vol. 48, pp. 45-56, 1998.

[94] CHPQA. *GUIDANCE NOTE 28: The Determination of Z Ratio*. Available: https://www.chpqa.com/guidance_notes/GUIDANCE_NOTE_28.pdf [Accessed: 01.06.2013]

[95] Danfoss. *The Heating Book - 8 steps to control of heating systems*. Available: http://heating.danfoss.com/Content/61078BB5-1E17-4CA2-

AC49-8A7CAC2BA687_MNU17424997_SIT54.html [Accessed: 23.07.2012]

[96] A. Seugwon, "Natural Gas and Electricity Optimal Power Flow," *PhD thesis, Oklahoma State University,* 2004.

[97] *MATPOWER*. Available: http://www.pserc.cornell.edu/matpower/ [Accessed: 03.04.2010]

[98] Y. Xing, A. Bagdanavicius, S. C. Lannon, M. Pirouti, and T. Bassett, "Low temperature district heating network planning with the focus on distribution energy losses," *The Fourth International Conference on Applied Energy (ICAE2012), Suzhou, China,* 2012.

[99] S. Ingram, S. Probert, and K. Jackson, "The Impact of Small Scale Embedded Generation Upon The Operating Parameters of Distribution Networks," *DTi New and Renewable Energy Program, K/EL/00303/04/01,* 2003.

[100] *IPSA Power* Available: http://www.ipsa-power.com/ [Accessed: 03.04.2013]

[101] T. Guo, M. I. Henwood, and M. van Ooijen, "An algorithm for combined heat and power economic dispatch," *Power Systems, IEEE Transactions on,* vol. 11, pp. 1778-1784, 1996.

[102] J. D. Glover, M. S. Sarma, and T. J. Overbye, *Power Systems Analysis & Design*: Thomson, 2008.

Appendix A - Hydraulic Calculation Methods

The objective of the hydraulic model is to determine the pipe mass flow rates $\dot{m}$ under the assumption that the nodal mass flow rates $\dot{m}_q$ are specified. The set of the hydraulic equations was written in the forms of unknown pipe mass flow rates $\dot{m}$, unknown pressure head *h*, or unknown corrective mass flow rates $\Delta\dot{m}$. The $\dot{m}$-equations solved by the Newton-Raphson method was described in Chapter 2. In this Appendix, the *h*-equations solved by the Newton-Raphson and the $\Delta\dot{m}$-equations solved by the Newton-Raphson and the Hardy-Cross method were explained by a simple example and a more complicated example.

A1 A Simple Example

A simple example of a pipe network with a loop is shown in Figure A.1.

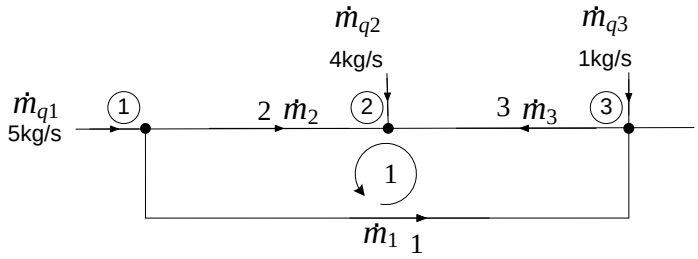

Figure A.1: A pipe network with a loop

For the pipe network, the nodal mass flow rates are $\dot{\boldsymbol{m}}_q = \begin{bmatrix} 5 \\ -4 \\ -1 \end{bmatrix}$.

It was assumed that the vector of the resistance coefficients of each pipe $\boldsymbol{K}$ is constant and is given by, $\boldsymbol{K} = \begin{bmatrix} 3 \\ 2 \\ 6 \end{bmatrix}$.

The network incidence matrix **A** and the loop incidence matrix **B** are:

$$\mathbf{A} = \begin{array}{c} \\ \text{Node No.} \\ 1 \\ 2 \\ 3 \end{array} \begin{array}{c} \begin{array}{ccc} \text{Pipe No.} & & \\ 1 & 2 & 3 \end{array} \\ \begin{bmatrix} 1 & -1 & 0 \\ 0 & 1 & 1 \\ -1 & 0 & -1 \end{bmatrix} \end{array} \qquad \mathbf{B} = \begin{array}{c} \\ \text{Loop No.} \\ 1 \end{array} \begin{array}{c} \begin{array}{ccc} \text{Pipe No.} & & \\ 1 & 2 & 3 \end{array} \\ \begin{bmatrix} 1 & -1 & 1 \end{bmatrix} \end{array}$$

a) ***ṁ*-equations**

The continuity equation for nodes 1 and 2 is

$$\begin{aligned} -\dot{m}_1 - \dot{m}_2 + 5 &= 0 \\ \dot{m}_2 + \dot{m}_3 - 4 &= 0 \end{aligned} \tag{A.1}$$

The loop pressure equation for loop 1 is

$$\begin{aligned} \boldsymbol{F_l}(\dot{\boldsymbol{m}}) &= \sum_{j=1}^{3} B_j K_j \dot{m}_j |\dot{m}_j| \\ &= 3\dot{m}_1|\dot{m}_1| - 2\dot{m}_2|\dot{m}_2| + 6\dot{m}_3|\dot{m}_3| = 0 \end{aligned} \tag{A.2}$$

b) ***h*-equations**

The mass flow rate is written in the form of the pressure head using equation (2.9)

$$\dot{m}_k = \left(\frac{|h_i - h_j|}{K_k} \right)^{1/2} \tag{A.3}$$

where $\dot{m}_k$ is the mass flow rate in pipe *k* between nodes *i* and *j*.

By substituting $\dot{m}_k$ in equation (A.1):

$$\begin{aligned} -\left(\frac{h_1 - h_3}{K_1} \right)^{1/2} - \left(\frac{h_1 - h_2}{K_2} \right)^{1/2} + 5 &= 0 \\ \left(\frac{h_1 - h_2}{K_2} \right)^{1/2} + \left(\frac{h_3 - h_2}{K_3} \right)^{1/2} - 4 &= 0 \end{aligned} \tag{A.4}$$

c) **Δ*ṁ*-equations**

Choose initial values of $\dot{\boldsymbol{m}}^{(0)}$ in each pipe, such that the continuity equation (A.1) is satisfied (e.g., $\dot{\boldsymbol{m}}^{(0)} = \begin{bmatrix} \dot{m}_1^{(0)} \\ \dot{m}_2^{(0)} \\ \dot{m}_3^{(0)} \end{bmatrix} = \begin{bmatrix} 3 \\ 2 \\ 2 \end{bmatrix}$). The mass flow rate in each pipe is replaced by an initial flow rate, denoted by $\dot{m}^{(0)}$, plus the unknown corrective flow rate that circulates through each pipe.

$$\begin{aligned} \boldsymbol{F_l} = \boldsymbol{BK\dot{m}}|\boldsymbol{\dot{m}}| &= \sum_{j=1}^{3} B_j K_j \dot{m}_j |\dot{m}_j| \\ &= 3\dot{m}_1|\dot{m}_1| - 2\dot{m}_2|\dot{m}_2| + 6\dot{m}_3|\dot{m}_3| \\ = 3\left(\dot{m}_1^{(0)} + \Delta\dot{m}\right)&\left|\left(\dot{m}_1^{(0)} + \Delta\dot{m}\right)\right| \\ &- 2\left(\dot{m}_2^{(0)} - \Delta\dot{m}\right)\left|\left(\dot{m}_2^{(0)} - \Delta\dot{m}\right)\right| \\ &+ 6\left(\dot{m}_3^{(0)} + \Delta\dot{m}\right)\left|\left(\dot{m}_3^{(0)} + \Delta\dot{m}\right)\right| = 0 \end{aligned} \tag{A.5}$$

Three systems of equations were described:

- Equations (2.27) and (2.28) with unknown variables $\dot{m}_1\ \dot{m}_2\ \dot{m}_3$
- Equation (A.4) with unknown variables $h_1\ h_2$
- Equation (A.5) with unknown variable $\Delta\dot{m}$

The number of $\dot{m}$-equations is equal to the number of pipes. The number of *h*-equations is equal to the number of nodes minus one. The number of $\Delta\dot{m}$-equations is equal to the number of loops.

A2 Solutions

The Newton-Raphson method for solving $\dot{m}$ -equations has been described in the hydraulic model in Chapter 2.

A2.1 *h*-equations using the Hardy-Cross method

The *h*-equations is solved using the Newton-Raphson method.
The iterative form of the Newton-Raphson method is

$$h^{(i+1)} = h^{(i)} - \boldsymbol{J^{-1}F}_h \tag{A.6}$$

where $\boldsymbol{F}_h$ is the pressure head mismatches.

The Jacobian matrix is formed similarly as the admittance matrix in electric power system. The Jacobian matrix for equation (A.4) is

$$J = \begin{bmatrix} -\frac{1}{2K_1\dot{m}_1} - \frac{1}{2K_2\dot{m}_2} & \frac{1}{2K_2\dot{m}_2} \\ \frac{1}{2K_2\dot{m}_2} & -\frac{1}{2K_2\dot{m}_2} - \frac{1}{2K_3\dot{m}_3} \end{bmatrix} \tag{A.7}$$

Assuming the pressure head at node 3 is the reference head h_3 = 10Pa, and the initial heads at nodes 1 and 2 are: h_1 = 20Pa, h_2 = 4Pa. For the first iteration, $h^{(1)} = h^{(0)} - \left(\boldsymbol{J}^{(0)}\right)^{-1}\boldsymbol{F}_h^{(0)} = [\,21.9089 \quad 3.9678 \quad 10.0000]^T$.

After 4251 iterations with the tolerance $\boldsymbol{\varepsilon}$ = 10^{-3}, the converged results are $\boldsymbol{h}$ = [21.9988 3.9976 10.0000]^T. By substituting $\boldsymbol{h}$ in equation (A.3), the calculated mass flow rates are $\dot{\boldsymbol{m}}$ = [1.9998 3.0002 1.0005]^T.

It was found that the *h*-equations with the nodal formulation encountered convergence difficulty in the case of improper selection of initial nodal head values.

A2.2 $\Delta\dot{\boldsymbol{m}}$-equations using the Newton-Raphson method

The unknown variables are the corrective mass flow rates in each pipe in $\Delta\dot{m}$-equations. The initial value of the mass flow rate in each pipe is chosen such that the continuity equation is satisfied. By changing the mass flow rates in all the pipes in loop *li* by the same amount $\Delta\dot{m}_{li}$, the increase or decrease in the flow into a junction is balanced by the exact same increase or decrease in the flow out, so that the continuity equation is still satisfied.

The mass flow rates within each pipe is calculated from the corrective mass flow rates in each loop

$$\dot{\boldsymbol{m}} = \dot{\boldsymbol{m}}^{(0)} + \boldsymbol{B}^T\Delta\dot{\boldsymbol{m}} \tag{A.8}$$

where $\Delta\dot{\boldsymbol{m}}$ is the n_l × 1 vector, n_l is the number of loops.
The iterative form of the Newton-Raphson method is

$$\Delta\dot{\boldsymbol{m}}^{(i+1)} = \Delta\dot{\boldsymbol{m}}^{(i)} - \boldsymbol{J}^{-1}\boldsymbol{F}_{\boldsymbol{l}} \tag{A.9}$$

The Jacobian matrix is

$$\boldsymbol{J} = \begin{bmatrix} \frac{\partial F_1}{\partial \Delta \dot{m}_1} & \cdots & \frac{\partial F_1}{\partial \Delta \dot{m}_{n_l}} \\ \vdots & \ddots & \vdots \\ \frac{\partial F_{n_l}}{\partial \Delta \dot{m}_1} & \cdots & \frac{\partial F_{n_l}}{\partial \Delta \dot{m}_{n_l}} \end{bmatrix} \tag{A.10}$$

The loop pressure mismatches are

$$\begin{aligned} \boldsymbol{F_l}(\dot{\boldsymbol{m}}) &= \boldsymbol{F_l}\left(\dot{\boldsymbol{m}}^{(0)} + \boldsymbol{B}^T \Delta \dot{\boldsymbol{m}}\right) \\ &= \sum_{j=1}^{n_p} B_{kj} K_j \left(\dot{m}_j^{(0)} + B_{kj} \Delta \dot{\boldsymbol{m}}_k\right) \left|\left(\dot{m}_j^{(0)} + B_{kj} \Delta \dot{\boldsymbol{m}}_k\right)\right| \end{aligned} \tag{A.11}$$

The derivative of $\boldsymbol{F_l}$ to $\Delta \dot{\boldsymbol{m}}$ ($\frac{\partial \boldsymbol{F_l}}{\partial \Delta \dot{\boldsymbol{m}}}$) is

$$\frac{\partial \boldsymbol{F_{l,k}}}{\partial \Delta \dot{\boldsymbol{m}}_j} = \begin{cases} \sum_{j=1}^{n_p} 2\left|B_{kj}\right| K_j \left|\dot{m}_j\right|, if\ j\ \in\ loop\ k \\ 2B_{kj} B_{k'j} K_j \left|\dot{m}_j\right|, if\ j \in loop\ k, j \in loop\ k' \end{cases} \tag{A.12}$$

For the network as shown in Figure A.1, the Jacobian matrix $\boldsymbol{J}$ is

$$\boldsymbol{J} = \frac{\partial \boldsymbol{F_l}}{\partial \Delta \dot{\boldsymbol{m}}} = 6|\dot{m}_1| + 4|\dot{m}_2| + 12|\dot{m}_3| \tag{A.13}$$

Initially assume $\Delta \dot{\boldsymbol{m}}^{(0)} = \boldsymbol{0}$.

For the first iteration,

$\Delta \dot{\boldsymbol{m}}^{(1)} = \Delta \dot{\boldsymbol{m}}^{(0)} - \left(\boldsymbol{J}^{(0)}\right)^{-1} \boldsymbol{F}_{\boldsymbol{l}}^{(0)} = 0 - \frac{43}{50} = -0.86.$

After **4** iterations with the tolerance $\boldsymbol{\varepsilon}$ = 10^{-3}, the converged results are: $\Delta \dot{\boldsymbol{m}} = -1.$

Thus, from equation (A.8),

$$\dot{\boldsymbol{m}} = \dot{\boldsymbol{m}}^{(0)} + \boldsymbol{B}^T \Delta \dot{\boldsymbol{m}} = \begin{bmatrix} 3 \\ 2 \\ 2 \end{bmatrix} + \begin{bmatrix} 1 \\ -1 \\ 1 \end{bmatrix} [-1] = \begin{bmatrix} 2 \\ 3 \\ 1 \end{bmatrix}.$$

A2.3 $\Delta \dot{\boldsymbol{m}}$-equations using the Hardy-Cross method

Hardy-Cross method was developed for hand calculations and solved one loop at a time instead of solving all loops simultaneously. The iterative form is

$$\Delta\dot{\boldsymbol{m}}^{(i+1)} = \Delta\dot{\boldsymbol{m}}^{(i)} - \frac{\boldsymbol{F_l}}{\frac{\partial \boldsymbol{F_l}}{\partial \Delta\dot{\boldsymbol{m}}}} = \Delta\dot{\boldsymbol{m}}^{(i)} - \frac{\boldsymbol{BK\dot{m}|\dot{m}|}}{2|\boldsymbol{B}|\boldsymbol{K}|\dot{\boldsymbol{m}}|} \tag{A.14}$$

The adjustments use the main diagonal of Jacobain matrix in the Newton-Raphson method. The adjustments of the pipe flow rates in all loops are

$$\frac{\boldsymbol{F_l}}{\frac{\partial \boldsymbol{F_l}}{\partial \Delta\dot{\boldsymbol{m}}}} = \frac{\sum_{j=1}^{n_p} B_{kj} K_j \dot{m}_j |\dot{m}_j|}{\sum_{j=1}^{n_p} 2|B_{kj}|K_j|\dot{m}_j|}, k = 1,2,\dots,n_l \tag{A.15}$$

where, n_p and n_l are the number of pipes and loops; k is the index of loops; $|\boldsymbol{B}|$ consists of elements '1' and '0'. For a pipe in two loops, the adjustments of its flow rate are cumulative. The procedure to calculate $\frac{\partial \boldsymbol{F_l}}{\partial \Delta\dot{\boldsymbol{m}}}$ is explained in the Newton-Raphson method.

Comparing to the Newton-Raphson method in the $\Delta\dot{m}$-equations, the Hardy Cross method simplifies the determination of the correction term by considering each loop independently rather than all loops simultaneously.

The steps of the hydraulic calculation for the network as shown in Figure A.1 are as follows:

1) Choose initial values of $\dot{\boldsymbol{m}}^{(0)}$ in each pipe, such that the continuity equation is satisfied (e.g., $\dot{\boldsymbol{m}}^{(0)} = \begin{bmatrix} \dot{m}_1^{(0)} \\ \dot{m}_2^{(0)} \\ \dot{m}_3^{(0)} \end{bmatrix} = \begin{bmatrix} 3 \\ 2 \\ 2 \end{bmatrix}$).

2) Calculate the sum of head loss around the loop using equation (A.5). For the first iteration,

$$\boldsymbol{F_l} = \boldsymbol{BK\dot{m}|\dot{m}|} = [1 \quad -1 \quad 1] \begin{bmatrix} 3 \\ 2 \\ 6 \end{bmatrix} \begin{bmatrix} 3 \\ 2 \\ 2 \end{bmatrix} \begin{bmatrix} 3 \\ 2 \\ 2 \end{bmatrix} = 27 - 8 + 24 = 43.$$

3) Calculate the derivative of the expression in step 2. For the first iteration,

$$2|\boldsymbol{B}|\boldsymbol{K}|\dot{\boldsymbol{m}}| = \sum_{j=1}^{n_p} 2|B_{kj}|K_j|\dot{m}_j| = 18 + 8 + 24 = 50.$$

4) Adjust the mass flow rates within each pipe in the loop by the same amount $\Delta\dot{\boldsymbol{m}}$. This adjustment is calculated by dividing the result from step 2 by the result from step 3. For the first iteration,

$\Delta\dot{\boldsymbol{m}} = -\frac{\boldsymbol{BK}\dot{\boldsymbol{m}}|\dot{\boldsymbol{m}}|}{2|\boldsymbol{B}|\boldsymbol{K}|\dot{\boldsymbol{m}}|} = -\frac{43}{50} = -0.86$. Thus,

$$\dot{\boldsymbol{m}}^{(1)} = \begin{bmatrix} \dot{m}_1^{(1)} \\ \dot{m}_2^{(1)} \\ \dot{m}_3^{(1)} \end{bmatrix} = \dot{\boldsymbol{m}}^{(0)} + \boldsymbol{B}^T\Delta\dot{\boldsymbol{m}} = \begin{bmatrix} \dot{m}_1^{(0)} + \Delta\dot{m} \\ \dot{m}_2^{(0)} - \Delta\dot{m} \\ \dot{m}_3^{(0)} + \Delta\dot{m} \end{bmatrix} = \begin{bmatrix} 2.14 \\ 2.86 \\ 1.14 \end{bmatrix}.$$

5) This procedure is repeated from step 2) until the maximum of $|\boldsymbol{F}_l|$ becomes less than $\boldsymbol{\varepsilon}$. After 4 iterations, the converged results are:

$$\dot{\boldsymbol{m}} = \begin{bmatrix} \dot{m}_1 \\ \dot{m}_2 \\ \dot{m}_3 \end{bmatrix} = \begin{bmatrix} 2 \\ 3 \\ 1 \end{bmatrix}.$$

A3 A Complicated Example

Another case represents a part of a district heating network with multi-loops is shown in Figure A.2. The network is supplied by node 1. The pipe parameters, nodal mass flow vector $\dot{\boldsymbol{m}}_q$, the network incidence matrix $\boldsymbol{A}$ and the loop incidence matrix $\boldsymbol{B}$ are listed in Table A.1-A.4.

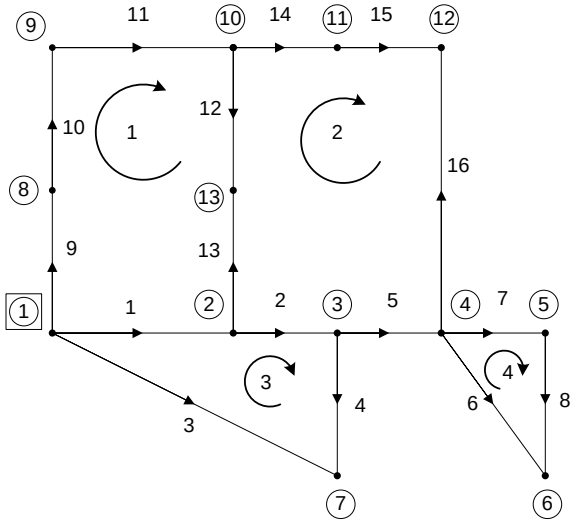

Figure A.2: A district heating network with multi-loops

Table A.1: Pipe parameters

Pipe No.	Node No. (start)	Node No. (end)	Diameter (m)	Length (m)	Roughness (mm)
1	1	2	0.25	200	0.025
2	2	3	0.20	80	0.025
3	1	7	0.05	352	0.025
4	3	7	0.05	112	0.025
5	3	4	0.20	240	0.025
6	4	6	0.05	328	0.025
7	4	5	0.15	96	0.025
8	5	6	0.125	248	0.025
9	1	8	0.08	160	0.025
10	8	9	0.05	104	0.025
11	9	10	0.05	208	0.025
12	10	13	0.15	200	0.025
13	2	13	0.30	48	0.025
14	10	11	0.10	120	0.025
15	11	12	0.08	208	0.025
16	4	12	0.10	280	0.025

Table A.2: Mass flow rate at each node

Node	1	2	3	4	5	6	7	8	9	10	11	12
$\dot{m}$	129.37	2.96	4.37	7.38	9.16	27.03	1.96	4.65	5.85	28.29	26.67	7.68

Table A.3: Data of the network incidence matrix A

		Pipe No.															
		1	2	3	4	5	6	7	8	9	10	11	12	13	14	15	16
Node No.	1	-1		-1						-1							
	2	1	-1											-1			
	3		1		-1	-1											
	4					1	-1	-1									-1
	5							1	-1								
	6						1		1								
	7			1	1												
	8									1	-1						
	9										1	-1					
	10											1	-1		-1		
	11														1	-1	
	12															1	1

Table A.4: Data of the loop incidence matrix B

		Pipe No.															
		1	2	3	4	5	6	7	8	9	10	11	12	13	14	15	16
Loop No.	1	-1								1	1	1	1	-1			
	2		-1			-1							-1	1	1	1	-1
	3	1	1	-1	1												
	4						-1	1	1								

A3.1 $\Delta\dot{m}$-equations using the Newton-Raphson method

For the network as shown in Figure A.2, the Jacobian matrix $\boldsymbol{J}$ is

$$\boldsymbol{J} = \begin{bmatrix} J_{11} & J_{12} & J_{13} & 0 \\ J_{21} & J_{22} & J_{23} & 0 \\ J_{31} & J_{32} & J_{33} & 0 \\ 0 & 0 & 0 & J_{44} \end{bmatrix} \tag{A.16}$$

where

$J_{kk} = \sum_{j=1}^{n_p} 2|B_{kj}|K_j|\dot{m}_j|,$

$J_{12} = J_{21} = 2B_{1,12}B_{2,12}K_{12}|\dot{m}_{12}| + 2B_{1,13}B_{2,13}K_{13}|\dot{m}_{13}|,$

$J_{13} = J_{31} = 2B_{1,1}B_{3,1}K_1|\dot{m}_1|,$

$J_{23} = J_{32} = 2B_{2,2}B_{3,2}K_2|\dot{m}_2|.$

After **6** iterations with the tolerance $\boldsymbol{\varepsilon}$=10^{-3}, the converged results are:

$\dot{\boldsymbol{m}}$ = [119.06 62.13 1.47 0.49 57.28 2.14 34.05 24.89 8.83 4.18 -1.67 -50.60 53.97 20.64 -6.03 13.71].

A3.2 $\Delta\dot{m}$-equations using the Hardy-Cross method

The steps of the hydraulic calculation for the network with 4 loops as shown in Figure A.2 are as follows

1) Choose initial values of $\dot{\boldsymbol{m}}^{(0)}$ in each pipe to satisfy the continuity equation:
   - Arbitrarily choose values for one pipe in each loop to form 4 augmented equations, for example, pipe 11 in loop 1, pipe 16 in

loop 2, pipe 3 in loop 3, pipe 6 in loop 4, e.g., set their values to 1 kg/s.

- Combine these augmented equations and the continuity equations to calculate the initial mass flow rates

  $\dot{\boldsymbol{m}}^{(0)}$ = [116.87 49.90 1.00 0.96 44.57 1.00 35.19 26.03 11.50 6.85 1.00 -60.64 64.01 33.35 6.68 1.00]^T.

2) Calculate the sum of head loss around each loop. For the first iteration, $\boldsymbol{F_l} = \boldsymbol{BK\dot{m}|\dot{m}|} = \begin{bmatrix} 20.24 \\ 31.75 \\ 2.40 \\ 7.38 \end{bmatrix}$.

3) Calculate the derivative of the expression in step 2. For the first iteration,

$$2|\boldsymbol{B}|\boldsymbol{K}|\dot{\boldsymbol{m}}| = \sum_{j=1}^{n_p} 2\left|B_{kj}\right|K_j\left|\dot{m}_j\right| = \begin{bmatrix} 12.17 \\ 3.09 \\ 6.35 \\ 5.16 \end{bmatrix}.$$

4) Adjust the flow in each pipe in the loop *li* by the same amount $\Delta\dot{m}_{li}$. This adjustment is calculated by dividing the result from step 2 by the result from step 3. For the first iteration,

$$\Delta\dot{\boldsymbol{m}}^{(1)} = -\frac{\boldsymbol{BK\dot{m}|\dot{m}|}}{2|\boldsymbol{B}|\boldsymbol{K}|\dot{\boldsymbol{m}}|} = -\begin{bmatrix} 20.24 \\ 31.75 \\ 2.40 \\ 7.38 \end{bmatrix} \Big/ \begin{bmatrix} 12.17 \\ 3.09 \\ 6.35 \\ 5.16 \end{bmatrix} = \begin{bmatrix} -1.66 \\ -10.28 \\ -0.38 \\ -1.43 \end{bmatrix},$$

$\therefore \dot{\boldsymbol{m}}^{(1)} = \dot{\boldsymbol{m}}^{(0)} + \boldsymbol{B}^T\Delta\dot{\boldsymbol{m}}^{(1)}$ =[118.16 59.80 1.38 0.58 54.85 2.43 33.76 24.60 9.84 5.19 -0.66 -52.02 55.39 23.07 -3.60 11.28] ^{T}.

5) This procedure is repeated from step 2) until the maximum element in $|\boldsymbol{F_l}|$ becomes less than $\boldsymbol{\varepsilon}$. After **7** iterations, the converged results are:

$\dot{\boldsymbol{m}}$ = [119.06 62.13 1.47 0.49 57.28 2.14 34.05 24.89 8.83 4.18 -1.67 -50.60 53.97 20.64 -6.03 13.71]^T.

A4 Summary

The hydraulic model of district heating networks in three systems of equations ($\dot{m}$-equations, *h*-equations, and $\Delta\dot{m}$-equations) by the Newton-Raphson or the Hardy-Cross method were explained with a simple example and a complicate example. The *h*-equations by the Newton-Raphson method was very sensitive to the initial values of the pressure head. The $\Delta\dot{m}$-equations used least number of equations.

The Newton-Raphson method considered all loops simultaneously. The Hardy-Cross method dealt with one loop at a time. Its adjustments used the main diagonal of the Jacobian matrix in the Newton-Raphson method. This was similar as PQ fast decoupled method to the Newton-Raphson method in electric power systems.

Appendix B - Derivation of the Temperature Drop Equation

The temperature at the outlet of a pipe is calculated using the temperature drop equation

$$T_{end} = (T_{start} - T_a)e^{-\frac{\lambda L}{C_p \dot{m}}} + T_a \quad \text{(B.1)}$$

where T_{start} and T_{end} are the temperatures at the start node and the end node of a pipe (°C); T_a is the ambient temperature (°C); λ is the overall heat transfer coefficient of each pipe per unit length (W/(m·K)); L is the length of each pipe (m); C_p is the specific heat of water (J/(kg·K)); and $\dot{m}$ is the mass flow rate (kg/s) within each pipe.

The derivation of the temperature drop equation (B.1) is as follows:

The rate of heat transfer from the water to the ambient through a pipe dx is given by

$$\frac{d\emptyset}{dt} = (T - T_a)\lambda dx \quad \text{(B.2)}$$

where T is the temperature of water at any time.

This heat transfer will cause the temperature of the water to change as shown in equation (B.3)

$$d\emptyset = C_p dm dT \quad \text{(B.3)}$$

Substitute $d\emptyset$ in equation (B.3) into equation (B.2)

$$\frac{C_p dm dT}{dt} = (T - T_a)\lambda dx \quad \text{(B.4)}$$

Rearrange equation (B.4)

$$\frac{dT}{(T-T_a)} = \frac{\lambda dx}{C_p dm} dt = \frac{\lambda dx}{C_p \dot{m}} \tag{B.5}$$

The integral of equation (B.5) is

$$\int_{T_{end}}^{T_{start}} \frac{dT}{(T-T_a)} = \int_0^L \frac{\lambda dx}{C_p \dot{m}} \tag{B.6}$$

Hence

$$In \frac{T_{start}-T_a}{T_{end}-T_a} = \frac{\lambda\, L}{C_p \dot{m}} \tag{B.7}$$

$$T_{end} - T_a = (T_{start} - T_a) e^{-\frac{\lambda L}{C_p \dot{m}}} \tag{B.8}$$

Appendix C - Data for the Example Networks

Table C.1: Data for the example networks in grid-connected mode

Electricity network
• The base power is 1MVA and the base voltage is 11kV. • Voltage magnitude of the CHP unit and the main grid are: $\|V_{1,source}\| = 1.05 p.u.$, $\|V_{grid}\| = 1.02 p.u.$ • Voltage angle of the main grid is: $\theta_4 = 0°$. • Active power of each load are: $P_{1,load} = P_{2,load} = 0.15 MW_e$. • Power factor of each load is: $\cos\Phi = 0.95$. • Impedance of each line is: $Y = 0.09 + j0.1577 p.u.$
Heat network
• $\Phi_{1,load} = \Phi_{2,load} = 0.3 MW_{th}$. • $T_{s1,source} = 100°C$, $T_{o1,load} = T_{o2,load} = 50°C$. • Ambient temperature is: $T_a = 10°C$. • The parameters of each pipe are: $D = 0.15m$, $\varepsilon = 1.25\times10^{-3}$ m, $\lambda = 0.2$ W/mK, $\mu = 0.294\times10^{-6} m^2/s$. $L_1 = L_2 = 400m$, $L_3 = 600m$. • Water density is: $\rho = 958.4 kg/m^3$. $C_p = 4182$ J/(kg·K)) = 4.182×10^{-3} MJ/(kg·K)).
Coupling components
• Heat-to-power ratio of the CHP unit is: $c_m = 1.3$. • Efficiency of a circulation pump is: $\eta_p = 0.65$. • Minimum allowable pressure head differential is: $H_c = 100m$. • Coefficient of performance (COP) of the heat pump is: COP = 3. • Fraction of electrical power generated from CHP unit modulated to drive the heat pump is: $\alpha = 40\%$.

Table C.2: Data for the example networks in islanded mode

Electricity network
• The base power is 1MVA and the base voltage is 11kV. • Voltage magnitude of the sources are: $\|V_{1,source}\| = 1.05 p.u.$, $\|V_{2,source}\| = 1.02 p.u.$ • Voltage angle of Source 2 at busbar 4 is: $\theta_4 = 0°$. • Active power of each load are: $P_{1,load} = P_{2,load} = 0.15\text{MW}_e$. • Power factor of each load is: $\cos\Phi = 0.95$. • Impedance of each line is: $Y = 0.09 + j0.1577 p.u.$
Heat network
• $\Phi_{1,load} = \Phi_{2,load} = \Phi_{2,load} = 0.3\text{MW}_{th}$. • $T_{s1,source} = T_{s1,source} = 100°C$, $T_{o1,load} = T_{o2,load} = T_{o3,load} = 50°C$. • Ambient temperature is: $T_a = 10°C$. • The parameters of each pipe are: $D = 0.15m$, $\varepsilon = 1.25 \times 10^{-3}m$, $\lambda = 0.2$ W/mK, $L = 400m$. • Water density is: $\rho = 958.4$ kg/m^3. $C_p = 4182$ J/(kg·K)) $= 4.182 \times 10^{-3}$ MJ/(kg·K)).
Coupling components
• The relations between heat and power generation of the CHP units are: $Z_1 = \frac{\emptyset_{CHP1}}{1.5 - P_{CHP1}} = 10$, $c_{m2} = \frac{\emptyset_{CHP2}}{P_{CHP2}} = 1.3$, where Z_1 is the Z ratio of CHP1; c_{m2} is the heat-to-power ratio of CHP2. • Efficiency of a circulation pump is: $\eta_p = 0.65$. • Minimum allowable pressure head differential is: $H_c = 100m$. • Coefficient of performance (COP) of the heat pump is: COP = 3. • Fraction of electrical power generated from CHP 1 modulated to drive the heat pump is: $\alpha = 40\%$.

Appendix D - Pipe Parameters for the Case Study

Table D.1: Pipe Parameters for the Barry Island Case Study in Chapter 4

Pipe No	From node	To node	Length (m)	Diameter (mm)	Heat transfer coefficient (W/mK)	Roughness (mm)
01	01	02	257.6	125	0.321	0.4
02	02	03	97.5	40	0.21	0.4
03	02	04	51	40	0.21	0.4
04	02	05	59.5	100	0.327	0.4
05	05	06	271.3	32	0.189	0.4
06	05	07	235.4	65	0.236	0.4
07	07	08	177.3	40	0.21	0.4
08	07	09	102.8	40	0.21	0.4
09	07	10	247.7	40	0.21	0.4
10	05	11	160.8	100	0.327	0.4
11	11	12	129.1	40	0.21	0.4
12	11	13	186.1	100	0.327	0.4
13	13	14	136.2	80	0.278	0.4
14	14	15	41.8	50	0.219	0.4
15	15	16	116.8	32	0.189	0.4
16	15	17	136.4	32	0.189	0.4
17	14	18	136.4	32	0.189	0.4
18	14	19	44.9	80	0.278	0.4
19	19	20	136.4	32	0.189	0.4
20	19	21	134.1	32	0.189	0.4
21	19	22	41.7	65	0.236	0.4
22	22	23	161.1	32	0.189	0.4
23	22	24	134.2	32	0.189	0.4
24	22	25	52.1	65	0.236	0.4
25	25	26	136	32	0.189	0.4
26	25	27	123.3	32	0.189	0.4
27	25	28	61.8	40	0.21	0.4
28	28	29	95.2	32	0.189	0.4
29	28	30	105.1	32	0.189	0.4
30	31	28	70.6	125	0.321	0.4
31	31	7	261.8	125	0.321	0.4
32	32	11	201.3	125	0.321	0.4

Appendix E - Network Incidence Matrix for the Case Study

Table E.1: Network incidence matrix for the Barry Island district heating network case study

Pipe No.

Node No.	1	2	3	4	5	6	7	8	9	10	11	12	13	14	15	16	17	18	19	20	21	22	23	24	25	26	27	28	29	30	31	32
1	-1																															
2	1	-1	-1	-1																												
3		1																														
4			1																													
5				1	-1	-1				-1																						
6					1																											
7						1	-1	-1	-1																						1	
8							1																									
9								1																								
10									1																							
11										1	-1	-1																				
12											1																					
13												1	-1																			
14													1	-1			-1	-1														
15														1	-1	-1																
16															1																	
17																1																
18																	1															
19																		1	-1	-1	-1											
20																			1													
21																				1												

22																					1	-1	-1	-1								
23																						1										
24																							1									
25																								1	-1	-1	-1					
26																									1							
27																										1						
28																											1	-1	-1	1		
29																												1				
30																													1			
31																														-1	-1	
32																																-1

Appendix F - Results Compared to SINCAL and IPSA for the Case Study

Table F.1: Temperatures and mass flow rates compared to SINCAL

	Supply temperature		Return temperature			Mass flow rate	
Node No.	Combined analysis	SINCAL	Combined analysis	SINCAL	Pipe No.	Combined analysis	SINCAL
1	70	70	29.6314	29.6312	1	4.7982	4.7971
2	69.7533	69.7532	29.7125	29.7123	2	0.6509	0.6509
3	69.3054	69.3054	30	30	3	0.8760	0.8760
4	69.5787	69.5788	30	30	4	3.2712	3.2702
5	69.4764	69.4762	29.6517	29.6514	5	0.6664	0.6664
6	68.3920	68.3918	30	30	6	-0.8802	-0.8724
7	69.6565	69.6564	29.6881	29.6881	7	0.6585	0.6585
8	68.8555	68.8552	30	30	8	0.6529	0.6529
9	69.1869	69.1866	30	30	9	0.6637	0.6637
10	68.5491	68.5488	30	30	10	3.4849	3.4762
11	69.3902	69.3901	29.7259	29.7257	11	0.6593	0.6592
12	68.8090	68.8089	30	30	12	4.1925	4.1899
13	69.1844	69.1842	29.7243	29.7241	13	4.1925	4.1839
14	69.0567	69.0564	29.7669	29.7668	14	1.0062	1.0061
15	68.9284	68.9280	29.7738	29.7738	15	0.5024	0.5024
16	68.3118	68.3121	30	30	16	0.5038	0.5037
17	68.2110	68.2112	30	30	17	0.5021	0.5021
18	68.3362	68.3357	30	30	18	2.1914	2.189
19	68.9764	68.9759	29.7605	29.7603	19	0.5031	0.5031
20	68.2575	68.2577	30	30	20	0.5030	0.5029
21	68.2693	68.2695	30	30	21	1.1852	1.1830
22	68.8315	68.8323	29.8015	29.8015	22	0.6699	0.6698
23	68.1949	68.1962	30	30	23	0.6681	0.6679
24	68.2992	68.3005	30	30	24	-0.1527	0.1608
25	69.7547	69.7549	29.7795	29.7796	25	0.6528	0.6528
26	69.1947	69.1949	30	30	26	0.6519	0.6519
27	69.2461	69.2464	30	30	27	-1.4574	-1.4594
28	69.8821	69.8821	29.7956	29.7956	28	0.6480	0.6480

29	69.4858	69.4858	30	30	29	0.6486	0.6486
30	69.4452	69.4452	30	30	30	2.7540	2.7560
31	70	70	29.6552	29.6554	31	3.5005	3.4987
32	70	70	29.5906	29.5905	32	2.2471	2.2471

Table F.2: Heat power compared to SINCAL

Heat power from Source 2 (heat slack)	
Combined analysis	SINCAL
0.8100	0.8099

Table F.3: Voltage magnitudes and angles compared to IPSA

	Voltage magnitude		Voltage angle	
Busbar No.	Combined analysis	IPSA	Combined analysis	IPSA
1	1.0488	1.0488	-0.63	-0.63
2	1.0488	1.0488	-0.63	-0.63
3	1.0490	1.0490	-0.66	-0.66
4	1.0493	1.0493	-0.71	-0.71
5	1.0499	1.0499	-0.74	-0.75
6	1.0499	1.0499	-0.75	-0.74
7	1.05	1.05	-0.72	-0.72
8	1.05	1.05	-0.76	-0.76
9	1.02	1.02	0	0

Table F.4: Electrical power compared to IPSA

Electrical power from Source 1 (electrical slack)	
Combined analysis	IPSA
0.8118	0.8118